FDOT-FHWA SPONSORED RESEARCH PROJECT

FINAL REPORT

Project Title: Elastomeric Bearing Pads Under Combined Loading

Contract No: BC352-16

Submitted

to:

Florida Department of Transportation
Tallahassee, Florida

by

Primus V. Mtenga, PhD, P.E.
Associate Professor in Structural Engineering
FAMU - FSU College of Engineering
Tallahassee, Florida

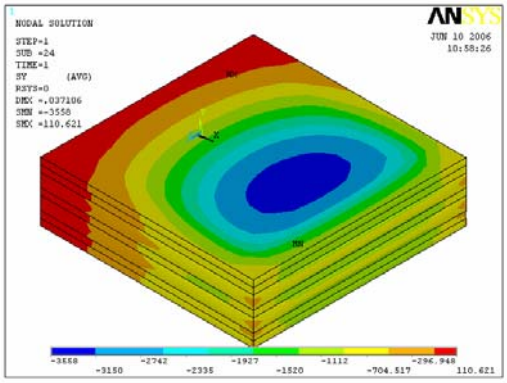

Project Manager:

Marcus Ansley, P.E.
Chief Structures Research Engineer
FDOT Structures Research Center

March 2007

DISCLAMER

The opinions, findings and conclusions expressed in this publication are those of the author and not necessarily those of the State of Florida Department of Transportation.

This material has not been edited by Florida Department of Transportation.

SI* (MODERN METRIC) CONVERSION FACTORS

APPROXIMATE CONVERSIONS TO SI UNITS

SYMBOL	WHEN YOU KNOW	MULTIPLY BY	TO FIND	SYMBOL
LENGTH				
in	inches	25.4	millimeters	mm
ft	feet	0.305	meters	m
yd	yards	0.914	meters	m
mi	miles	1.61	kilometers	km

SYMBOL	WHEN YOU KNOW	MULTIPLY BY	TO FIND	SYMBOL
AREA				
in^2	squareinches	645.2	square millimeters	mm^2
ft^2	squarefeet	0.093	square meters	m^2
yd^2	square yard	0.836	square meters	m^2
ac	acres	0.405	hectares	ha
mi^2	square miles	2.59	square kilometers	km^2

SYMBOL	WHEN YOU KNOW	MULTIPLY BY	TO FIND	SYMBOL
VOLUME				
fl oz	fluid ounces	29.57	milliliters	mL
gal	gallons	3.785	liters	L
ft^3	cubic feet	0.028	cubic meters	m^3
yd^3	cubic yards	0.765	cubic meters	m^3
NOTE: volumes greater than 1000 L shall be shown in m^3				

SYMBOL	WHEN YOU KNOW	MULTIPLY BY	TO FIND	SYMBOL
MASS				
oz	ounces	28.35	grams	g
lb	pounds	0.454	kilograms	kg
T	short tons (2000 lb)	0.907	megagrams (or "metric ton")	Mg (or "t")

SYMBOL	WHEN YOU KNOW	MULTIPLY BY	TO FIND	SYMBOL
TEMPERATURE (exact degrees)				
^oF	Fahrenheit	5 (F-32)/9 or (F-32)/1.8	Celsius	^oC

SYMBOL	WHEN YOU KNOW	MULTIPLY BY	TO FIND	SYMBOL
ILLUMINATION				
fc	foot-candles	10.76	lux	lx
fl	foot-Lamberts	3.426	candela/m^2	cd/m^2

SYMBOL	WHEN YOU KNOW	MULTIPLY BY	TO FIND	SYMBOL
FORCE and PRESSURE or STRESS				
lbf	poundforce	4.45	newtons	N
lbf/in^2	poundforce per square inch	6.89	kilopascals	kPa

APPROXIMATE CONVERSIONS TO SI UNITS

SYMBOL	WHEN YOU KNOW	MULTIPLY BY	TO FIND	SYMBOL
LENGTH				
mm	millimeters	0.039	inches	in
m	meters	3.28	feet	ft
m	meters	1.09	yards	yd
km	kilometers	0.621	miles	mi

SYMBOL	WHEN YOU KNOW	MULTIPLY BY	TO FIND	SYMBOL
AREA				
mm^2	square millimeters	0.0016	square inches	in^2
m^2	square meters	10.764	square feet	ft^2
m^2	square meters	1.195	square yards	yd^2
ha	hectares	2.47	acres	ac
km^2	square kilometers	0.386	square miles	mi^2

SYMBOL	WHEN YOU KNOW	MULTIPLY BY	TO FIND	SYMBOL
VOLUME				
mL	milliliters	0.034	fluid ounces	fl oz
L	liters	0.264	gallons	gal
m^3	cubic meters	35.314	cubic feet	ft^3
m^3	cubic meters	1.307	cubic yards	yd^3

SYMBOL	WHEN YOU KNOW	MULTIPLY BY	TO FIND	SYMBOL
MASS				
g	grams	0.035	ounces	oz
kg	kilograms	2.202	pounds	lb
Mg (or "t")	megagrams (or "metric ton")	1.103	short tons (2000 lb)	T

SYMBOL	WHEN YOU KNOW	MULTIPLY BY	TO FIND	SYMBOL
TEMPERATURE (exact degrees)				
^{o}C	Celsius	1.8C+32	Fahrenheit	^{o}F

SYMBOL	WHEN YOU KNOW	MULTIPLY BY	TO FIND	SYMBOL
ILLUMINATION				
lx	lux	0.0929	foot-candles	fc
cd/m^2	candela/m^2	0.2919	foot-Lamberts	fl

SYMBOL	WHEN YOU KNOW	MULTIPLY BY	TO FIND	SYMBOL
FORCE and PRESSURE or STRESS				
N	newtons	0.225	poundforce	lbf
kPa	kilopascals	0.145	poundforce per square inch	lbf/in^2

*SI is the symbol for the International System of Units. Appropriate rounding should be made to comply with Section 4 of ASTM E380

1. Report No. **BC352-16**	2. Government Accession No.	3. Recipient's Catalog No.
4. Title and Subtitle **Elastomeric Bearing Pads Under Combined Loading**		5. Report Date **August 2006** 6. Performing Organization Code **FSU PRJ. No. 00944**
7. Author(s) **Primus V. Mtenga, PhD, P.E.**		8. Performing Organization Report No. **FSU PRJ. No. 00944**
9. Performing Organization Name and Address **FAMU - FSU College of Engineering 2525 Pottsdamer St. , Tallahassee, FL 32310**		10. Work Unit No. (TRAIS) 11. Contract or Grant No. **BC352-16**
12. Sponsoring Agency Name and Address **Florida Department of Transportation**		13. Type of Report and Period Covered **Sep. 30, 2003 - Sep 30, 2005** 14. Sponsoring Agency Code
15. Supplementary Notes		

16. Abstract

According to current AASHTO specification the bearing capacity of a pad subjected to rotation drops very rapidly as the bearing dimension B increases and as the angle of rotation increases. The capacity obtained by the AASHTO equation was found to be much less than what was observed to be working in the field. The objective of this project is to formulate a new design criteria for steel reinforced elastomeric bridge bearing pads subjected to axial loading and rotation.. In this study a number of bearing pads were subjected to a combination of axial loading followed by cyclic rotational loading up to million cycles. The shear modulus, G, of the material plays an important role in determining the bearing capacity. In order to determine the G value for the pads used in the tests, a nondestructive technique was developed for that purpose. In addition, analytical modeling of the pads was conducted using finite element techniques. ANSYS, a commercially available finite element analysis software package, was used to conduct the analytical study.

From the analytical studies and pressure sensor reading in the testing it was evident that there is a core at the middle where the stresses are the highest. Moreover, the elastomer layers reveals bulging in the lower end of the rotation just as was evidenced in the test samples. From these results one can observe the fact that the high compressive stress core moves toward the end subjected to the most compression. This behavior is in agreement with the experimental results, i.e., failure that was limited to the lower end of the rotation.

Based on these experimental and analytical studies a new design equation for cases involving rotation was developed. The new equation or design procedure was formulated under the assumption that the lower side of the rotation, the end subjected to the most compression, will fail and can be eliminated. The resulting capacity of the pad will be that of a reduced pad.

17. Key Word	18. Distribution Statement		
19. Security Classif. (of this report)	20. Security Classif. (of this page)	21. No. of Pages	22. Price

TABLE OF CONTENTS

LIST OF FIGURES

EXECUTIVE SUMMARY

ELASTOMERIC BRIDGE BEARING PADS UNDER COMBINED LOADING

PROBLEM STATEMENT

Elastomeric bearing pads have been in use for many years. This type of bearing pad has proven to be economical and requires minimum maintenance. Recent changes in the AASHTO specification have led to an increase in required calculations with rather restrictive rotational requirements. Rotations in the bearing pad may be significant in the following cases: a) during the construction phase as any existing camber is recovered upon the introduction of the dead loads, b) at simply supported beam-ends where rotation must be allowed to mirror the zero moment assumption and c) when there is skew or in curved girders the bearing pads may be subjected to bi-axial rotation in addition to the vertical compression.

According to current AASHTO specification the bearing capacity of a pad subjected to rotation is given as

$$P = A\cdot\left[1.875\cdot G\cdot S\cdot\left[1 - 0.200\cdot\left(\frac{\theta_{max}}{n}\right)\cdot\left(\frac{B}{h_{ri}}\right)^2\right]\right]$$

where A is the bearing area, B is the bearing dimension perpendicular to the axis of rotation , G is elastomer shear modulus, h_{ri} is the thickness of a single layer of the bearing, n is the number of elastomer layers and P is the bearing capacity.

As can be seen from the above equation, the capacity drops very rapidly as the dimension B increases and as the angle of rotation increases. The capacity obtained by this equation was found to be much less than what was observed to be working in the field.

OBJECTIVES

The primary objectives of this study were:

1. To investigate the behavior of steel reinforced elastomeric bridge bearings under the combination of axial and rotational loading.
2. To examine the validity of limitations of the AASHTO specifications (Eq. 14.7.5.3.5-2) especially under large rotations.
3. To make modifications as necessary and develop design criteria for steel reinforced elastomeric bridge bearing pads.
4. To determine and propose design procedures to be used to update or modify FDOT elastomeric bearing pad design standards.

FINDINGS AND CONCLUSIONS

The evaluation of the current AASHTO specification on elastomeric bearing pads subjected to rotation showed that there was a significant discrepancy between the computed bearing capacity and what was observed to work in the field. In this study a number of bearing pads were subjected to a combination of axial loading and cyclic rotational loading up to a million cycles. The shear modulus, G, of the material plays an important role in determining the bearing capacity. In order to determine the G value for the pads used in the tests, a nondestructive technique was developed for that purpose. In addition, analytical modeling of the pads was conducted using finite element techniques. ANSYS, a commercially available finite element analysis software package, was used to conduct the analytical study.

From the testing bulging and elastomer separation at the end, where compression strain was a maximum, was found to be the dominant failure as shown below.

Failed 8x8 Bearing Pad Samples

From the analytical studies and experimental pressure sensor reading in the testing it was evident that there is a core at the middle where the stresses are the highest. Moreover, the elastomer layers reveal bulging in the end with the maximum compression strain just as evidenced in the test samples. From these results one can observe the fact that the high compressive stress core moves towards the end of with the maximum compression strain. This behavior is in agreement with the experimental results, i.e., failure was limited to the end with the maximum compression strain.

Based on these experimental and analytical studies a new design equation for cases involving rotation was developed. The new equation or design procedure was formulated under the assumption that pad damage will be limited to the high compression end which can be neglected in the capacity computations. Thus the capacity of the pad will be that of a reduced pad.

Therefore the new formulation will be as follows:

$$P_\theta := 1.66 \cdot G \cdot S_{nw} \cdot A_{nw}$$

where

A_{nw} the area of the reduced pad area equal to $B_{nw} \cdot W$

S_{nw} the shape factor of the reduced pad size.

$$S_{nw} := \frac{B_{nw} \cdot W}{2 \cdot h_{ri} \cdot \left(B_{nw} + W\right)}$$

$$B_{nw} := \begin{cases} B & \text{if } \theta = 0 \\ \dfrac{B \cdot E_c \cdot \theta + 1.66 \cdot G \cdot S \cdot h_{ri}}{2 \cdot E_c \cdot \theta} & \text{otherwise} \end{cases}$$

$$B_{nw} := \text{if}\left(B_{nw} > B, B, B_{nw}\right)$$

$E_c := E_0 \cdot \left(1 + 2 \cdot \phi \cdot S^2\right)$ the effective compression modulus

$E_0 = 4.515 \cdot G - 0.488 \cdot MPa$ where G is in MPa (for SI units)

$E_0 = 4.515 \cdot G - 0.071 \cdot ksi$ where G is in ksi (for US customary units)

S the shape factor of the pad.

$$S := \frac{B \cdot W}{2 \cdot h_{ri} \cdot (B + W)}$$

$\phi = 0.445 + \dfrac{0.16 \cdot MPa}{G}$ where G is in MPa (for SI units)

$\phi = 0.445 + \dfrac{0.023 \cdot ksi}{G}$ where G is in ksi (for US customary units)

CHAPTER 1: INTRODUCTION

Elastomeric bearing pads have been in use for many years. This type of bearing pad has proven to be economical and requires minimum maintenance. Recent changes in the AASHTO specification have lead to an increase in required calculations with rather restrictive rotational requirements. Rotations in the bearing pad may be significant in the following cases:

a) During the construction phase as any existing camber (in both pre-stressed concrete girders and in steel girders) is recovered upon the introduction of the dead loads. This type of rotation occurs only once and at a time when the compressive load on the pad is at its minimum.

b) At the simply supported beam-ends where rotation must be allowed to mirror the zero moment assumption. By considering the elastic condition (Slope Deflection Method) the expected rotation in this case can be approximated as:

$$\theta_L = \frac{M_F L}{2EI} \qquad \text{……..…… (1.1)}$$

where θ_L = girder end rotation, thus the rotation in the elastomeric bearing pad

L = span of the girder

M_F = Moment that will prevent rotation at the end (fixed end moment).

EI = Flexural rigidity of the girder (modulus of elasticity x moment of inertia).

From the above expression (Eq. 1), it can be seen that the rotation at the bearing pad will increase as a function of the span. Since the fixed end moment M_F will increase with span then the rotation will be proportional to the square of the span length. Pad rotation will therefore be critical to large spans which will also have higher beam end reactions. Recent girder failures that may be attributed to insufficient rotational capacity of elastomeric bearing pads at the simply supported end (expansion point end) have been observed during the investigation of Jacksonville Skyway girder cracking (Mtenga 2001).

This type of rotation will be cyclic in nature since it is partly caused by traffic loading. In cases for which the girder may be placed at grade the resulting total rotation may be several times the rotation of Equation. 1.

c) When there is skew or curved girders the bearing pads may be subjected to bi-axial rotation in addition to the vertical compression.

These rotations have some influence on the performance of the bearing pads. As shown in the sketches presented in Figure 1.1, the rotation will cause some additional compression and increases the tendency of pad “walk-out” when acting in combination with axial compression and shear loading. The limited understanding of the combined loading behavior is one of the reasons why the recently modified specifications have a rather restrictive rotational requirement. In this proposed study the combined rotation, shear and compressive axial loading will be investigated.

From the results of this study we expect to ascertain the design criterion of reinforced elastomeric pads when we have the combination of shear loading, direct bearing and rotation in the bearing pad.

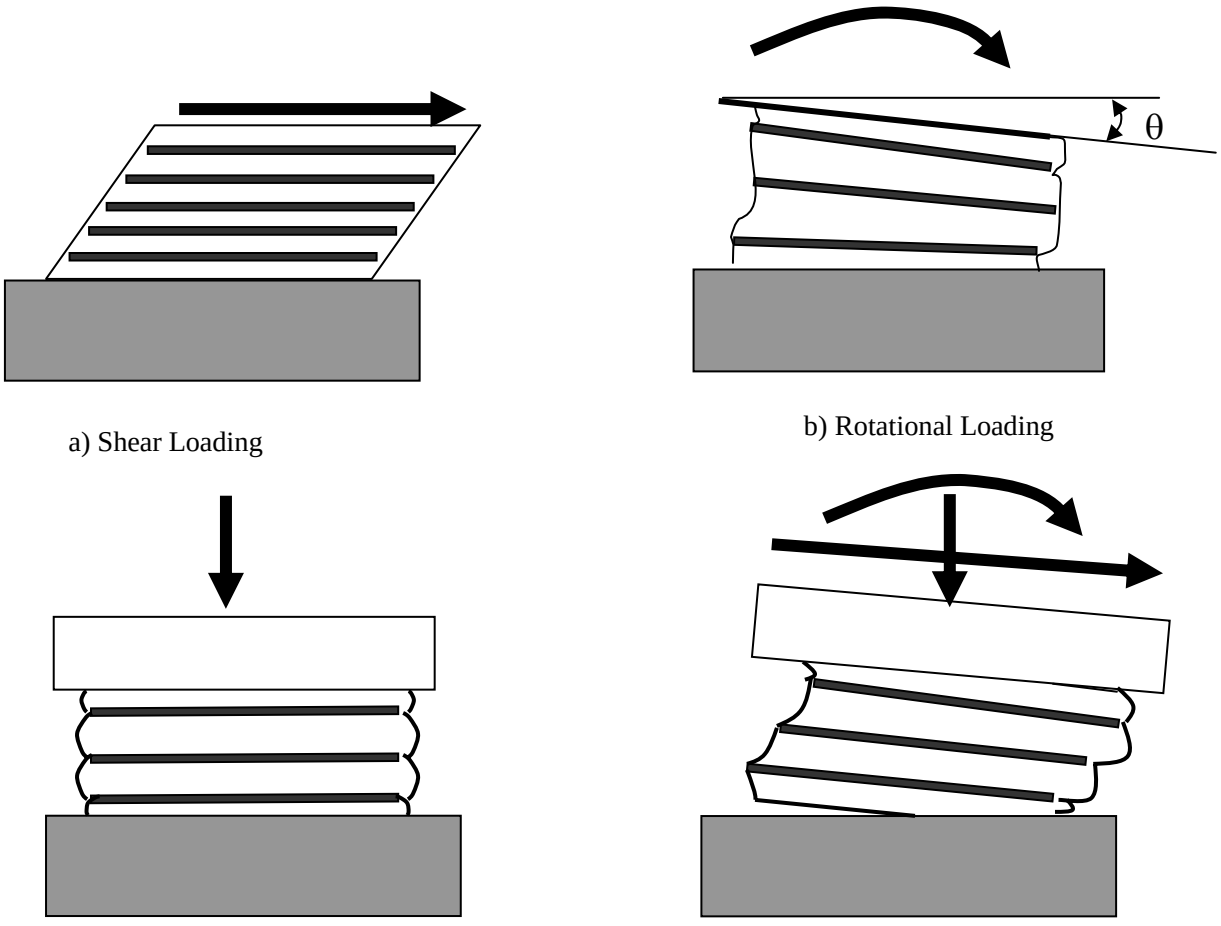

a) Shear Loading

b) Rotational Loading

c) Compressive Loading

d) Combined Loading

Figure 1.1 Sketches of Steel Reinforced Elastomeric Pads Possible Loading Cases

Shown in Figure 1.2 is the capacity of a steel reinforced elastomeric bearing pads computed in accordance to AASHTO specification, i.e.

With rotation the capacity given by AASHTO Eq. 14.7.5.3.5-2 as:

$$P = A_{db,dw}\cdot\left[1.875\cdot G\cdot S_{db,dw}\cdot\left[1-0.200\cdot\left(\frac{\theta_{max}}{n}\right)\cdot\left(\frac{B_{db}}{h_{ri}}\right)^2\right]\right] \quad \text{..... (1.2)}$$

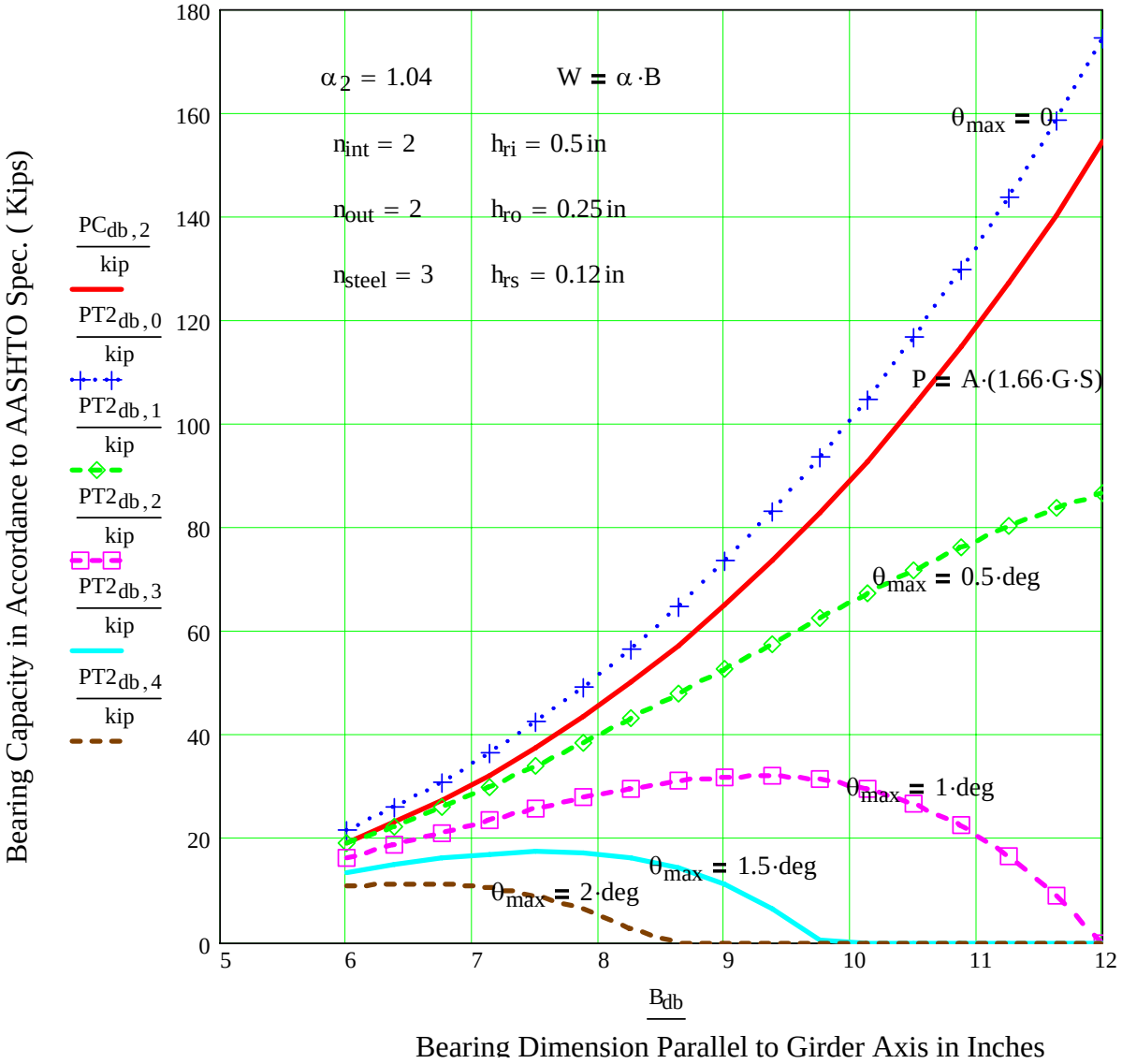

Figure 1.2 Capacity of a Square Steel Reinforced Elastomeric Pads for With Respect to Maximum Rotation as Computed Using AASHTO Formulae

From Figure 1.2, parameters can be defined as follows:

$\alpha_2 = \dfrac{W}{B}$ Ratio, $\quad n_{int} =$ number of internal elastomer layers

n_{out} = number of outside elastomer layers, h_{ri} = thickness of internal elastomer layers

h_{ro} = thickness of outside elastomer layer, h_{rs} = thickness of steel reinforcement plate

Without rotation (pure compression) the capacity is given by AASHTO Eq. 14.7.5.3.2-1 as

$$P = A\cdot(1.66\cdot G\cdot S) \quad \text{.....(1.3)}$$

where A = the bearing area

B = bearing dimension

G = elastomer shear modulus

h_{ri} = thickness of a single layer of the bearing

n = number of elastomer layers

P = bearing capacity

θ_{max} = maximum rotation at an axis perpendicular to dimension B (Fig 2.3)

S is known as shape factor, which is a measure of the area free to bulge, given by the expression by Eq. 1.4.

$$S = \frac{B\cdot W}{2\cdot(B + W)\cdot h_{ri}} \quad \text{.....(1.4)}$$

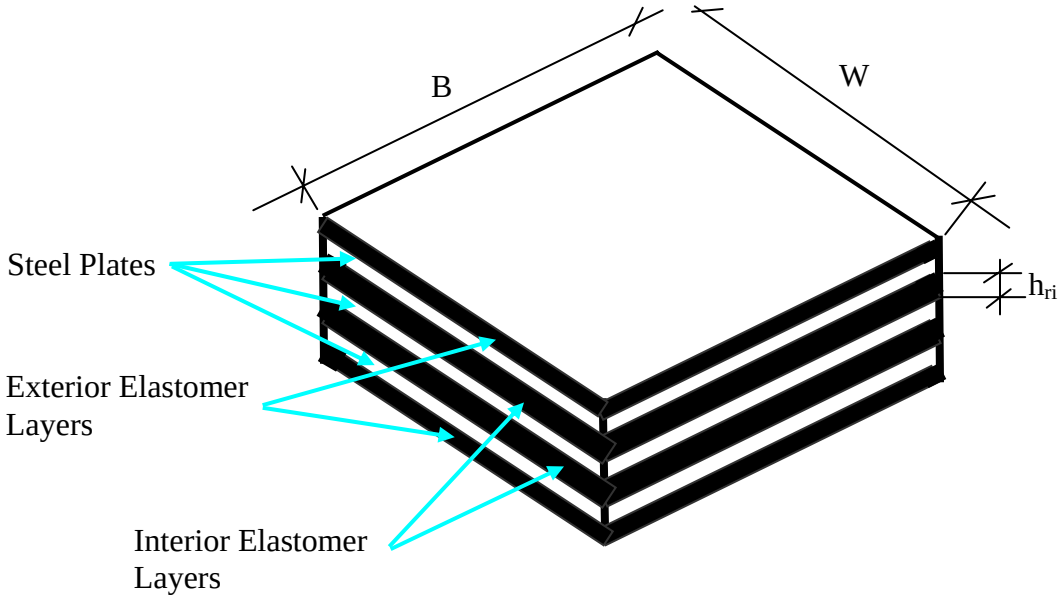

Figure 1.3 A Typical Construction of Steel Reinforced Elastomeric Bearing Pad

Based on what is presented in Figure 1.2, one can observe the following:

a) There is discrepancy between the case of pure compression and the rotation per the AASHTO formulae as the angle of rotation approaches zero, i.e. equivalent to pure compression.
b) At small bearing sizes the angle of rotation appears to have little sensitivity as far as its impact on the bearing capacity is concerned.
c) For moderate to large size bearings, large values of rotation have a huge impact on the capacity of the bearing.

Research Objectives

Given what is discussed above, the following are the primary objectives of this study:

1. To investigate the behavior of steel reinforced elastomeric bridge bearings under the combination of axial and rotational loading.
2. To examine the validity of limitations of AASHTO specifications (Eq. 14.7.5.3.5-2 as demonstrated in Figure 1.2) especially under large rotations.
3. To make modification as necessary and develop design criteria for steel reinforced elastomeric bridge bearing pads.
4. To determine and propose design procedures to be used to update or modify FDOT elastomeric bearing pad design standards.

CHAPTER 2: BACKGROUND

Elastomeric bridge bearings are placed between bridge superstructure and bridge sub-structure to accommodate possible movements between these two main parts of the bridge. Therefore, as placed, the elastomeric bearing pads will be subjected to gravity loads (live loads and dead load) causing vertical deformations, horizontal deformations due to seasonal thermal-elongation of the bridge superstructure and rotations due to flexural loads on the superstructure. The pads must be able to accommodate these deformations ensuring a safe transfer of the forces from the superstructure to the substructure while maintaining the bridge functionality and stability both in the short-term and the long-term.

According the National Cooperative Highway Research Program (NCHRP-449) report, elastomeric bearing bridge which have been used since 1950, have demonstrated remarkably good performance. A recent survey (Chen and Yura 1995) found only a few cases of poor bearing performance. Some of these cases of poor performance have been, deterioration resulting from large shear strains of plain pads (unreinforced pads) and pad walk-out. These walk-out problems were traced to excessive paraffin wax in the rubber (Muscarella and Yura 1995, McDonald 1999).

Steel-reinforced elastomeric bearings are one of the most widely used bridge-support systems because they are effective. While having high compressive stiffness, they are flexible enough in shear to prevent the transfer of harmful shear forces to the sub-structure. Moreover, they do not have any moving parts which may freeze, thus causing uneven distribution of applied loads or impairment in the absorption of vibrations. They are simple to install, weather-resistant, have low initial installation costs, and require little or no

associated maintenance. The elastomer in elastomeric bearings is flexible under shear stress, but comparatively stiff against compressive and volumetric change. Steel plates, installed as shown in Figure 2.1(b) below, restrain the bulging of elastomer and provides a large increase in stiffness under compressive load. This permits steel reinforced elastomeric bearing pads to support relatively large compressive loads while accommodating large translations and rotations. (Roeder and Stanton 1997)

Currently the most commonly used rubber bearing pads are the steel reinforced elastomeric bearing pads (Figure 2.1). Shown in Fig. 2.1.is a schematic of reinforced elastomeric bearing pads. The construction of these pads is done by vulcanizing the elastomer on to layers of equally spaced steel plates as shown in Figure 2.1 (b).

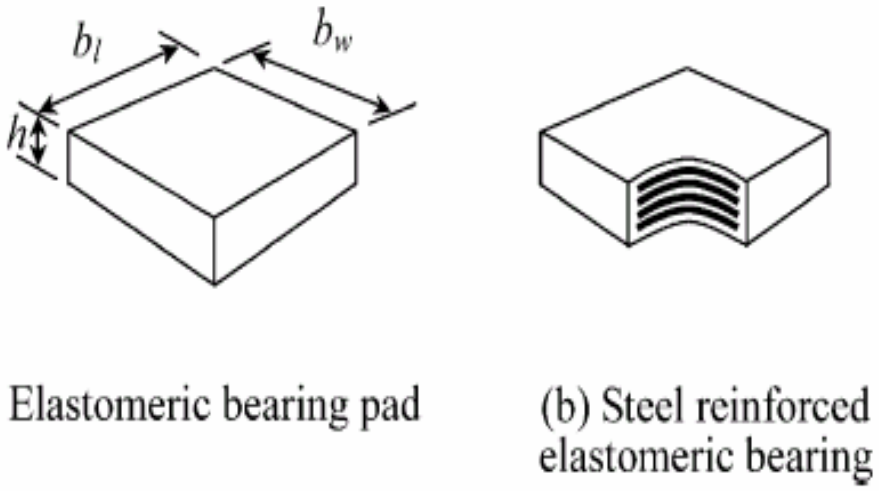

Figure 2.1 Schematic of Steel Reinforced Elatomeric Bearing Pad

When loads are applied to the bearing pad the elastomer material undergoes both axial and lateral deformation which leads to some bulging. Figure 2.2 shows the effect of

compression on elastomeric bearings. As the un-deformed pad (Fig 2.2(a)) is placed between rigid surfaces (Figure 2.2(b), compression bulging will occur as shown in Fig 2.2(c). However, when the pad is reinforced with steel plates, the steel plates act as rigid surfaces, thus limiting the bulging to the material between the plates as shown in Figure 2.2(d).

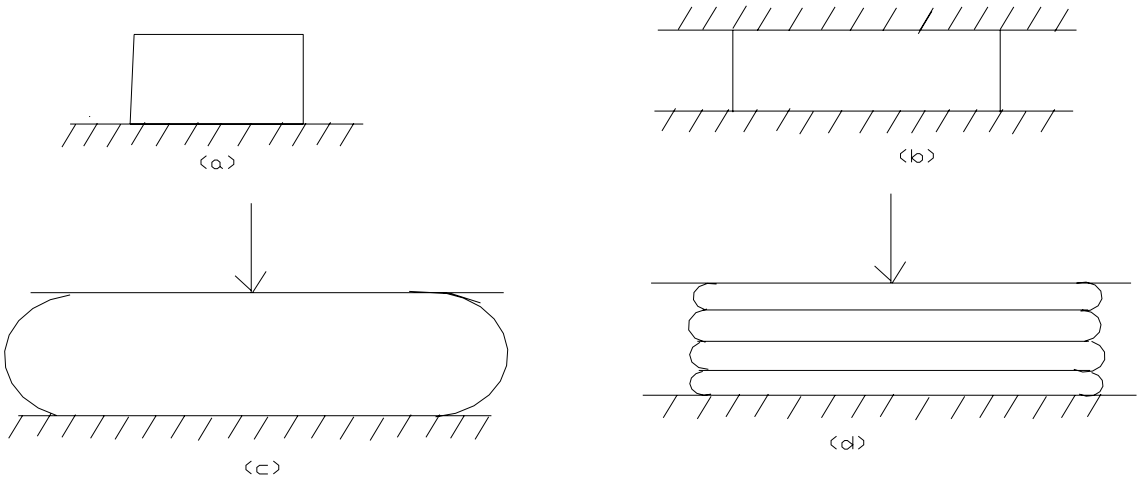

Figure 2.2. Compressive behavior of Elastomeric bearing Pad.

Muscarella and Yura (1995) conducted test on elastomeric bearing pads to determine the physical properties at low temperature, by using AASHTO 251-97, the specimens of different grades were tested from the temperatures of $-40^{o}F$ to $-71^{o}F$, the samples were immersed in cooled dry ice and liquid hydrogen, then the specimens were held as cantilever beams and removed and examined. The results from the tests satisfied AASHTO 251-97.

Clark and Moultrap (1966) performed tests on plain neoprene, butyl rubber and chlorinated butyl rubber pads, the objective of the tests was to evaluate elastomeric bearing

pads under low temperature, the test indicated that neoprene stiffens under low temperature to a greater extent than the other two materials and also becomes more brittle under accelerated aging.

Kurt Miller from Axel Product Inc (Experimental Loading Conditions Used to Implement Hyper elastic and Plastic Material Models) conducted experiments on plastics and elastomers. For elastomeric materials, experiments in multiple strain states such as simple tension, planar tension and biaxial extension, provided stress-strain data that allowed the variables in the material model to be fitted. For plastics and elastomers, tests were performed using a single pull-to-failure mode of up to 400% strain. The elastomer materials were tested in accordance with ASTM D412 and the plastics with ASTM D638 specifications. The elastomer test results are presented (Fig 2.3)

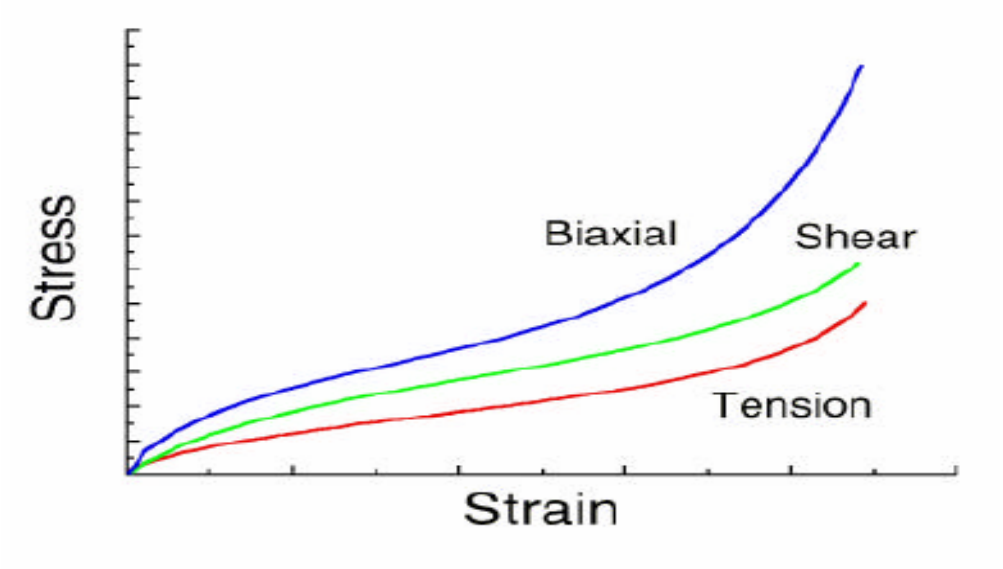

Fig 2.3. Typical Stress-Strain Curve of Elastomers

In these tests the elastomer was loaded and unloaded in a stepping manner first step was three cycles with strains ranging from +10% to -10% In the next step the strain was increased by 10% both ways, that is, three cycles with strain range of +20% to -20% . The 10% strain increments were repeated up to a strain range of +100% to -100%. Presented in Figure 2.4 below are the results of such cyclic loading.

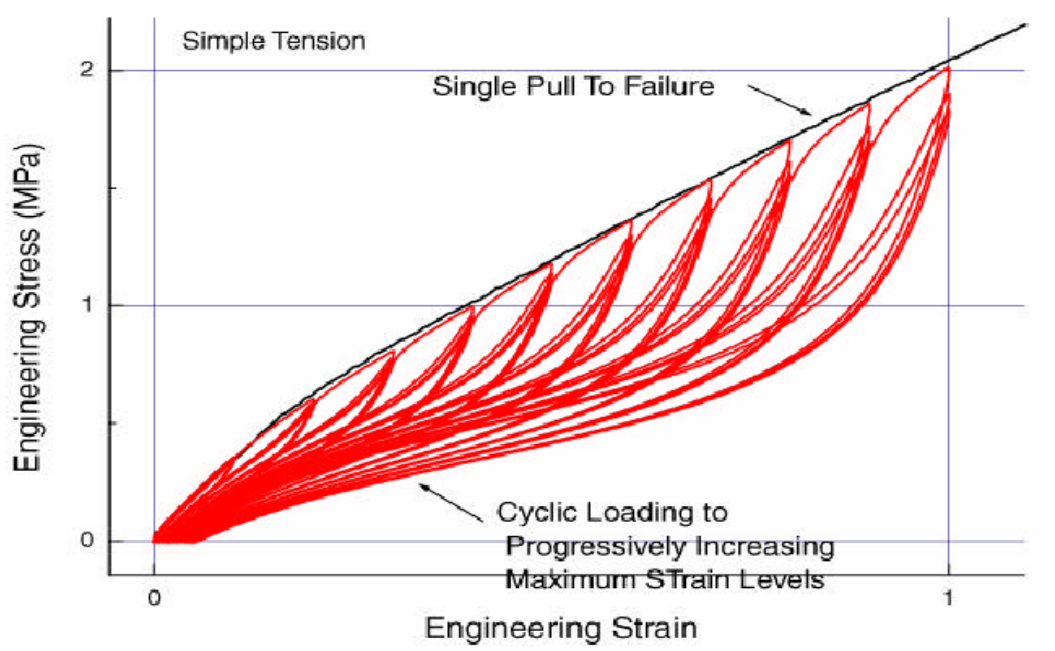

Fig 2.4. Stress-Stain Plot for Elastomer Cyclic Loading

From the test, researcher, observed two effects. The first effect is that, repeated stretching to a particular strain level causes the stress strain curve to soften significantly and change its original shape. The second effect is that each time the elastomer is stretched to a new larger maximum strain, additional softening and additional shape changes occur.

Elastomer hardness:

Hardness is defined as ‘’reversible, elastic deformation produced by the specially shape indentor under specified loads’’ Hardness is the commonly measured in International Rubber Hardness Degree (IRHD) or shore “A” Durometer point. For commonly used elastomers , the hardness ranges from 45 to 65 Durometer points (*Muscarella and Yura 1995).*

The behavior of the bearing pad is highly dependent on the shear modulus of the elastomer material. According to Lindley (1992) the shear modulus is highly correlated to the hardness of the elastomer material. Given in Table 2.1 below are values of shear modulus at 50% strain for various elastomer hardness values.

Table 2.1 Elastomer Shear Modulus for Elastomer of Varying Hardness

HARDNESS	45-55	55-65	65-75
Shear modulus (Mpa)	0.53-0.75	0.75-1.05	1.05-1.40
Shear modulus (ksi)	77-110	110-150	150-200

Pad Reinforcement

Bearing pads are usually reinforced with steel shims sandwiched in between layers of the elastomer material. The primary purpose of the steel shims are to reduce high bulging of the elastomer. These steel shims experience bending stress as well as tensile stress. The most significant stress are the traverse tensile stress transferred to the shims as the elastomer experiences bulging

In recent years a number of studies have been conducted to investigate the performance of steel shim reinforced bearing pads. Muscarella and Yura (1995) conducted compressive tests on both unreinforced and reinforced bearing pads. From the results of these tests it was concluded that pads without reinforcement or slightly reinforced deformed excessively under compressive stresses. Furthermore it was concluded that the thickness of the elastomer material layer has influence on the performance of the pad.

Stanton and Roeder (1982) reported that steel reinforced pads behavior is quite different compared to plain bearing pads. Under uniaxial compression the flexible elastomer would shorten significantly and sustain large increases in its plan dimensions. But the steel layers restrain this lateral expansion which restrains the bulging pattern and increase the stiffness under compressive load. This permits a steel reinforced elastomeric bearing to support relatively large compressive loads while accommodating large translations and rotations.

Dawn et al (1990) studied the effect of the compression test on different bearing pads. The study involved cotton duck bearing pads, reinforced and plain elastomeric bearing pads. The results showed that the compressive capacities of cotton duck bearing pads are larger than other bearing pads. Also the ultimate compressive stress was influence by the shape factor. The shape factor influence is much less pronounced for Cotton duck bearing pads (CDP) as compared to steel-reinforced elastomeric bearings and plain elastomeric pads. Presented in Figure 2.5 are the results of this study by Dawn. From this study it was concluded that the shape factor has influence on the compressive and rotational stiffness, but little effect on the translational stiffness.

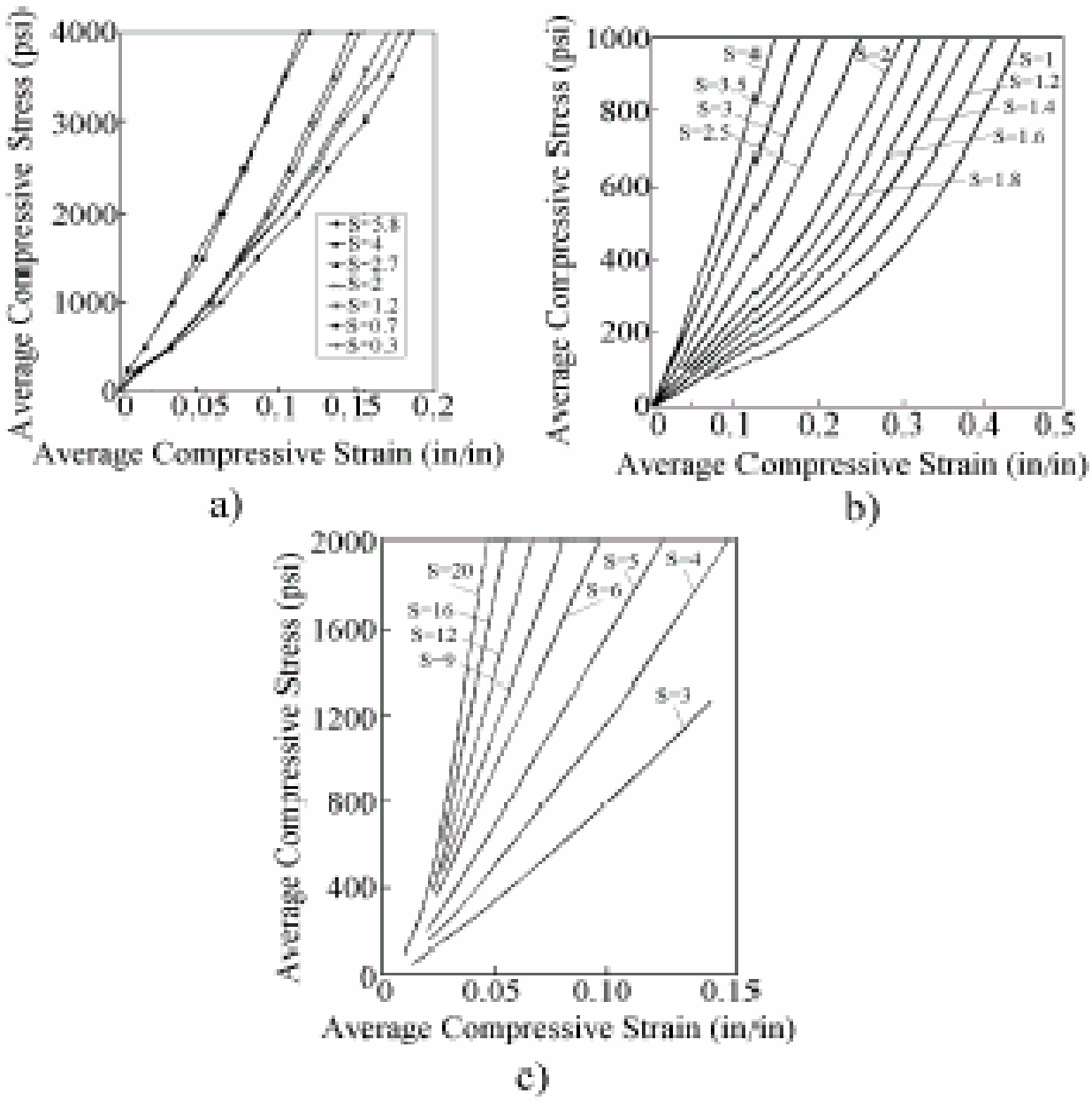

Fig 2.5. Average Compressive Stress and Strain as Function of Shape Factor; [a) CDP, [b) PEP, and [c] Steel Reinforced Elastomeric Bearings [*Extracted from Dawn (1990)]*

Reinforced Bearing Pads Subjected to Rotational Loading

Bridge bearings rotate because of deflections due to traffic loading, temperature gradient and construction tolerances. Rotations due to construction tolerances and camber may remain nearly constant for the life of the bridge. But rotations due to vehicle load are dynamic and occur many times in the life of the bridge. Rotations damage bridge bearings because of concentrated compressive strains which may develop on one edge of the bearing. Also rotation may cause uplift or local separation between the bearing and the bridge structure which may lead to some local distress. Uplift effects lead to local bearing strains and local damage on Polytetrafluoroethylene (PTFE) sliding surfaces. If the bridge has larger cyclic rotations pot bearings are often used, rotation in pot bearings may occur about any axis and are accommodated by deformation of the elastomeric pad. Pot bearings can sustain many rotation cycles with little or no damage. Several techniques have been used to reduce the abrasion and wear of the pot bearing. One is application of lubricants which have proven to be efficient and have been used regularly to minimize wear and abrasion, but with time some lubricants becomes less effective. Silicone grease, graphite powder and PTFE sheets have all been used as lubricants. Silicone grease has proven to be the most effective.

Cyclic rotation may also cause damage to the sealing rings of pot bearings. Flat brass rings types are more susceptible to ring fracture and elastomer leakage, while circular brass rings are susceptible to severe wear.

Behavior of steel reinforced elastomeric bearing pads under shear loading

Bridge bearings accommodate translation movement caused by thermal effects, creep, shrinkage of superstructure and dynamic loading caused by the traffic load. Elastomeric

bearings are normally designed to accommodate these translational movements through shearing deformation of the elastomer. Jain (1998) conducted horizontal shear tests to study the behavior of laminated bearings and the effect of the loading cycle. The effects of cyclic loading on the laminated rubber bearings were studied. The bearings were subjected to ten cycles of a sinusoidal waveform with a constant amplitude of ± 10KN and ± 15KN at a frequency of 0.5 Hz. In addition, the bearings were tested under a reversed cyclic horizontal load with the amplitude increasing from 2.5 KN to 15.0 KN at frequencies of 0.1 Hz and 1 Hz respectively. Two load cycles were applied at each amplitude level. The test results revealed a stable hysteretic behavior without any significant amount of stiffness degradation. Furthermore it was observed that the horizontal stiffness seems to be unaffected by the frequency of loading. However, the value of damping was reduced as the frequency of loading was increased. The load deflection behavior of bearings under vertical and horizontal loading was found to be non-linear. The vertical stiffness was found to increase with respect to strain increases, while horizontal stiffness was found to decreases with respect to strain increases.

Yura and Muscarella (1995) conducted an inclined compression-shear test for plain and laminated bearing pads. The test set up was designed to duplicate the dead load weight and the daily thermal deformation response of the bridge girder. The test specimens were sandwiched between sets of metal plates with slopes of 1:10 and 1:20. As a compressive force was applied, the inclined surfaces provided normal and shear forces to the bearing pads. According to the authors, the inclined compression setup was capable of estimating full-scale behavior of laminated bearing pads but didn’t give an accurate value of shear modulus for plain bearing pads. This test set up is reported as being used by Topkaya (2004). A further

discussion of this test method, including our proposed new method of determining shear modulus of the elastomer, is discussed in Chapter 3

Fatigue failure

Fatigue is caused by cyclic loading induced by traffic flow and daily temperature change. English et al (1994) reported that compressive load combined with cyclic shear deformations causes fatigue cracks that are visible in the interface of the elastomer and the reinforcement steel plates. It was further reported that the rate creaking and its magnitude depends on several factors. These factors include magnitudes of applied loads and properties of elastomer material. When fatique cracks are allowed to propagate a loss of axial or shear stiffness may occur. Ozell and Diniz (1960) conducted shear fatigue tests on plain neoprene bearing pads. The tests involved different bearing pads sizes, loaded to a compressive stress of 815 psi and then subjected to a cyclic shear up to 1 million cycles at a frequency of 2 Hz. The results showed extensive cracking at the interfaces of the steel plates and elastomer.

Stability

Buckling will occur if the height of the bearings is too high compared to the width. The shear deformation controls the buckling of bearing pads. The AASHTO specification provides criteria for design of bearing pads for buckling control. To control buckling the height is limited by the movement requirements, the length of elastomer, base dimensions and total thickness of bearing pads and also depends upon the shear modulus. If the elastomeric bearing pads buckle under the compression load, the bearing should be designed

to accommodate buckling effect. According to AASHTO specifications the following equations must be satisfied:

For pads susceptible to sideway

$$\sigma t \leq \left[\frac{G}{\left[\frac{3.84(hrt/L)}{S\sqrt{1+2.0L/W}} - \frac{2.67}{S(S+2.0)(1+L/4W)} \right]} \right] \quad \text{.................................... 2.1}$$

And for bearings that are restrained against sideways they must satisfy

$$\sigma t \leq \left[\frac{G}{\left[\frac{1.92(hrt/L)}{S\sqrt{1+2.0L/W}} - \frac{2.67}{S(S+2.0)(1+L/4W)} \right]} \right] \quad \text{.......................2.2}$$

The shape factor and flexural rigidity (EI) are the most important parameters in design elastomeric bearing pads. These parameters increase the bearing stability, reduce the deflection of the bearing pads and increase the compression load carried by bearing pads. The flexural response of the laminated system is different compared to un-reinforced bearings. For reinforced bearings, the bending stiffness is increased significantly due to the presence of the steel plates compared to the stiffness of plain bearing pads.

Delamination /separation of the elastomer from the reinforcements

Delamination of elastomer is not a critical failure mode in bearing pads. Delamination defects in layered composite materials may occur due to a various reasons. The major

reasons include low energy impact and manufacturing defects such as poor interfacial bonding between the elastomer and steel shims. The presence of delamination defects may influence post-buckling behavior of the whole bearing pad. Improvements in the quality control of the pad manufacturing helps in minimizing delamination failures. The reinforcing steel plates, which are meant to restrain the Poison effect, are subjected to in-plane tensile stresses. From this stress state there exist the potential of yield or rupture of the reinforcing steel plates. Unlike delamination, failure of the reinforcement will cause immediate and disastrous degradation of bearing performances.

Bearing slip:

In recent years bearing slip has become a significant serviceability issue for bridges. Bearings will slip if they are subjected to excessive horizontal force. Those forces may be caused by shrinkage and creep of prestressed concrete girders, girder placement at extreme temperatures and construction misalignment. Roeder and Stanton (1982) indicated that slip is more likely for plain bearings than a steel reinforced bearing. Bearing slip is attributed to a low coefficient of friction between the pad elastomer and the bridge superstructure. The researchers conclude that a plain bearing subjected to a compression load will not slip at its edges if the shape factor is less than or equal to half of the coefficient of friction between the bearing pad and the bridge superstructure.

Bridge movements

Bridge movement may be caused by factors such as bridge skew, curvature effects, initial camber, traffic loading, misalignment or construction tolerances, settlement of supports and thermal effects. Changes of the ambient temperatures and creep deformations of

the materials can cause longitudinal movement of a bridge deck. These factors increases both rotation and compression deformation, thus affecting the performance of the bearing pad both at the service level and at ultimate capacity.

Skewed bridges move both longitudinally and transversely, and curved bridges move both radially and tangentially. Yazdani (2000) conducted research on the interaction of the support boundary condition of bridge girders and different bridge parameters. The test results showed that the skew angle parameter has a significant effect on bridge performance. According to this study, it was concluded that bridges with higher skew angles require bearing pads with a higher shear modulus so as to reduce the midpoint deflection. Lower skew angles may experience an uplift effect at the end girder supports and may cause a loss of contact with the bearing pads.

Initial camber of bridge girders and out of level support surfaces induce bearing rotation. Initial camber may cause a large rotation on the bearing that can grow smaller as the construction of the bridge progresses. Rotation due to initial camber and construction are the largest components of bearing rotation. If the bearing is installed at an intermediate stage of construction, deflections and rotations due to the weight of the deck and construction equipment must be added to the effects of temperature and live load. The direction of loads, movements and rotations must also be considered, since it is inappropriate to simplify the absolute magnitudes of these design requirements. Rational design requires considering the worst possible combination of those conditions without designing for unrealistic or impossible combinations. In many cases it may be economical to install the bearing with an initial offset or to adjust the position of the bearing after construction has started. Those procedures can be used to minimize the adverse effect of these temporary initial conditions.

Ambient temperature may cause a thermal translation of the bearing pads. Changes in the temperature gradient induces bending and deflection which may reduce the bearing performance. Maximum and minimum bridge temperatures are defined depending upon whether the location is a cold or moderate climate. The change in average bridge temperature, between the installation temperature and the design extreme temperatures is used to compute the positive and negative movements. It should be further noted that a given temperature change can cause thermal movement in all directions. This means that a short, wide bridge may experience greater transverse movement than longitudinal movement.

CHAPTER 3: SHEAR MODULUS DETERMINATION

The shear modulus value, G, plays an important role in the determination of the bearing capacity of the elastomeric bridge bearing pads. This parameter governs the nature and magnitude of the force that is transferred to the bridge abutments. According to NCHRP Report 449 for satisfactory design the shear modulus of the bearing has to be determined reliably. This need led to efforts by Muscarella and Yura at the University of Texas at Austin to propose a "cost effective, easy test method" to determine the shear modulus for full-size elastomeric pads. They named their proposed method the Inclined Compression Test. The proposed inclined compression test Figure 3.2, has some draw backs. These include 1) simultaneous variation in both the shear force and the normal force in the bearing pad, 2) non-symmetrical bulging of the bearing pad due to the normal force component as the lateral movable middle wedge is allowed to move. This contributes to the measured lateral displacement that is assumed to have been caused by the lateral force component, and 3) in the inclined compression test setup two bearing pads are tested at the same time making it difficult to determine the independent properties.

In North America the design of Steel Reinforced Elatomeric Bearing Pads (SREBP) is governed by the *American Association of Highway and Transportation Officials (AASHTO) Standard Specifications for Highway Bridges*. Over the years the AASHTO design requirements have undergone significant changes. These changes have included the reduction of the design compressive stress. In the current AASHTO Specification edition the following design equations are applicable:

When the pad is subjected to compressive force only AASHTO limits the normal design compressive stress to:

$$\sigma = 1.66 \cdot G \cdot S \qquad \text{..... (1)}$$

When the bearing pad is subject to rotation, the maximum axial compressive stress is limited to

$$\sigma = 1.875 \cdot G \cdot S \cdot \left[1 - 0.200 \cdot \left(\frac{\theta_{max}}{n} \right) \cdot \left(\frac{B}{h_{ri}} \right)^2 \right] \qquad \text{..... (2)}$$

where ***S*** is the shape factor , which is the ratio of the bearing area to the surface area free to bulge, i.e.

$$S = \frac{BL}{2 (B + L) h_{ri}} \qquad \text{.....(3)}$$

B is the dimension of the bearing pad parallel to the length of the beam

L is the dimension of the bearing pad perpendicular to the length of the beam

h_{ri} is the depth of the thickest elastomer layer between the reinforcement steel plates

θ_{max} is maximum rotation of the beam at the bearing.

G is the shear modulus of the elastomer material.

As it can be observed in Equations 1 and 2 the shear modulus value, G, plays an important role in the determination of the bearing capacity of elastomeric pads. This parameter governs the nature and magnitude of the force that is transferred to the bridge abutments. According to NCHRP Report 449 (NCHRP 2001) for satisfactory design the shear modulus of the

bearing has to be determined reliably. This led to efforts by Muscarella and Yura at the University of Texas at Austin to propose a “cost effective, easy test method” to determine the shear modulus for full-size elastomeric pads. They named their proposed method the Inclined Compression Test.

THE INCLINED COMPRESSION TEST.

In the inclined compression test setup, developed at the University of Texas at Austin, two bearing pads are sandwiched between three inclined aluminum platens as shown in the sketch in Figure 3.1.

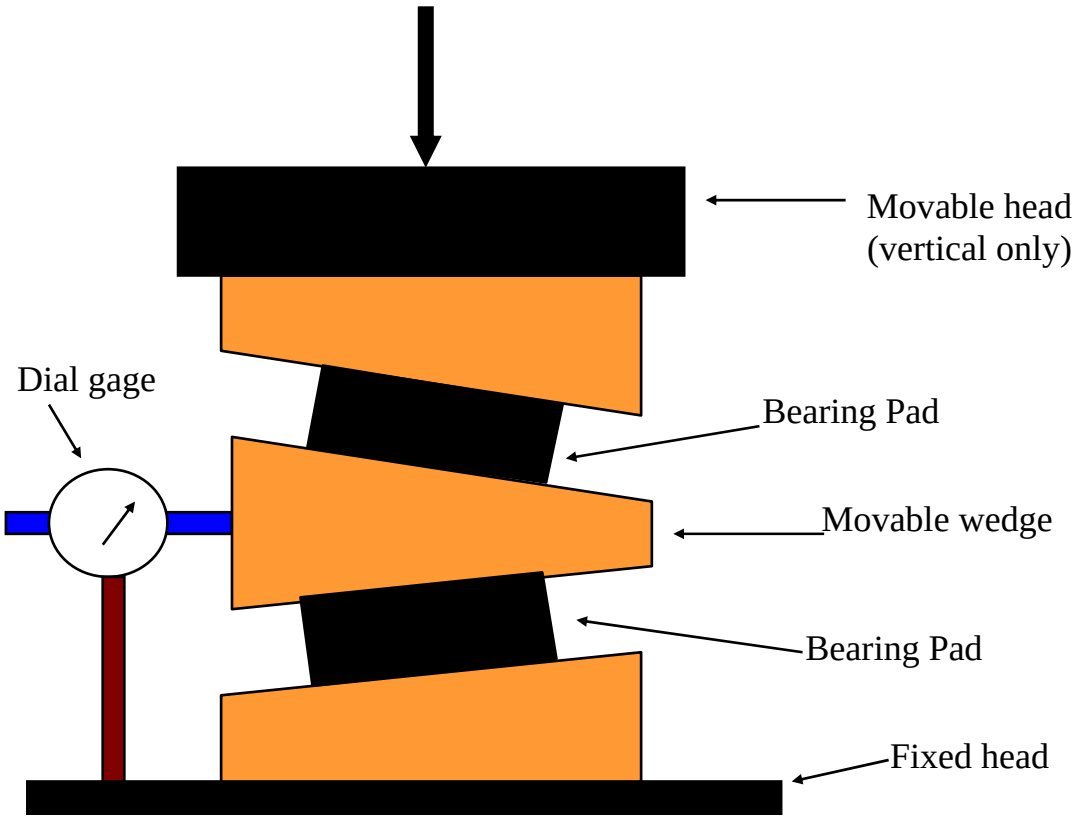

Figure 3.2 Sketch of Inclined Compression Test Proposed by Yura, et al.

The metal wedge between the two bearing pads is free to move both vertically and laterally as the system is loaded. The inclined surfaces can have slopes ranging from of 1:10 to 1:20. A displacement gage measures the lateral movement of the middle wedge. This lateral displacement is then used in the determination of the shear strain. The shear force is taken to be H = s x W, where s is the slope of the inclined surfaces and W is the total vertical compressive force. The shear stress, shear strain and shear modulus can then be computed as

Shear stress

$$\tau = \frac{s \cdot W}{A} \qquad \text{..... (4)}$$

Shear strain

$$\gamma = \frac{\Delta_s}{h_{rt}} \qquad \text{..... (5)}$$

Shear modulus

$$G = \frac{\tau}{\gamma} = \frac{s \cdot W \cdot h_{rt}}{A \cdot \Delta_s} \qquad \text{..... (6)}$$

In this test setup both the shearing force and the normal force will vary throughout the test period.

This proposed test has two major draw backs:

1. The normal stress has an influence on the magnitude of the determined shear modulus. Thus the situation in which the normal stress in the bearing pad is constantly varying has some influence on the results.

2. When the elastomer is compressed bulging takes place. In cases where the rubber material is between two surfaces which are restrained from moving laterally the bulging will be symmetrical. However, when the bulging takes place in a situation where lateral movements are allowed and enabled by the lateral component along the slope, the bulging will no longer be symmetrical. As shown in Figure 3.2, the non-symmetrical bulging will have the tendency of moving the middle wedge laterally, even without a lateral load. Thus the lateral displacement measured in the inclined compression test setup is not due to the lateral force component alone. This non-symmetrical bulging may have not been that detrimental in the University of Texas tests because of the existence of steel reinforcement, which limited the bulging in the layers .

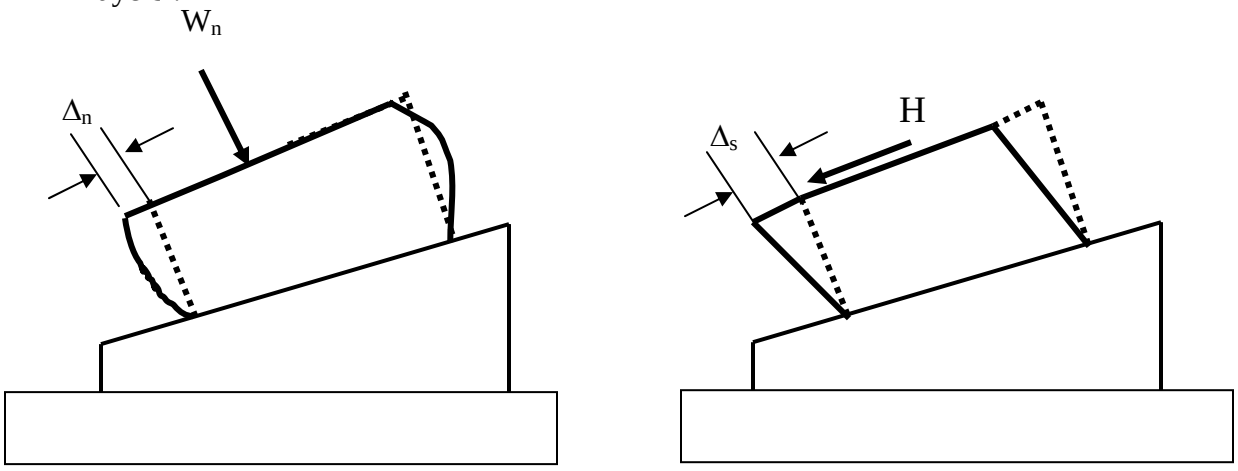

(a) Non-symmetrical Bulging Because of Movable Wedge

(b) Lateral Displacement Due to Shear Force Component

Figure 3.3 Schematics of the Inclined Compression Behavior

3. In the inclined compression test setup two bearing pads test specimens are used at the same time. This means that only the average modulus of the two pads is determined directly.

The above observations instigated a search for an alternative easy and economical method of determining the shear modulus of full size bearing pads.

Proposed Shear Modulus Test Setup

The proposed shear modulus test setup consists of two systems of applying loads that can be controlled separately. This provides the ability to apply the compressive load in the "symmetrical" state thus avoiding non-symmetrical bulging. In addition the two independent loading systems allows the determination of the shear modulus at a constant normal force.

Shown in Figure 3.3 is a schematic of the proposed testing setup. This consists of a vertically movable top plate that is free to slide against a vertical steel channel. A bottom plate that is free to move horizontally on a set of well lubricated ball bearings is provided. At opposite ends of the top and bottom plates, stoppers were provided. Steel shims were used against the stoppers to account for the variable depth of the bearing reinforcement. In this proposed shear test the shear force is introduced to the bearing pad by pulling the horizontally movable bottom plate, which in turn transfers the pull to one edge of the bottom bearing pad reinforcement plate. The top horizontally fixed plate resists the introduced force at the other end by bearing on the top reinforcement. This arrangement allows the introduction of shear force in the bearing pad independent of the vertical load. Presented in Figure 3.4 is a picture

of the assembled test unit. The shown test unit is equipped with two ENERPAC actuators each capable of applying a force up to 50-kips.

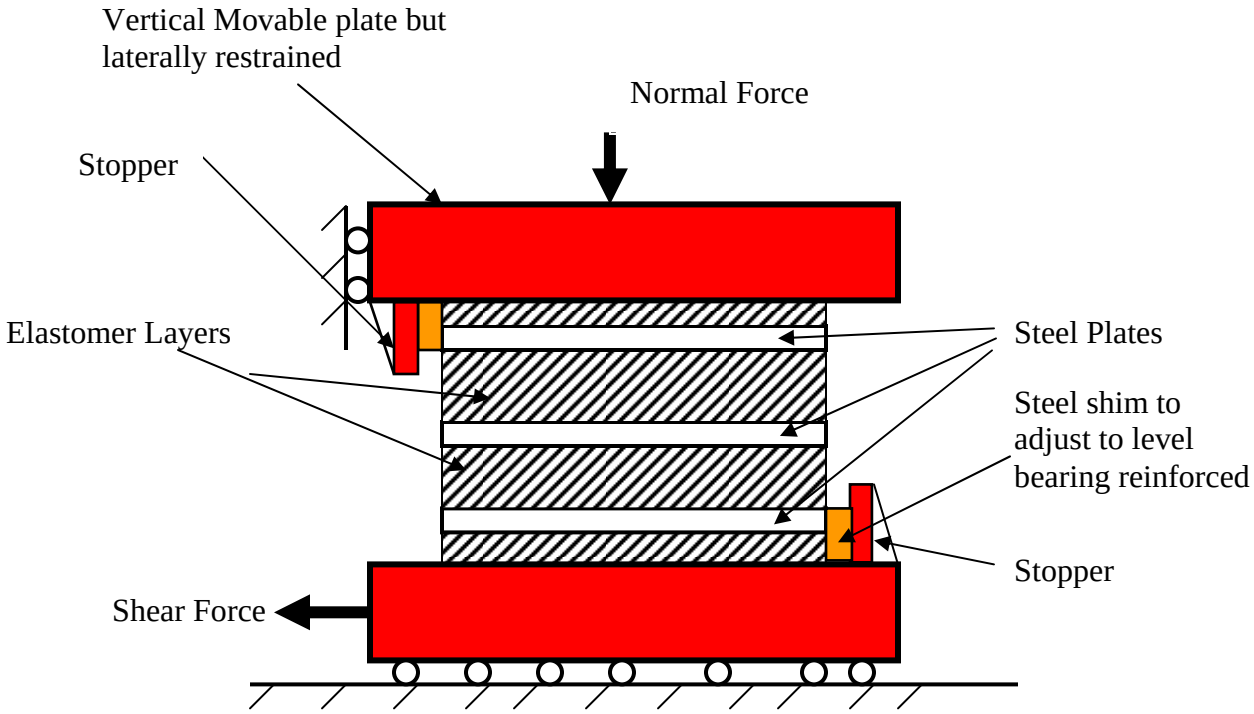

Figure 4.3 Schematics of Proposed Shear Testing Set-up

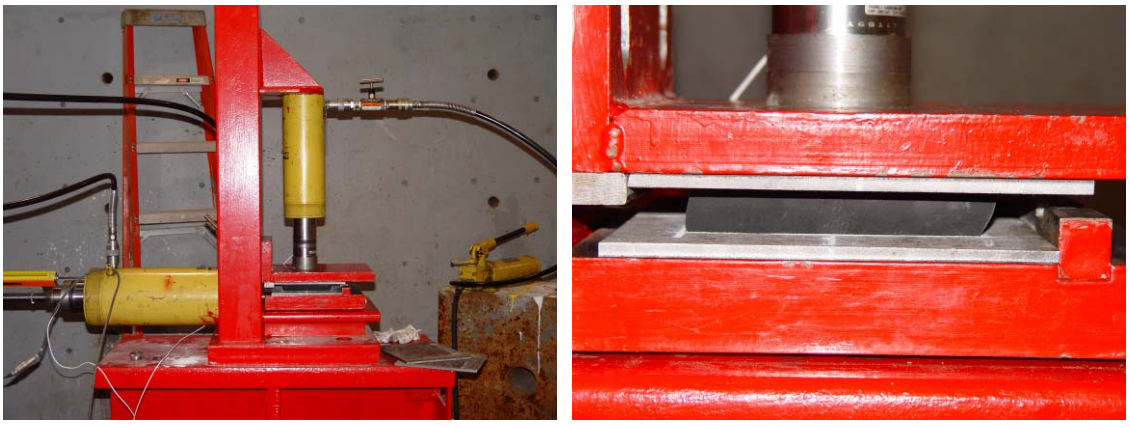

Figure 3.4: In-lab Testing Equipment

Test Procedures

After the fabrication of the aforementioned shear modulus test, a number of tests were conducted using the device.

Test Specimen

Bearing pads specified to have rubber material of 50 durometer hardness were ordered from a manufacturer. The sizes ordered were as presented in Table 1. The supplied bearing pads were prepared for testing by trimming off the side rubber material to expose the steel reinforcement edges. This was done to allow the appropriate adjustment of the stopper steel shims to match the steel edges. This was necessary to make sure that the shear force is transferred to the outer steel reinforcement plates. For the rectangular pads the shear was introduced along the shorter length.

Table 3.1 Test Sample

ALL PADS: 2-1/16 THICK & 50 DUROMETER NEOPREME

Qnty	B (in)	L (in)
10	3	6
10	6	6
10	4	8
10	6	8
10	8	8
10	5	10

Instrumentation and Testing

Load cells were mounted to monitor both the vertical load and the horizontal load. An LVDT was installed to monitor the horizontal displacement of the horizontally movable plate. All sensors were connected to a data logger that was set to sample the data every 0.5 seconds. The data was collected continuously until all of the loading cycles were completed.

For each tested pad the testing started by first applying a compressive force to the pad at a rate such that the desired load was reached in 3-minutes. While the compression was being applied the horizontal displacement was monitored for lateral movement. After attaining the desired normal load the horizontal shear load was applied. The rate of loading was adjusted such that the complete cycle of loading and unloading was attained in 5 to 6-minutes for all the bearing pads tested.

Each test pad was subjected to a total of four (4) loading cycles at the same compressive load. This shear modulus was computed using the slope of the line between two points as shown in Figure 3.5

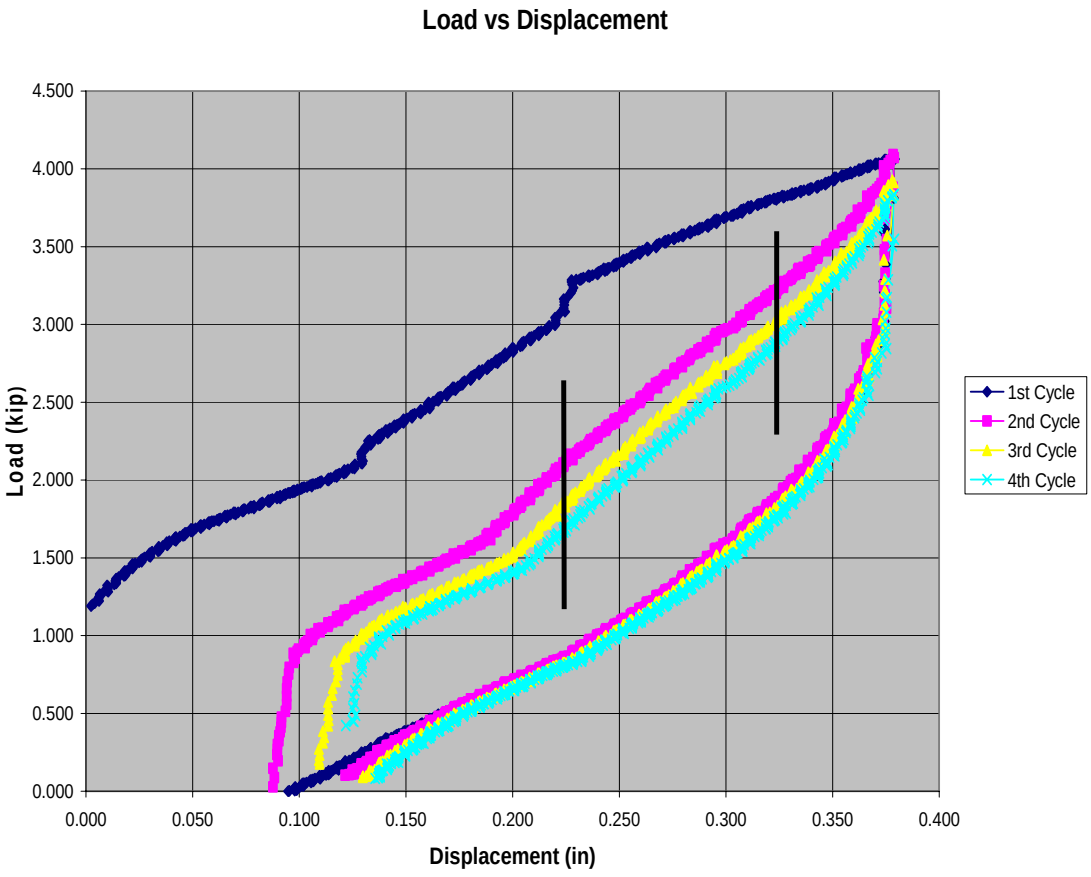

Figure 3.5: Load vs. Displacement

Test Results

The results of the testing conducted are presented in Figure 3.6 to Figure 3.9. Each data point is an average of three tests on similar pads. Presented in Figure 3.6 is the variation of shear modulus as a function normal stress. The variation of the shear modulus with respect to the area subjected to shear is presented in Figure 3.7. The variation of the shear modulus with respect to the shape factor is presented in Figure 3.8. The variation of the shear modulus with respect to the pad length subjected to shear is presented in Figure 3.9**.** In each of these the best trend line is plotted. The test data is presented in Table 3.1.

Table 3.1: Results of NDE Shear Test on Bearing Pads

SHEAR MODULUS SUMMARY

S/N	ID	Shear Modulus G (MPa) 1^{st} LC	Shear Modulus G (MPa) 4^{th} LC	Shear Modulus G (MPa) 1^{st} UL	Shear Modulus G (MPa) 4^{th} UL	shape Factor
1	8"x8"	1.0062	0.9389	0.9357	0.9635	1.8300
2	8"x8"	0.9937	0.977	1.0118	0.9636	1.8300
3	8"x8"	0.7573	0.8069	0.7399	0.6909	1.8300
Avg. Shear Value		0.9191	0.9076	0.8958	0.8727	1.8300

S/N	ID	Shear Modulus G (MPa) 1^{st} LC	Shear Modulus G (MPa) 4^{th} LC	Shear Modulus G (MPa) 1^{st} UL	Shear Modulus G (MPa) 4^{th} UL	shape Factor
1	6"x8"	0.6719	0.9733	0.5141	0.8414	1.5600
2	6"x8"	0.8246	0.8203	0.4801	0.505	1.5600
3	6"x8"	0.6933	0.7045	0.6155	0.5885	1.5600
Average Shear modulus		0.7299	0.8327	0.5366	0.6450	1.5600
S/N	ID	Shear Modulus G (MPa)	Shear Modulus G (MPa)	Shear Modulus G (MPa)	Shear Modulus G (MPa)	shape Factor

		1st LC	4th LC	1st UL	4th UL	
1	6"x6"	0.8764	0.9612	0.8094	0.8175	1.3700
2	6"x6"	0.7921	0.9832	0.8088	0.763	1.3700
3	6"x6"	0.9153	0.8937	0.8616	0.7769	1.3700
Average Shear modulus		0.8613	0.9460	0.8266	0.7858	1.3700

S/N	ID	Shear Modulus G (MPa) 1st LC	Shear Modulus G (MPa) 4th LC	Shear Modulus G (MPa) 1st UL	Shear Modulus G (MPa) 4th UL	shape Factor
1	5"x10"	0.86	0.8772	0.8153	0.8447	1.3900
2	5"x10"	0.9693	0.987	0.9339	0.9428	1.3900
3	5"x10"	0.8178	0.8836	0.8069	0.8277	1.3900
Average Shear modulus		0.8824	0.9159	0.8520	0.8717	1.3900

S/N	ID	Shear Modulus G (MPa) 1st LC	Shear Modulus G (MPa) 4th LC	Shear Modulus G (MPa) 1st UL	Shear Modulus G (MPa) 4th UL	shape Factor
1	4"x8"	0.6941	0.6981	0.6657	0.6098	1.1900
2	4"x8"	0.7942	0.8469	0.8469	0.8134	1.1900
3	4"x8"	0.5817	0.6095	0.611	0.6071	1.1900
Average Shear modulus		0.6900	0.7182	0.7079	0.6768	1.1900

Abbreviation LC loading cycle UL unloading cycle

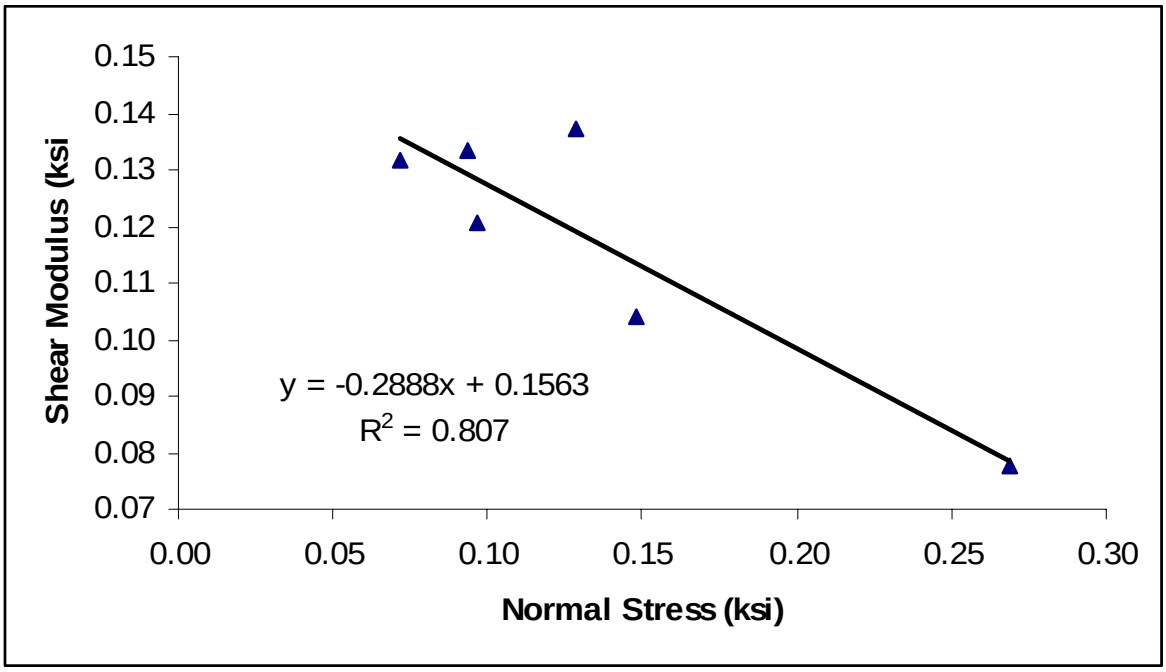

Figure 3.6 Variation of Shear Modulus with Respect to Normal Stress

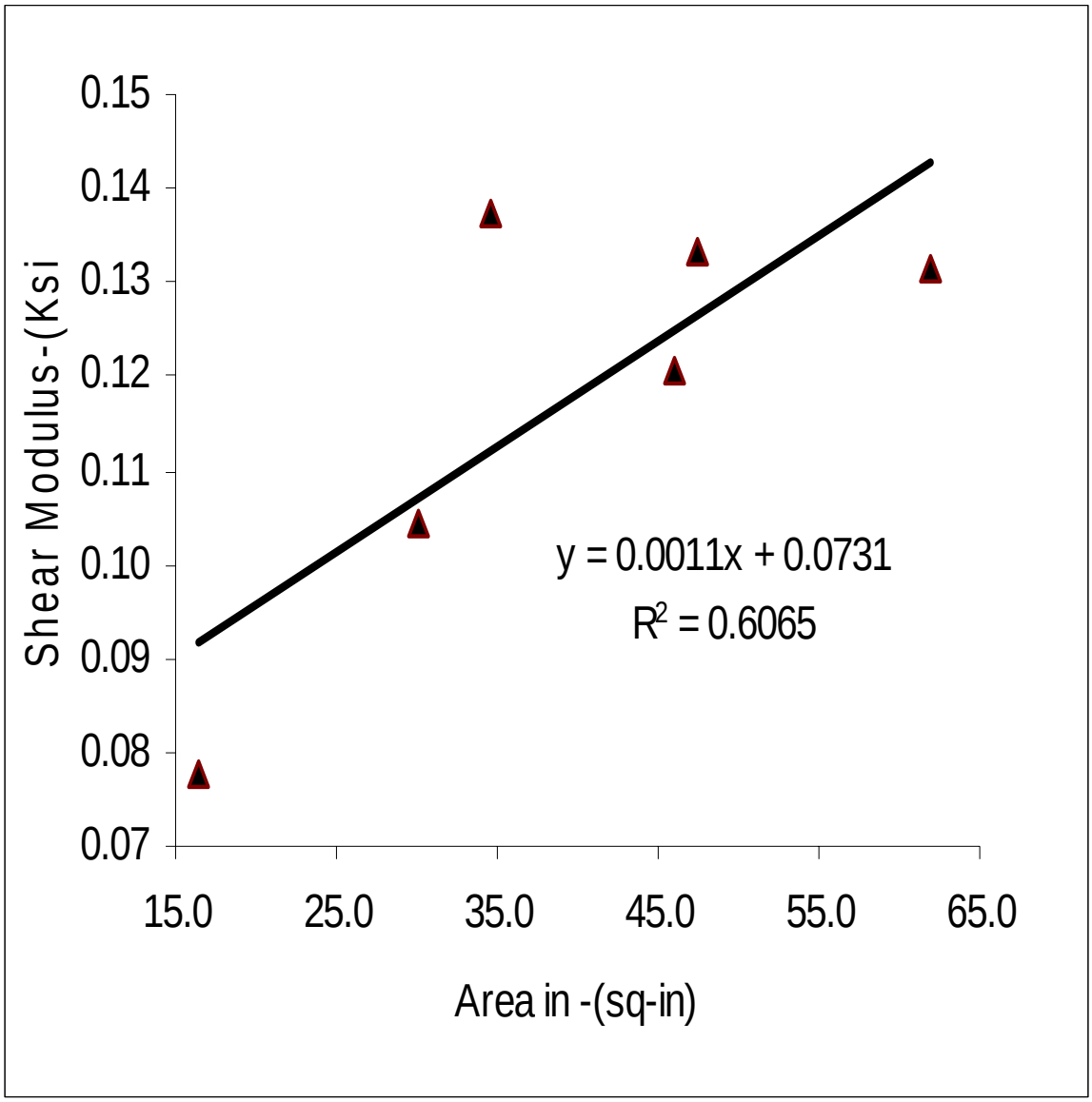

Figure 3.7 Variation of Shear Modulus with Respect to Area in Shear

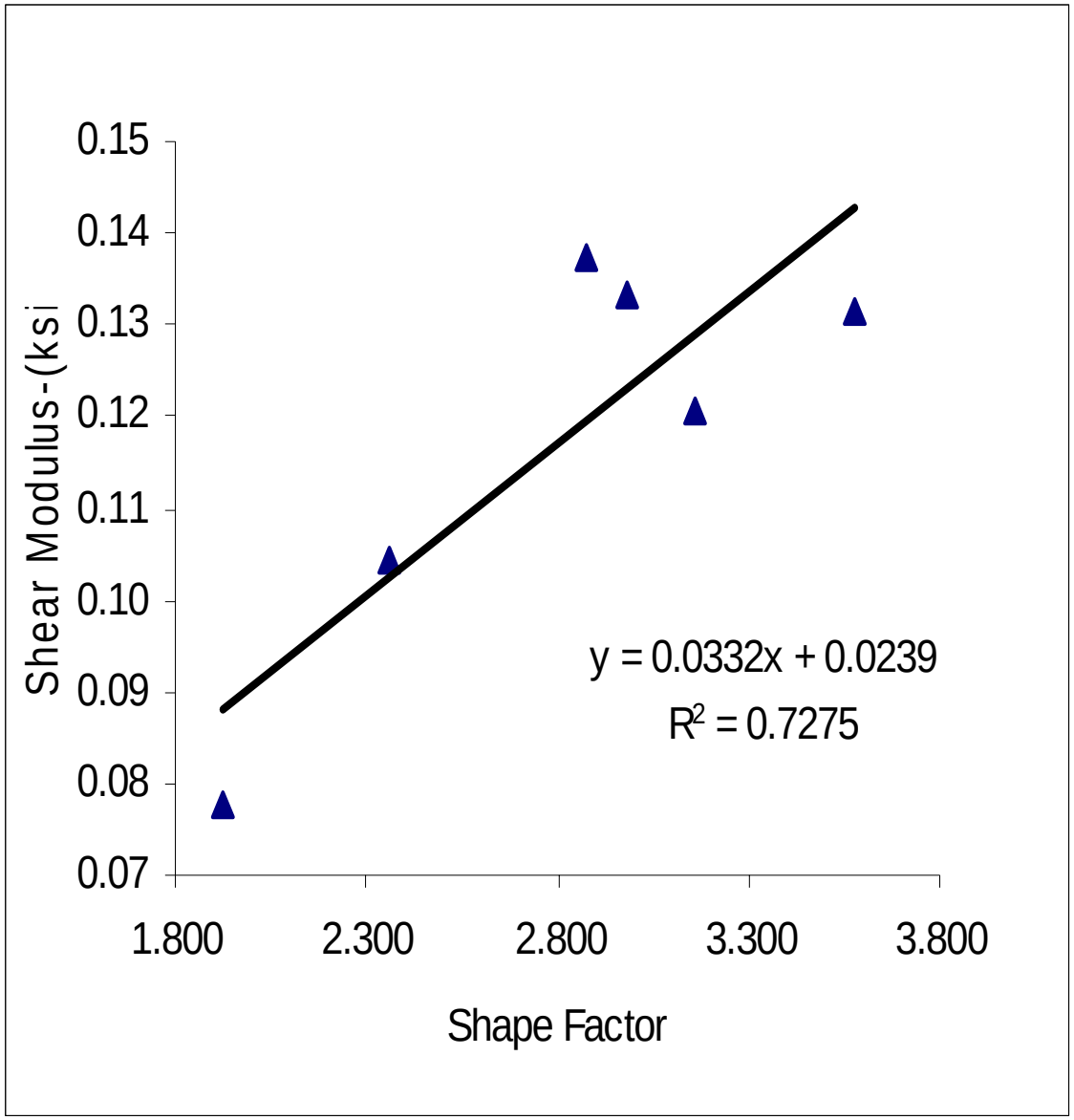

Figure 3.8 Variation of Shear Modulus with Respect to Shape Factor

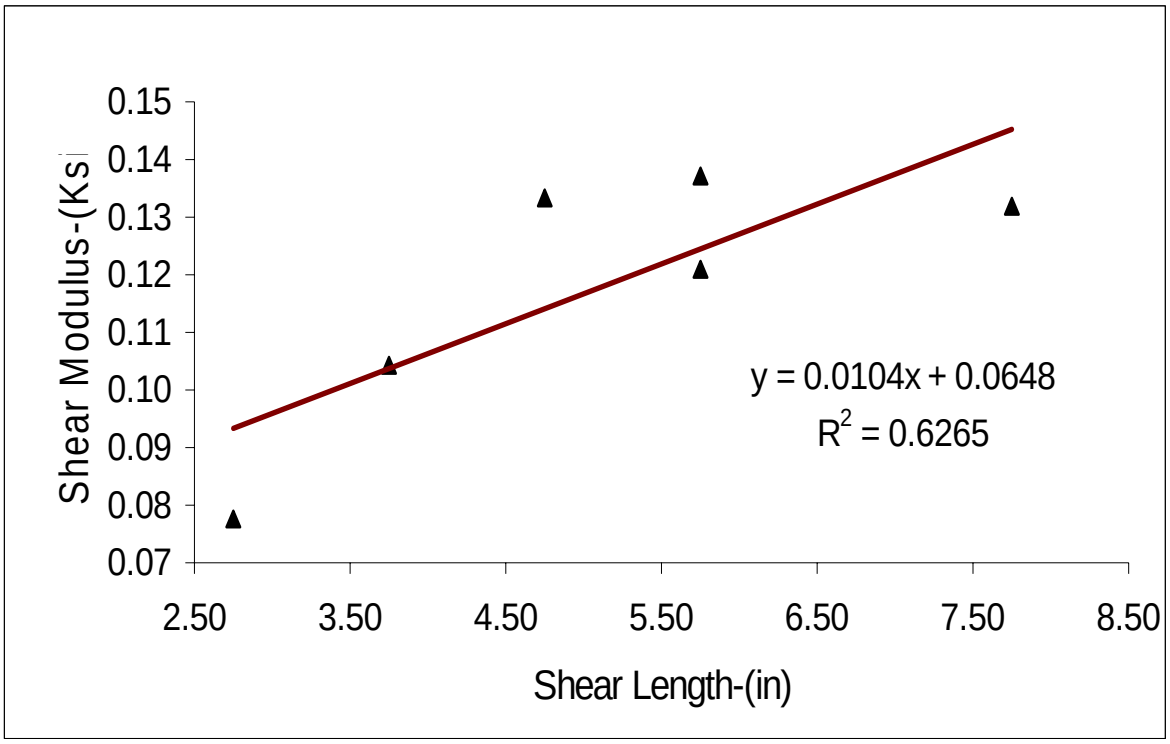

Figure 3.9 Variation of Shear Modulus with Respect to Shear Area Length

Discusion

As shown in the results above it is only the normal stress that has a high correlation to the shear modulus as indicated by the high R^2 values. A stepwise multivariate analysis was conducted using the SAS statistical analysis package. A 95% confidence limit was adopted from this multivariate analysis. From this analysis the normal stress was found to be the parameter that has significant influence on the value of the shear modulus.

Conclusions and Recommendations

From this study following conclusions can be drawn:

1. The magnitude of the shear modulus is negatively influence by the level of normal stress in the bearing pad.

2. The Texas inclined compression test setup which has normal stress varying at the same time as the shear stress needs to be adjusted to take in to consideration the influence the normal stress has on the value of the shear modulus.

The following recommendation can be made:

There is need to develop a shear modulus standard that will look at all the parameters that have impact on the shear modulus value.

CHAPTER 4: COMBINED LOADING TEST

Combined Loading Test Setup

The system used to conduct the combined loading was fabricated with the assistance of the Florida Department of Transportation (FDOT) Structures Laboratory, specifically for the proposed testing. This system consisted of 1) a heavy W-Section acting as the rigid platform beam 2) a second lighter W-section to provide the rotational leverage (pivot beam) 3) a system of plates to hold the test pad and pressure sensors, 4) a circular rod placed between the pivot beam and a top plate and 5) 1-inch threaded roads to maintain the applied compressive load during the rotational cyclic loading.

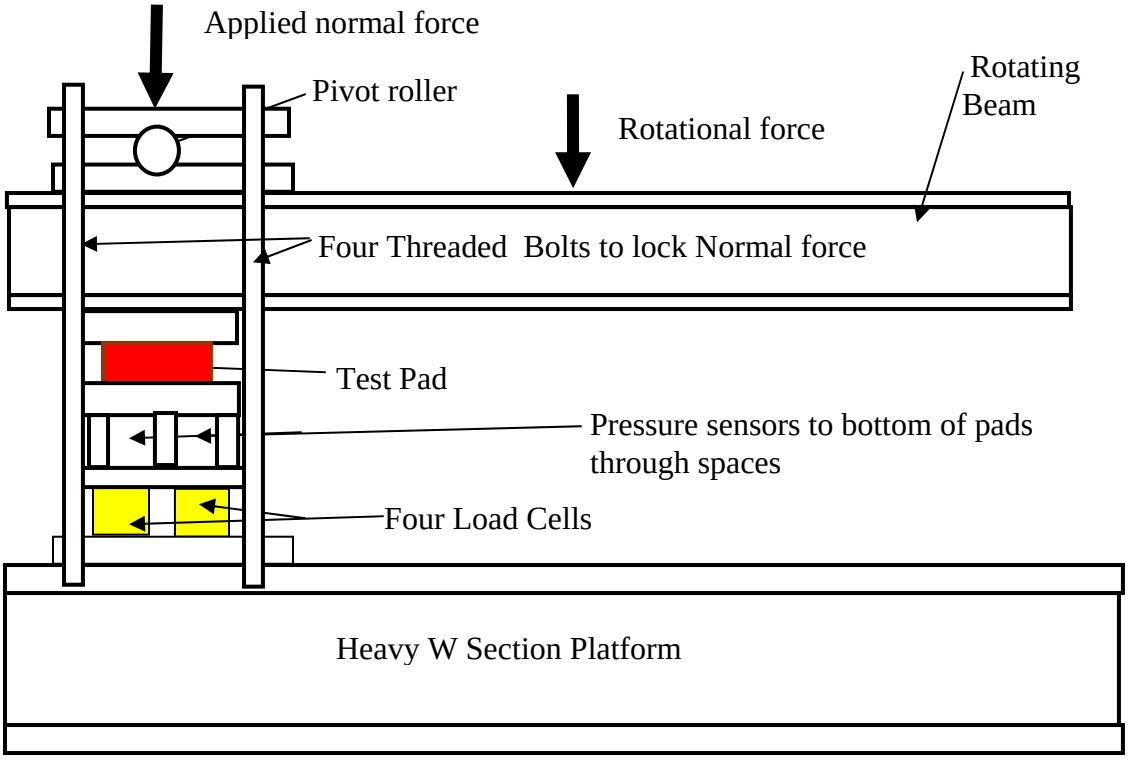

Figure 4.1 Schematic of the Combined Loading Arrangement

Shown in Figure 4.1 and Figure 4.2 are two different views of the loading testing system. As it can be seen from these two views of the assembly a long pivot beam was used to provide flexibility in the testing. By varying the distance of the actuator from the center of the rotation the magnitude of the force required to cause the desired rotation was varied. Moreover, the position of the rotational actuator determined the required travel stroke and the frequency to which the loading could be applied due to the limitations of the hydraulic system running the actuators.

Presented in Figure 4.3 is the bottom plate system showing the load cells and pressure sensors used to monitor reactions and pressures during the testing. Presented in Figure 4.4 is a detailed view of the top of the bottom plate system. A restraining plate was provided at the top after experiencing pad walk-out problems during initial testing.

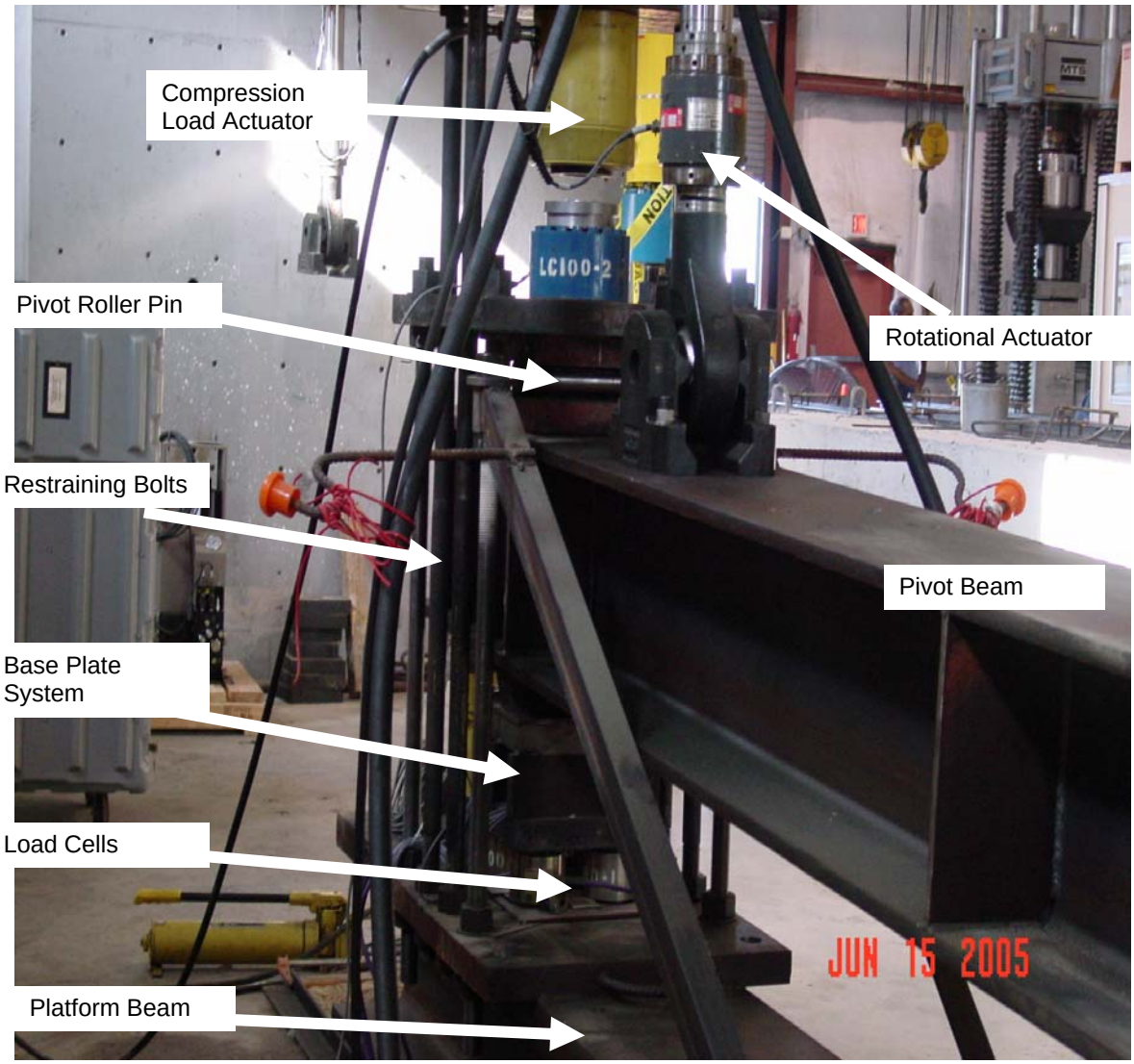

Figure 4.1 View 1 of the Combined Loading Testing Assembly

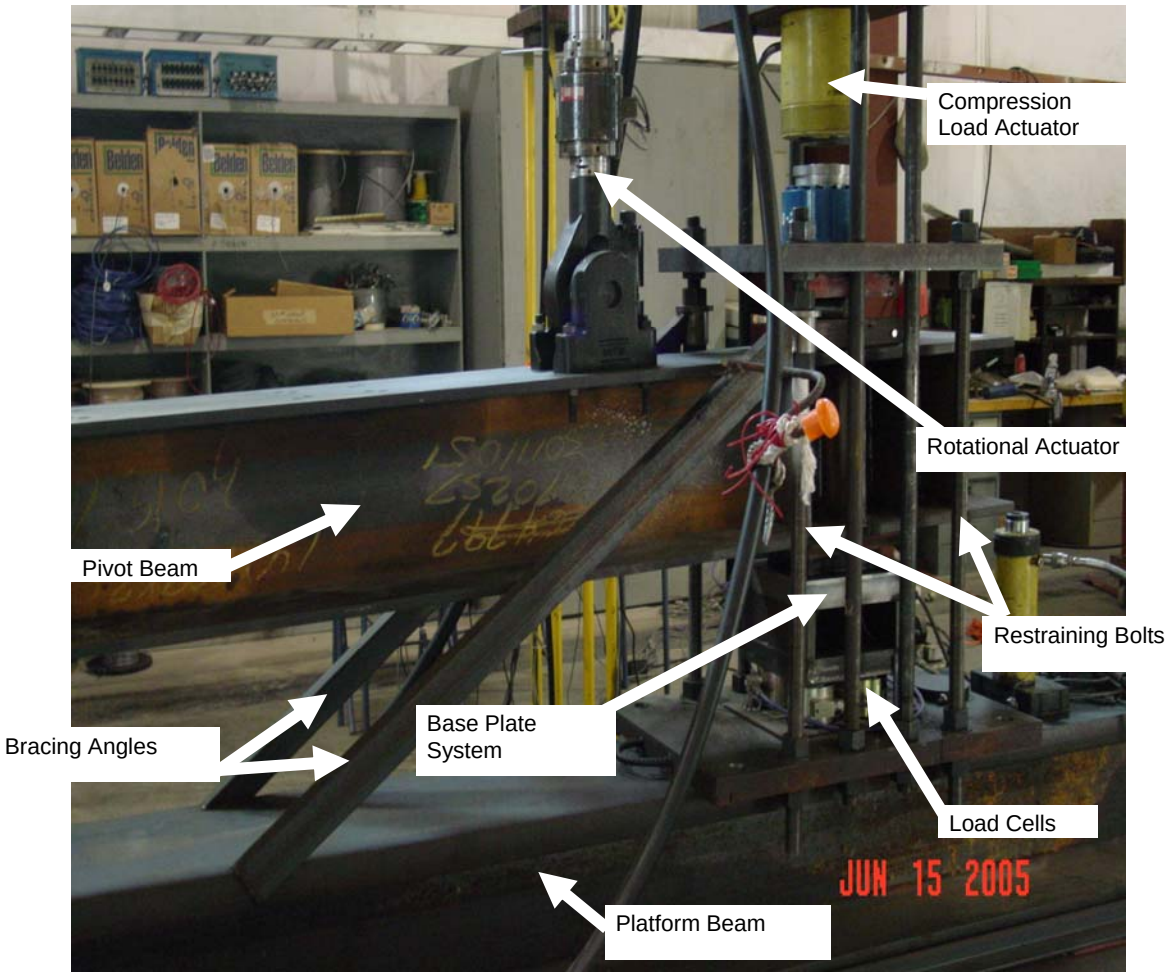

Figure 4.2 View 2 of the Combined Loading Testing Assembly

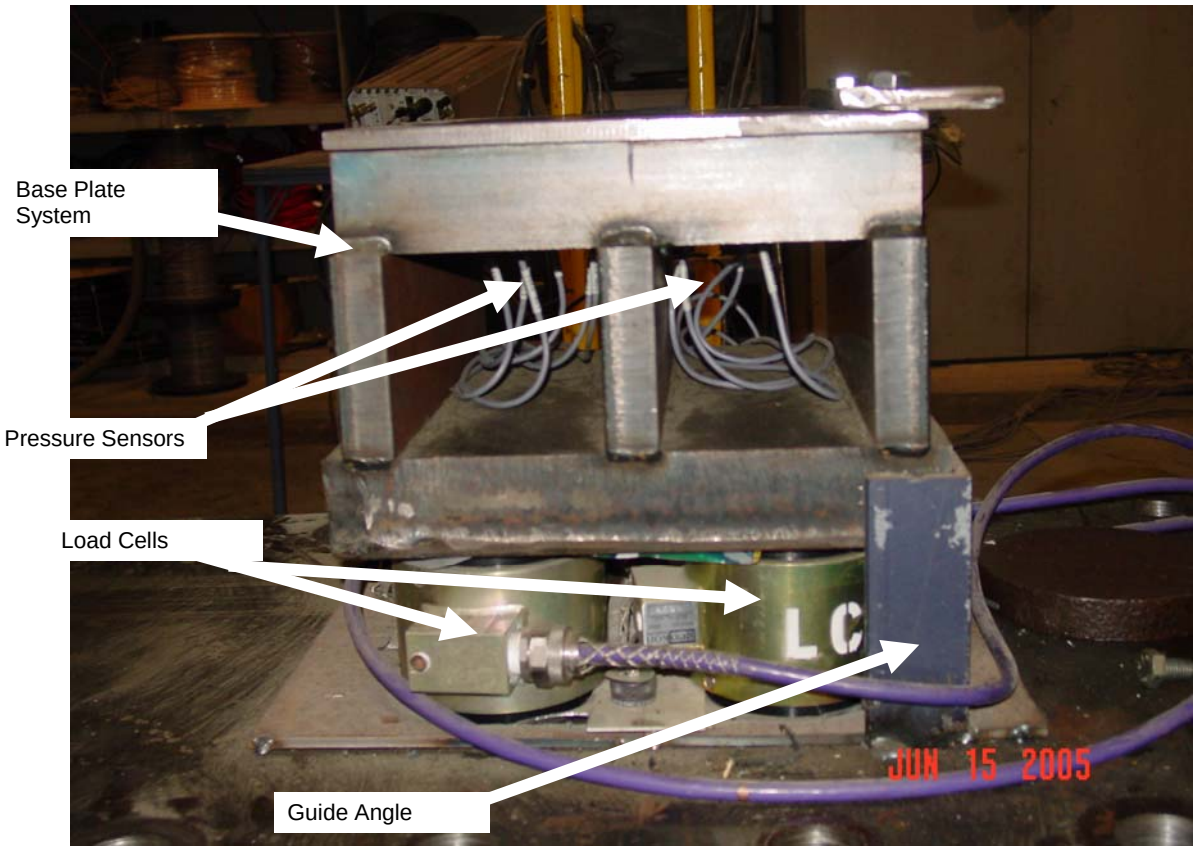

Figure 4.3 The Bottom Plate System

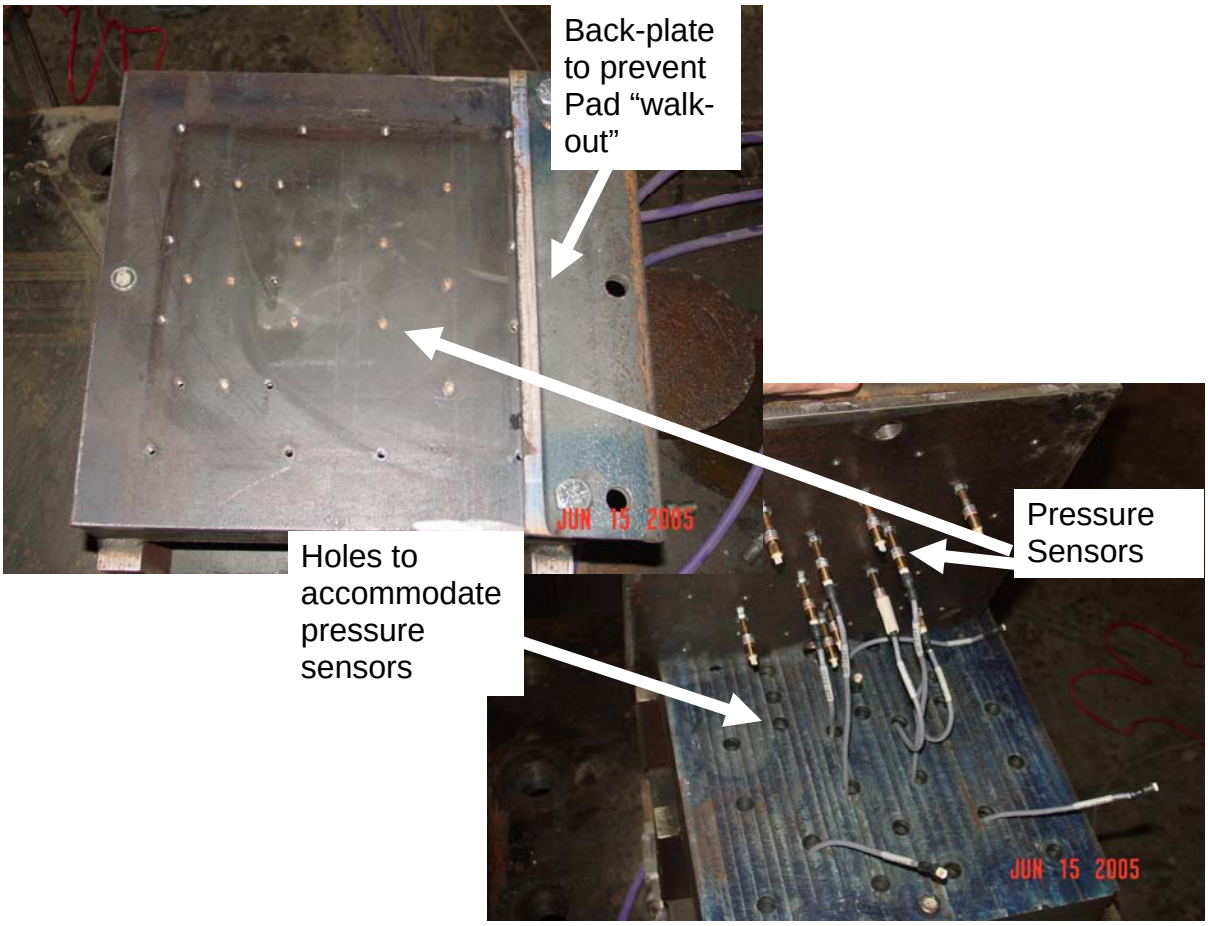

Figure 4.4 Detailed View of the Top of the Bottom Plate System

Presented in Figures 4.5 and 4.6 are the placements of the pressure gages for the various bearing pads.

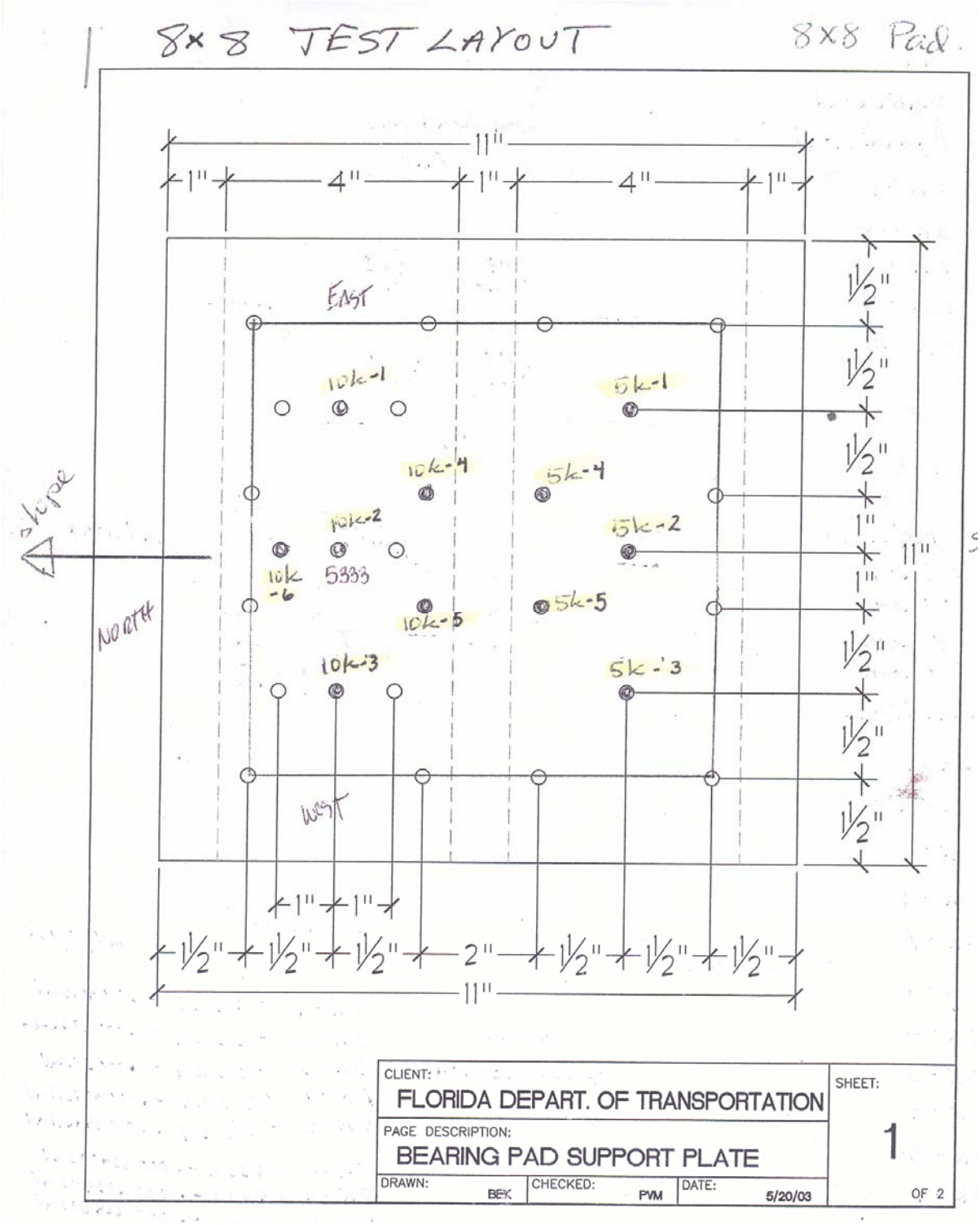

Figure 4.5: **Pressure Gage Set-up for a 8x8 Bearing Pad**

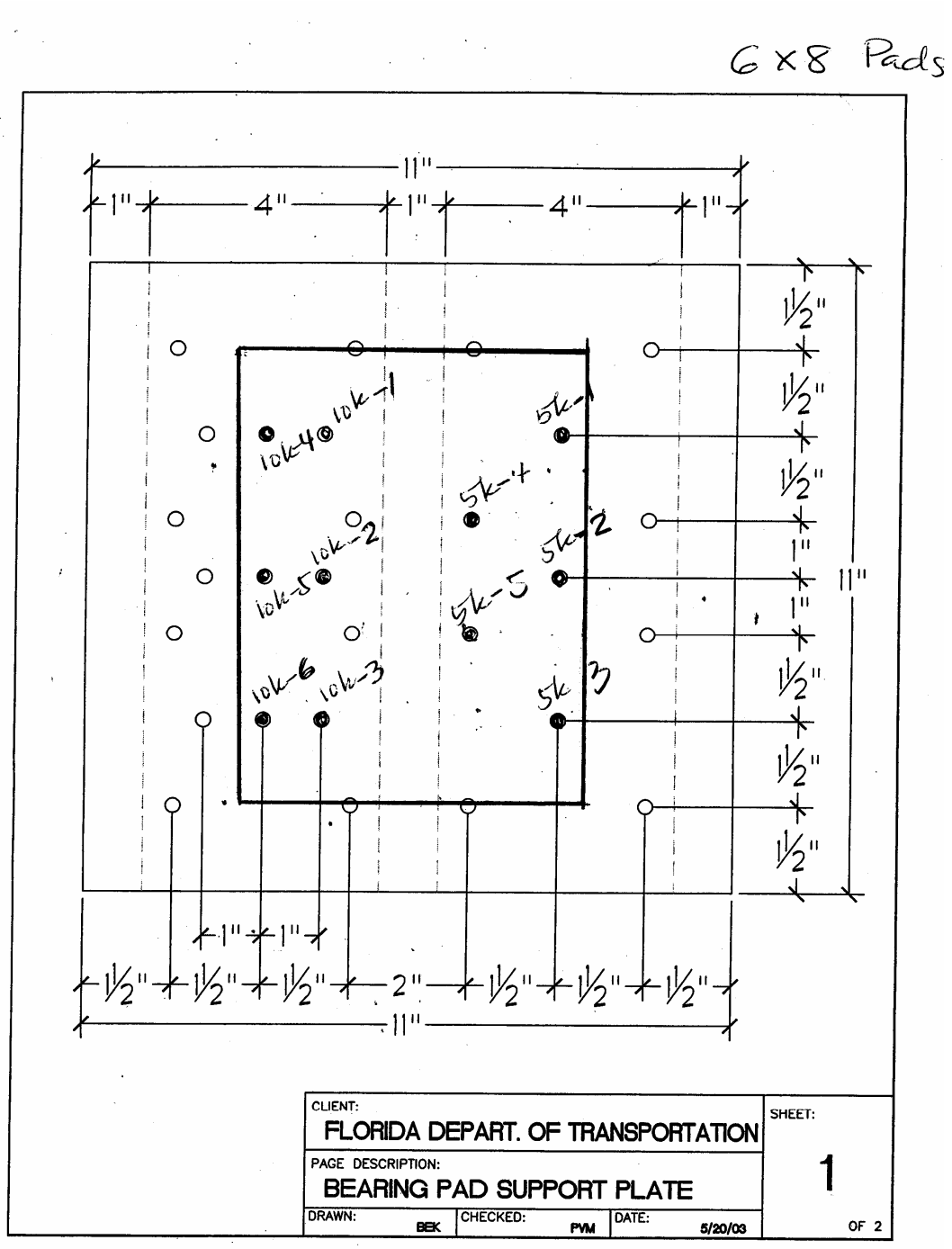

Figure 4.6: Pressure Gage Set-up for a 6x8 Bearing Pad

CHAPTER 5: ANALYTICAL MODEL

An analytical model was created using ANSYS software, a commercially available Finite Element Analysis (FEA) package. The elastomer material was model using SOLID 185 elements and the steel parts, including the top and bottom plates, were modeled by SOLID 45 elements. The element capabilities, as described by the ANSYS manual, are described below.

SOLID185 Element

SOLID185 is used for the 3-D modeling of solid structures. It is defined by eight nodes having three degrees of freedom at each node: translations in the nodal x, y, and z directions. The element has plasticity, hyperelasticity, stress stiffening, creep, large deflection, and large strain capabilities. It also has mixed formulation capability for simulating deformations of nearly incompressible elastoplastic materials, and fully incompressible hyperelastic materials. The element is defined by eight nodes and the orthotropic material properties. The default element coordinate system is along global directions.

SOLID185 Element Technology

SOLID185 uses the selective reduced integration method. This method helps to prevent volumetric mesh locking in nearly incompressible cases, which is the situation in the case in this study. This option replaces volumetric strain at the Gauss integration point with the average volumetric strain of the elements. However, this method can not prevent any shear locking in bending dominated problems.

SOLID45 Element

SOLID45 is used for the 3-D modeling of solid structures. The element is defined by eight nodes having three degrees of freedom at each node: translations in the nodal x, y, and z directions. The element has plasticity, creep, swelling, stress stiffening, large deflection, and large strain capabilities.

The element is defined by eight nodes and the orthotropic material properties. Orthotropic material directions correspond to the element coordinate directions.

This element also supports uniform reduced (1 point) integration with hourglass control. Using uniform reduced integration provides the following advantages when running a nonlinear analysis:

- Less cpu time is required for element stiffness formation and stress/strain calculations to achieve a comparable accuracy to the FULL integration option.
- The length of the element history saved record is about 1/7th as much as when the full integration (2 X 2 X 2) is used for the same number of elements.
- Nonlinear convergence characteristic of the option is generally far superior to the default full integration with extra displacement shape.
- The analysis will not suffer from volumetric locking which can be caused by plasticity or other incompressible material properties.

An analysis using uniform reduced integration can have the following disadvantages:

- The analysis is not as accurate as the full integration method, which is apparent in the linear analysis for the same mesh.
- The analysis cannot capture the bending behavior with a single layer of elements; for example, in the case of a fixed-end cantilever with a lateral point load, modeled by one layer of elements laterally. Instead, four elements are usually recommended.

Contact Elements

The interface between the bearing pad and the top and bottom plates were modeled using **CONTACT** and **TARGET** elements. With this modeling slippage and separation (uplift) of the pad from the lower and upper plates was permissible.

CONTA174 Element

According to the ANSYS manual, **CONTA174** is used to represent contact and sliding between 3-D “target” surfaces (TARGE170) and a deformable surface, defined by this element. The element is applicable to 3-D structural and coupled field contact analyses.

TARGE170 Element

According to the ANSYS manual, **TARGE170** is used to represent various 3-D “target” surfaces for the associated contact elements (CONTA173, CONTA174, CONTA175, and CONTA176). The contact elements themselves overlay the solid elements describing the boundary of a deformable body and are potentially in contact with the target surface, defined by TARGE170. This target surface is discretized by a set of target segment elements

(TARGE170) and is paired with its associated contact surface via a shared real constant set. You can impose any translational or rotational displacement, temperature, voltage, and magnetic potential on the target segment element. You can also impose forces and moments on target elements. For rigid target surfaces, these elements can easily model complex target shapes. For flexible targets, these elements will overlay the solid elements describing the boundary of the deformable target body.

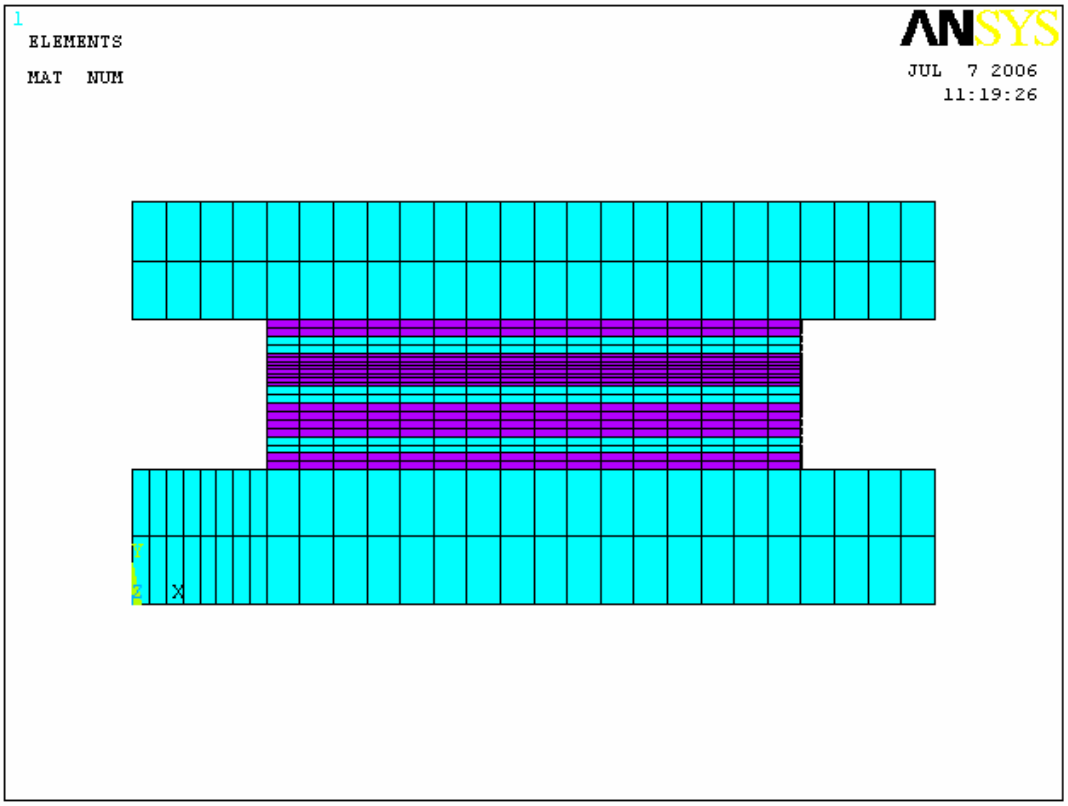

Figure 5.1 X-Y View of the Pad and Supporting and Loading Plate Mesh

Presented in Figure 5.1 and Figure 5.2 are typical meshing of a 8x8 bearing pad.

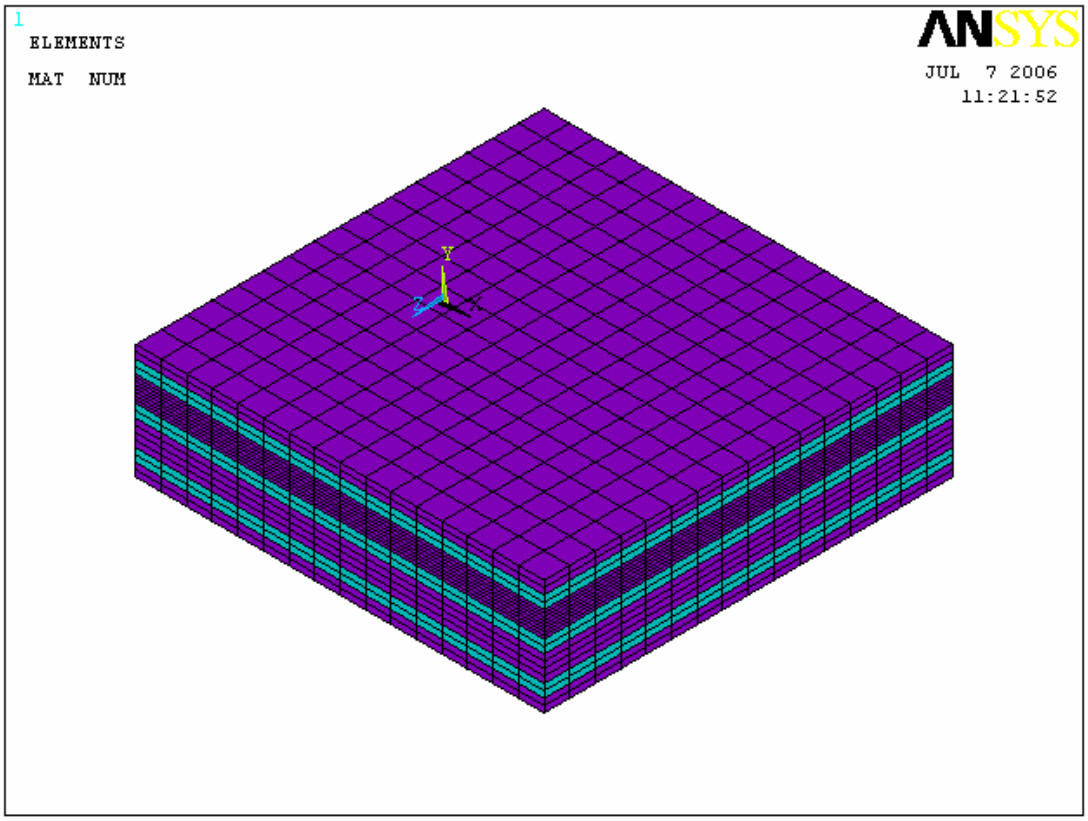

Figure 5.2 A 3-D View of the Bearing Pad Mesh

Material Properties

The material model has much influence on the FEA results. In this modeling all the steel parts were assumed to behave as a linear elastic model with the following parameters:

Modulus of elasticity E_s = 29,000,000 psi

Poisson ratio ν = 0.30

The elastomer material was assumed to behave in an hyper-elastic non-liner material. According to the result of shear modulus test, as presented in Chapter 3, the shear modulus, G, was found to be correlated to the average normal stress. Furthermore, Gent (1970) has found that the effective compression modulus was a function of the shape factor of the

bearing pad. Gent found the effective compression modulus to be related to the shear modulus as follows.

$$E_c := E_0 \cdot \left(1 + 2 \cdot \phi \cdot S^2\right)$$

where

S = is the bearing pad shape factor

$$E_0 = 4.515 \cdot G - 0.071$$

G = Shear modulus (in ksi) as determined in Chapter 3 (Table 3.2)

$$\phi = 0.445 + \frac{0.023}{G}$$

As noted in the literature the elastomer exhibits a stress hardening behavior. In this simulation a bilinear stress hardening material model was adopted.

A sketch of the bilinear model used in this study is presented in Figure 5.3. The exact values were dependent on the pad size which had influence on the shape factor. The hardening factor a was taken to be 1.2 in this study. In reality this factor is not constant, rather it varies continuously, thus making it necessary to use multlinear model. Since there was no sufficient data to support the continuously varying hardening behavior, a bilinear model, as presented in Figure 5.3, was adopted.

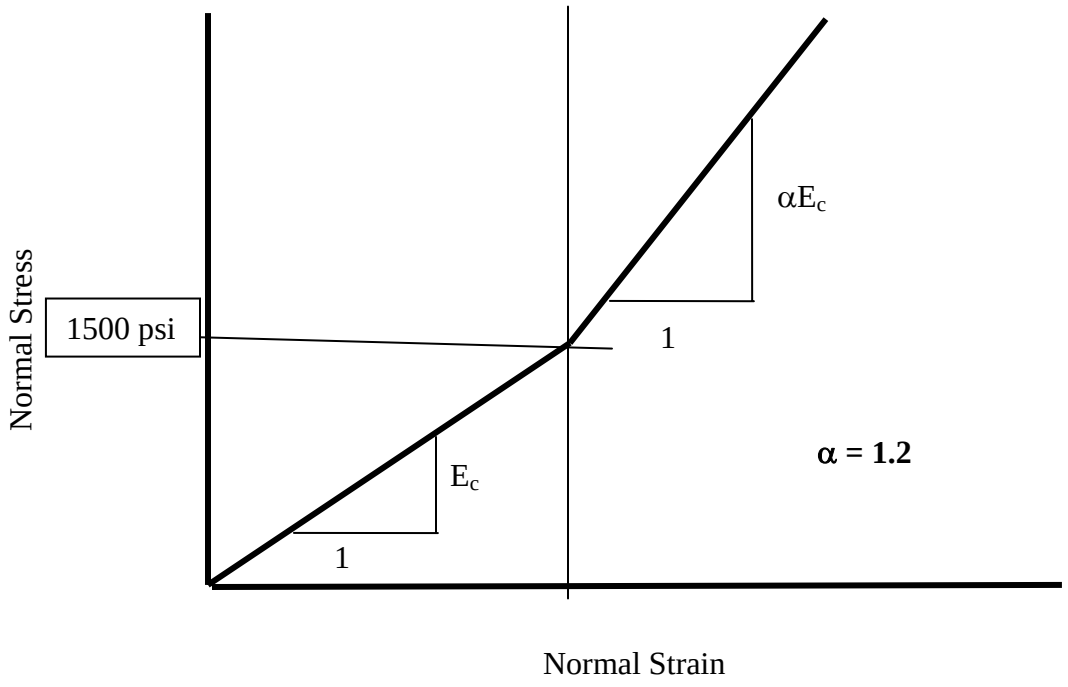

5.3 Elastomer Stress-Strain Material Model Used in FEA Model

CHAPTER 6: RESULTS AND DISCUSSION

Presented in this chapter are the results of the combined loading tests as well as the FEA results. Presented in Fig. 6.1 are examples of failed pads. As it can be observed in Figure 6.1 (a), the elastomer, between the reinforcement steel plates at the end with the high compression strains, bulged permanently out of the of the plane of the pad. This tearing of the pad occurred after loading cycles ranging from 7 to 24-thousand for the various samples tested. A cut through the failed samples (after applying 1-million load cycles) showed that this bulging failure was limited to a relatively small region of the end of the pad. The sketch on Figure 6.1(b) shows the general geometry of the failed elastomer wedge. Evaluations of the failure surfaces were conducted using an electron microscope. Presented in Figures 6.2 and 6.3 are the electron microscope surface scans. The surface morphology presented in Figure 6.2 shows evidence for shear failure and delamination. Striations as shown in Figure 6.3 are indications of fatigue failure. From these surfaces scans it can be argued that the predominant mode of failure is shear failure. Even the fatigue failure is in the sliding mode, i.e, shear failure.

Presented in Figures 6.4, 6.6, 6.8, 6.10 and 6.12 are the pressure variations across the bottom surface of the pad. These pressures were recorded by the pressure sensors after various load cycles as indicated in the figures. KCY stands for a thousand load cycles. The pressure of each sensor was normalized by its value for the initial load cycles that is before any sign of bulging failure. These pressure ratios are presented in Figures 6.5, 6.7, 6.9, 6.11 and 6.13.

Fig. 6.1: Predominant Pad Failure Mode

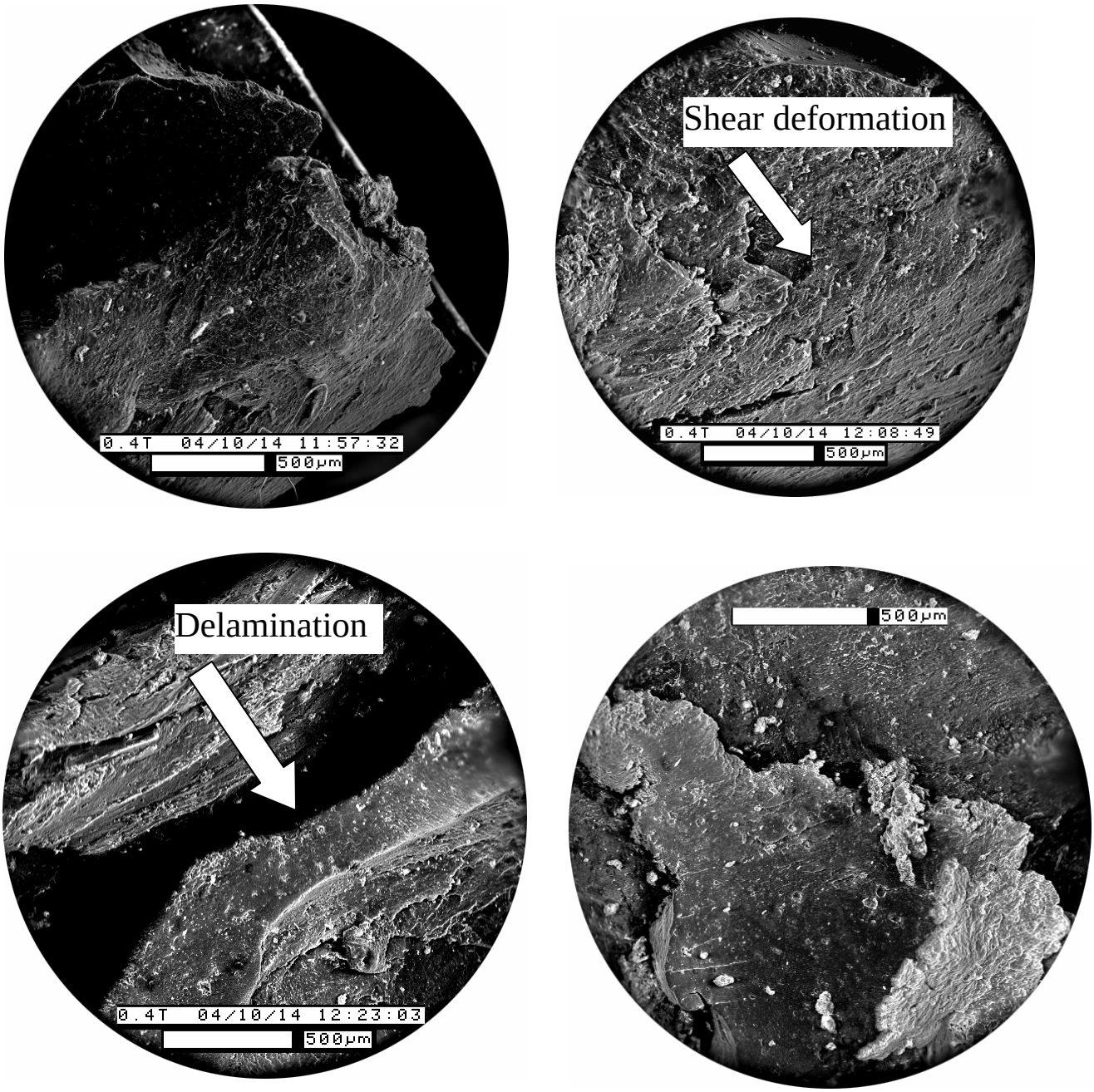

Fig. 6.2: Electron Microscope Scans of the Failed Surfaces: Evidence of Shear and Delamination

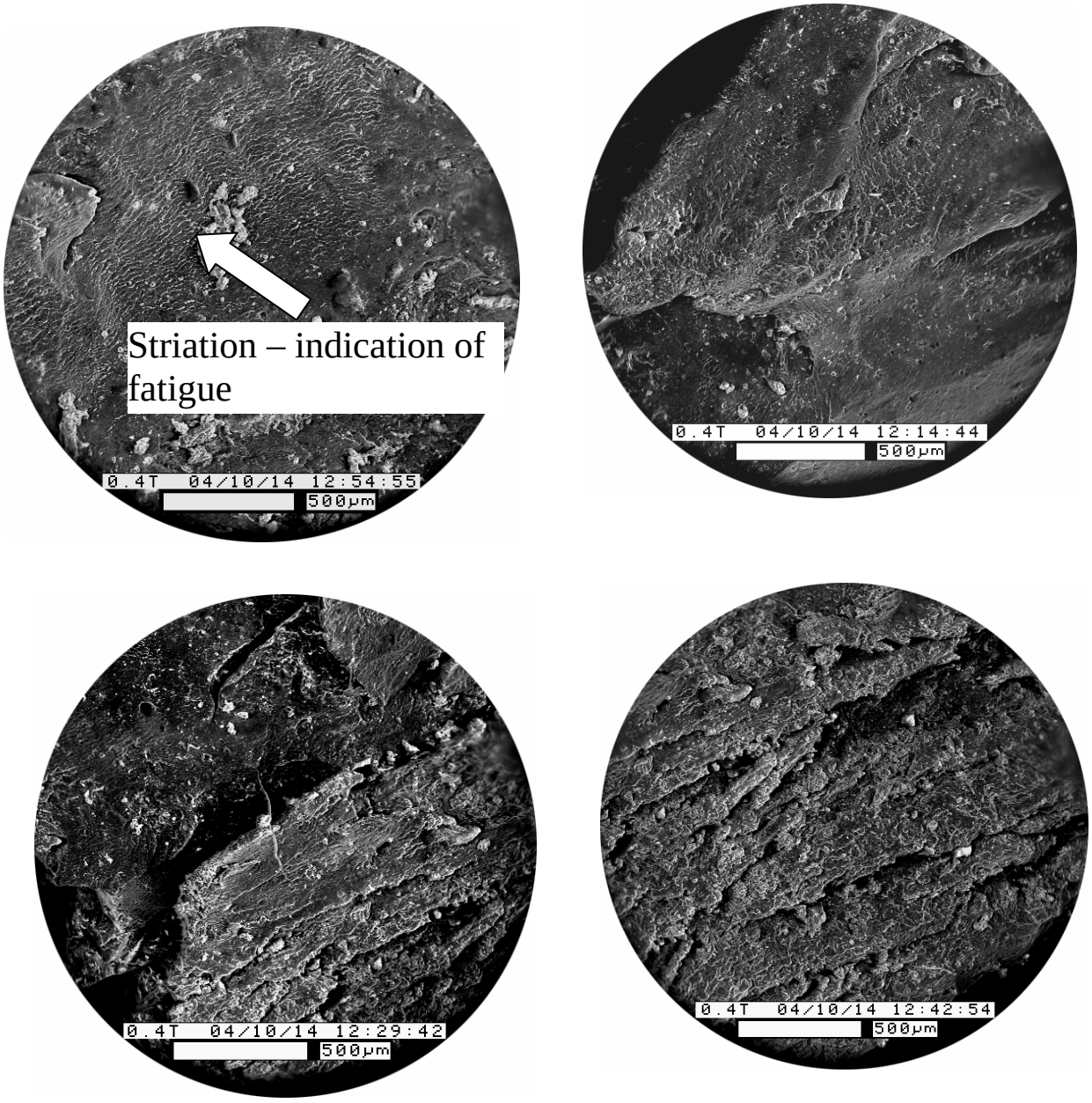

Fig. 6.3: Electron Microscope Scan of the Failed Surfaces: Evidence of Fatigue Failure

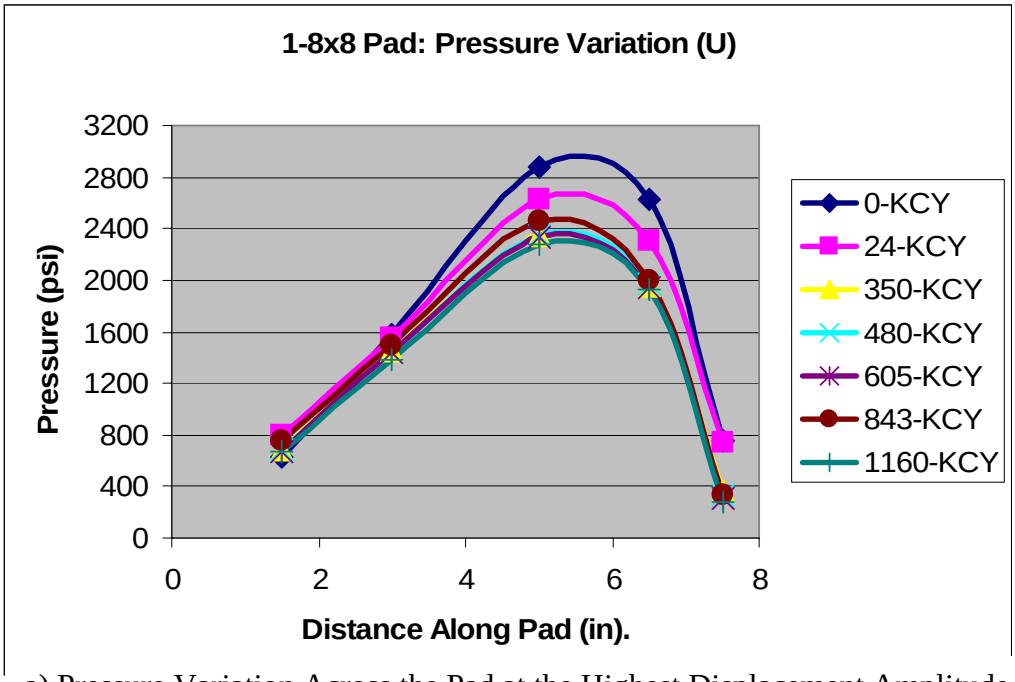

a) Pressure Variation Across the Pad at the Highest Displacement Amplitude

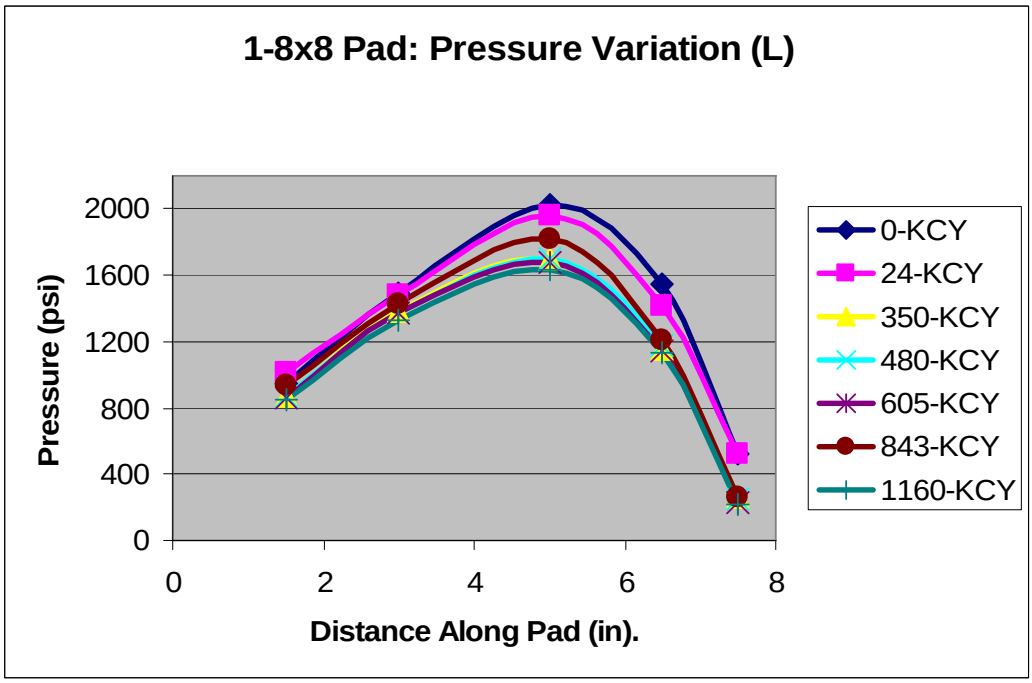

b) Pressure Variation Across the Pad at the Lowest Displacement Amplitude

Figure 6.4. Pressure Variation for 1-8x8 Pad

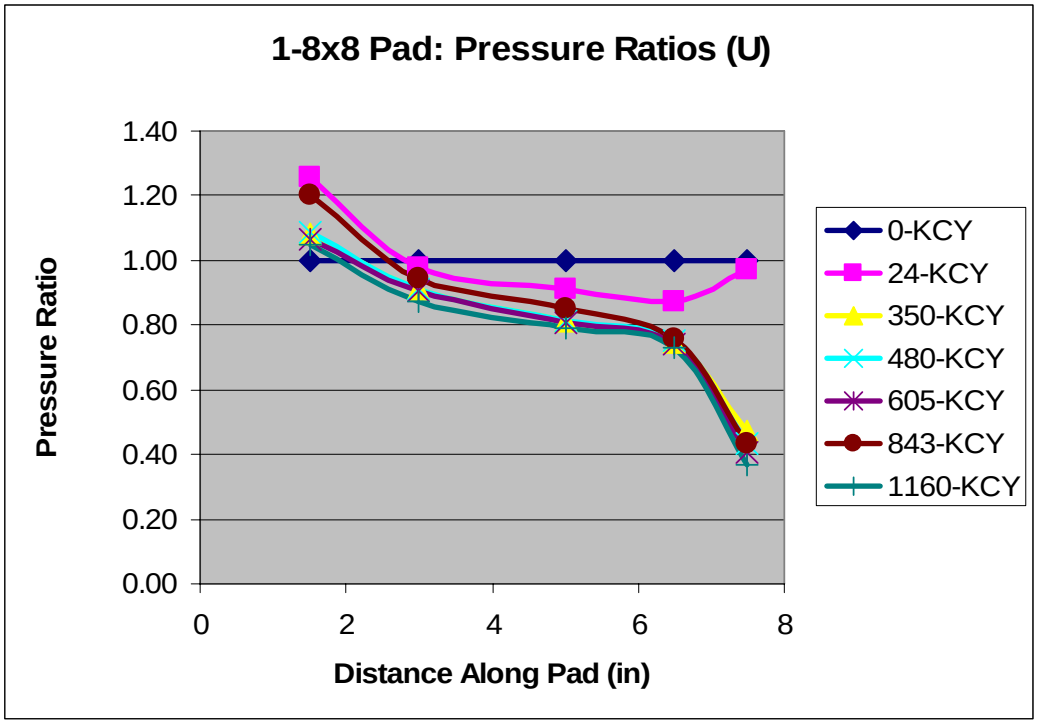

a) Pressure Ratio Variation Across the Pad at the Highest Displacement Amplitude

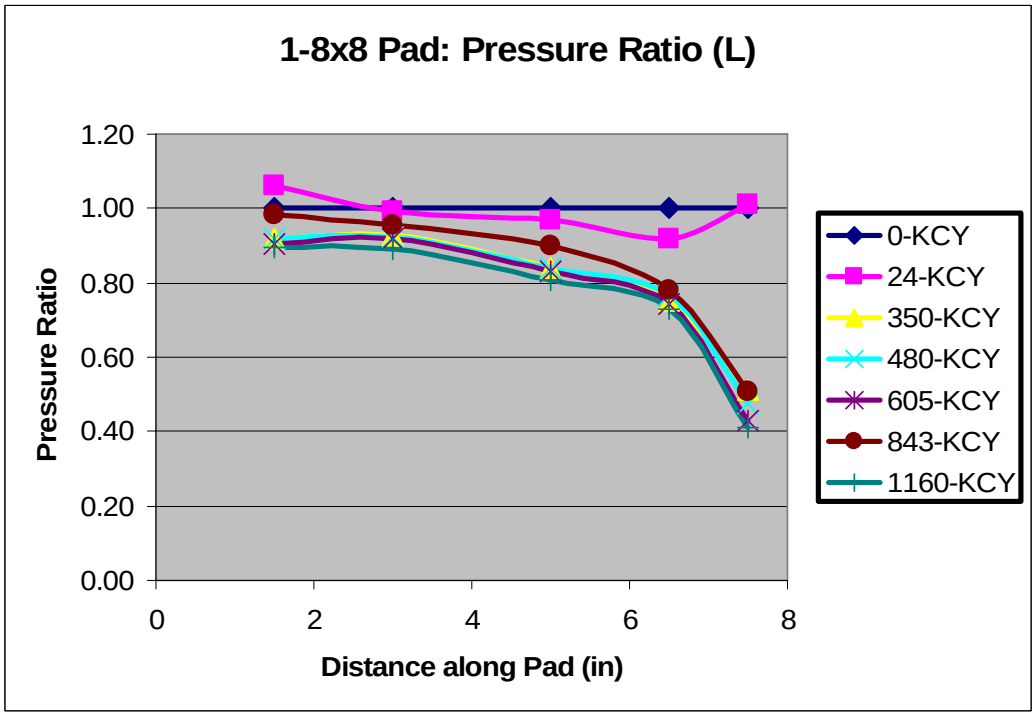

b) Pressure Ratio Variation Across the Pad at the Lowest Displacement Amplitude

Figure 6.5. Pressure Ratio Variation for 1-8x8 Pad

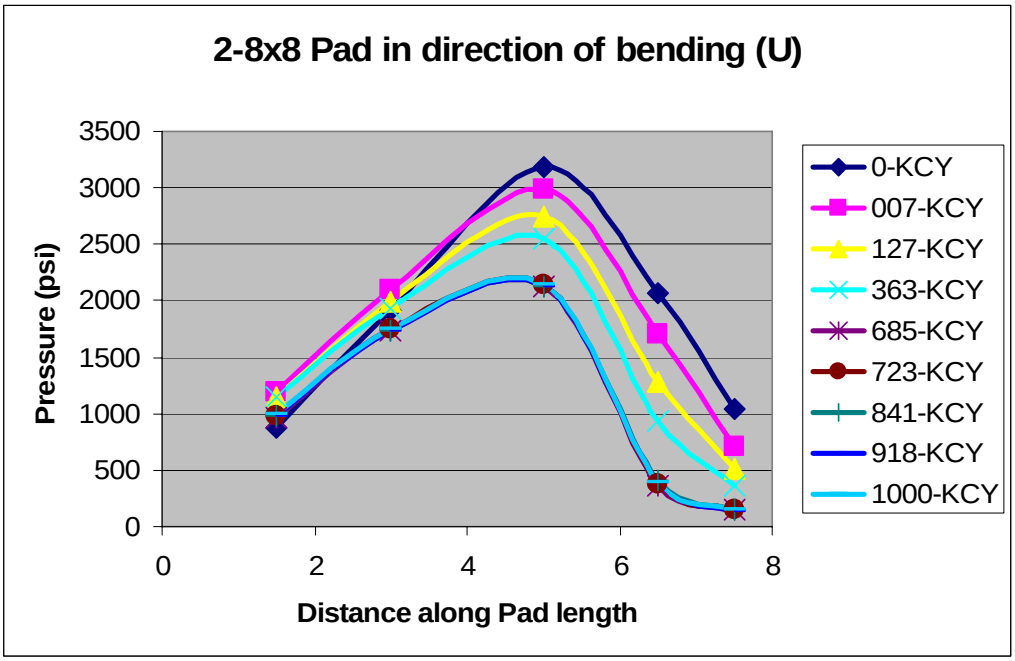

a) Pressure Variation Across the Pad at the Highest Displacement Amplitude

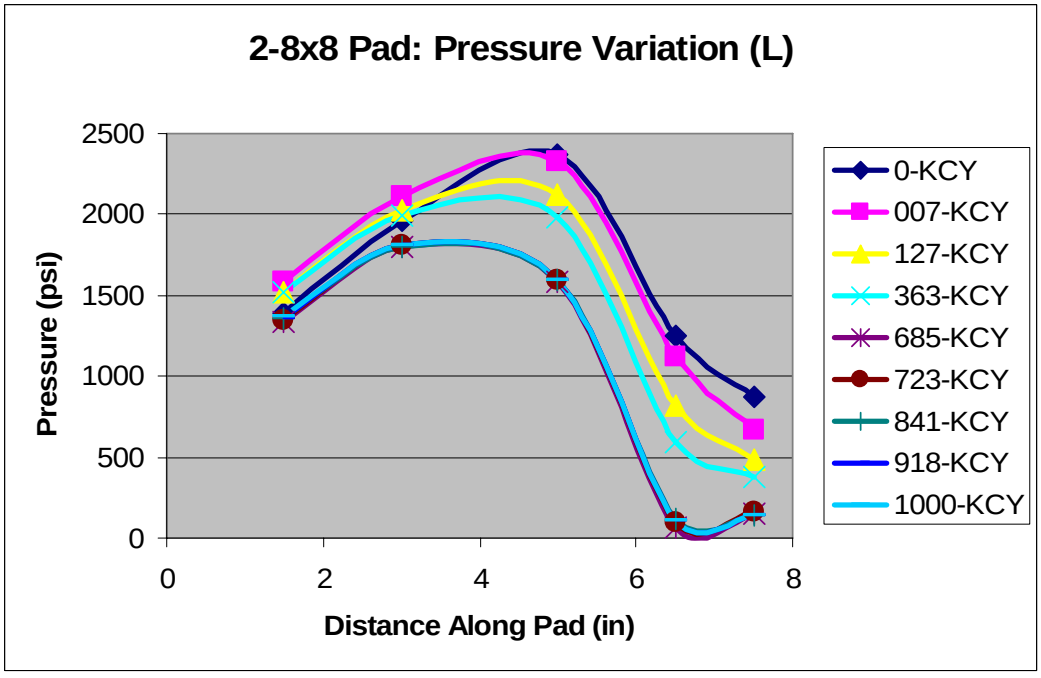

b) Pressure Variation Across the Pad at the Lowest Displacement Amplitude

Figure 6.6. Pressure Variation for 2-8x8 Pad

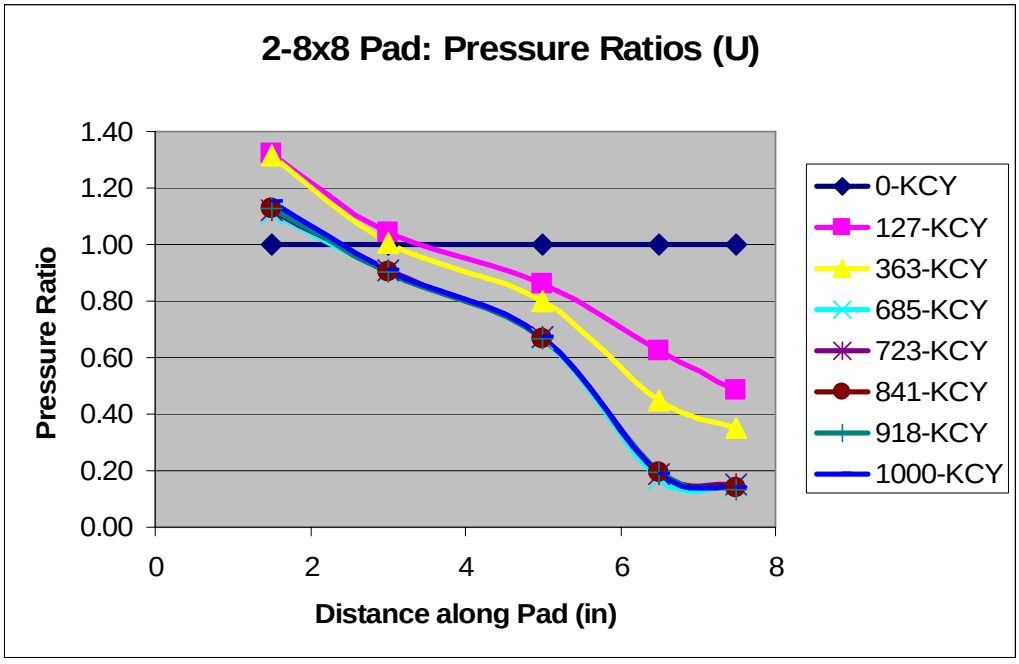

a) Pressure Ratio Variation Across the Pad at the Highest Displacement Amplitude

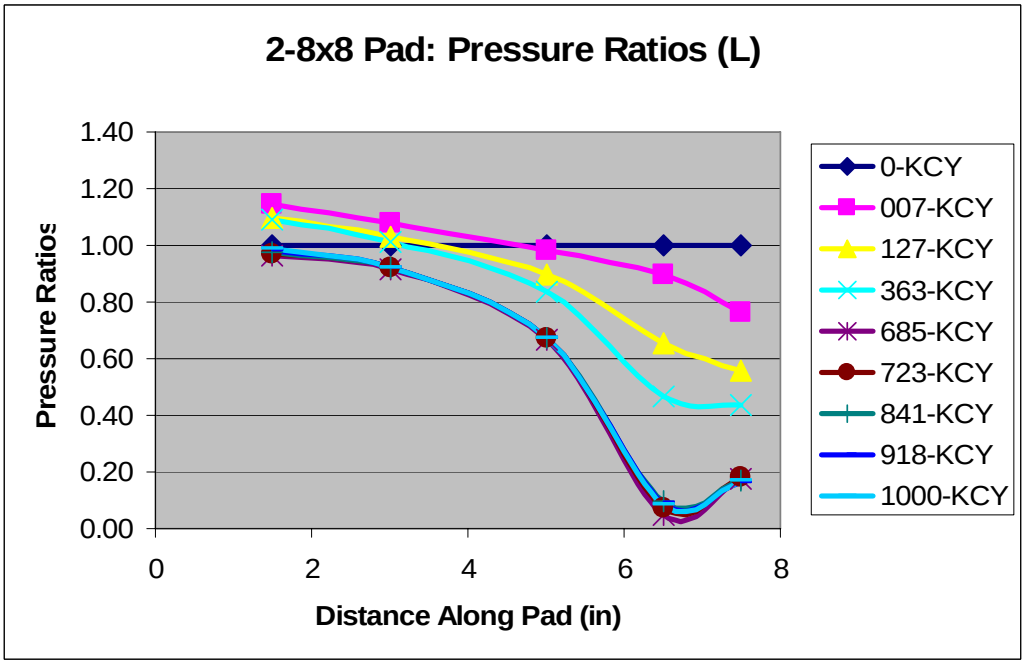

b) Pressure Ratio Variation Across the Pad at the Lowest Displacement Amplitude

Figure 6.7. Pressure Ratio Variation for 2-8x8 Pad

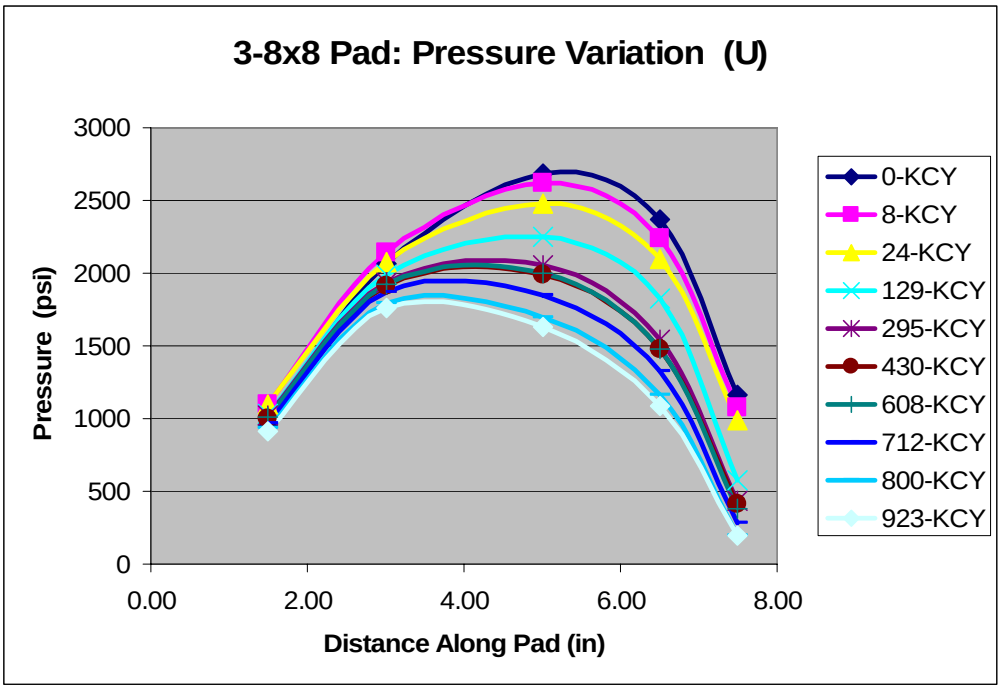

a) Pressure Variation Across the Pad at the Highest Displacement Amplitude

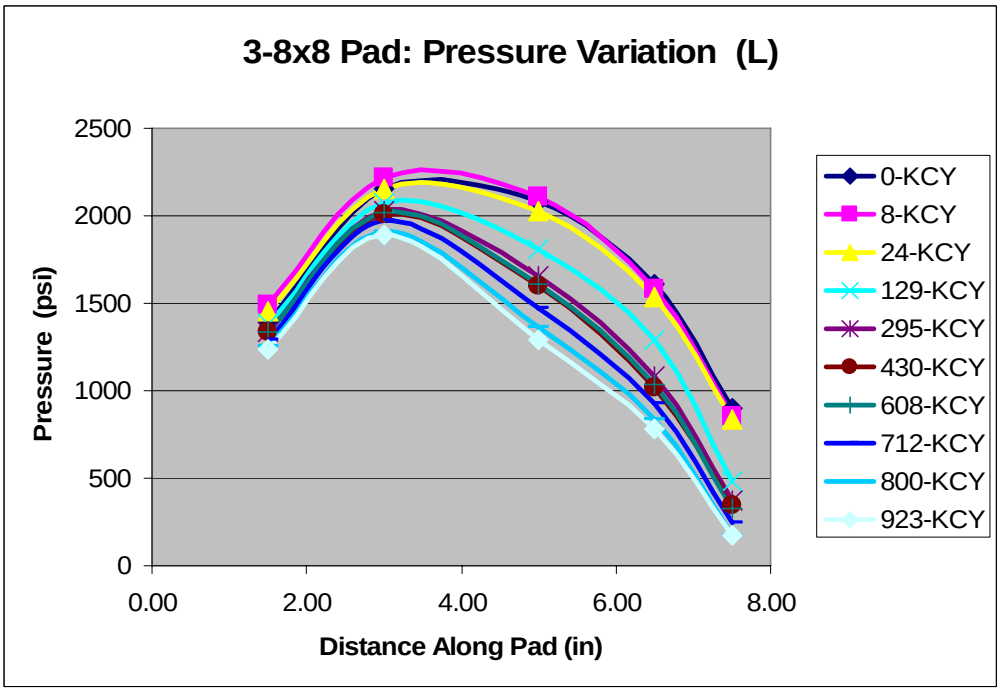

b) Pressure Variation Across the Pad at the Lowest Displacement Amplitude

Figure 6.8. Pressure Variation for 3-8x8 Pad

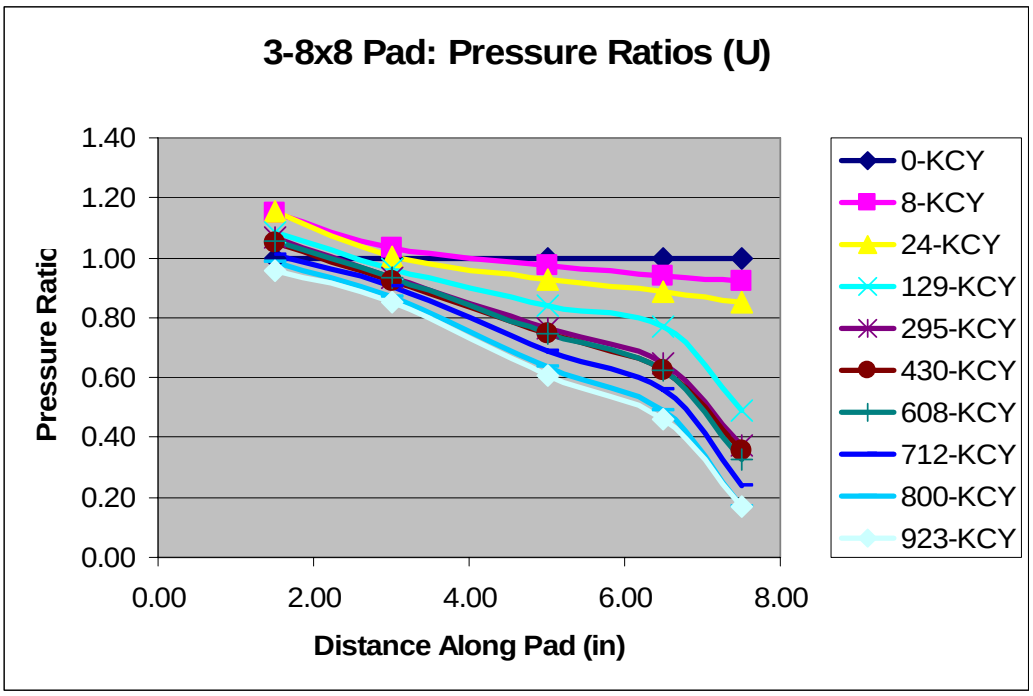

a) Pressure Ratio Variation Across the Pad at the Highest Displacement Amplitude

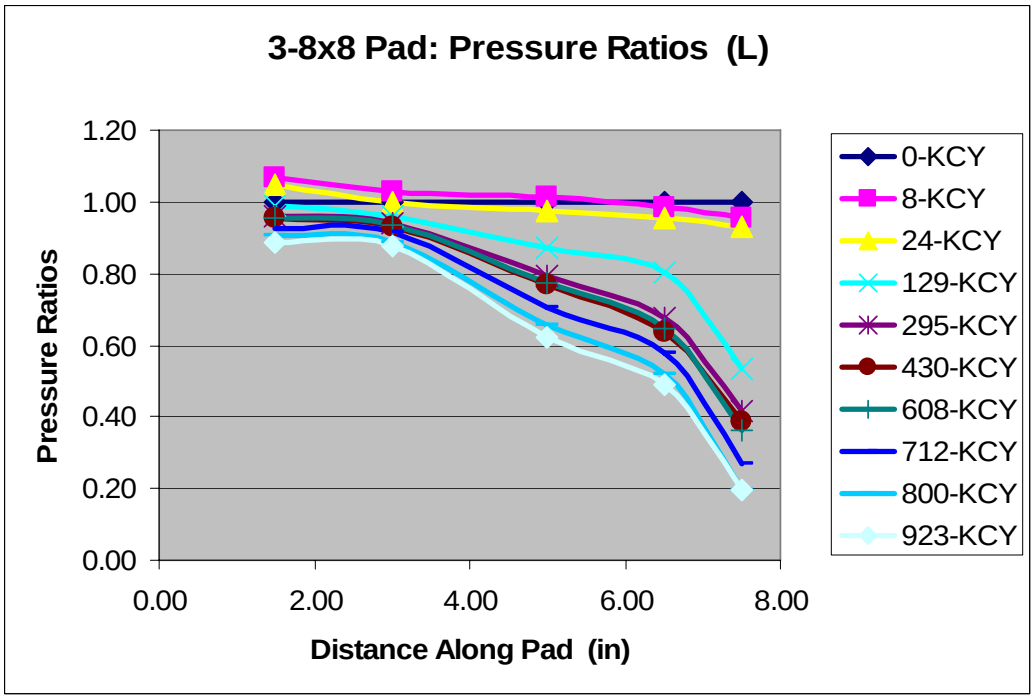

b) Pressure Ratio Variation Across the Pad at the Lowest Displacement Amplitude

Figure 6.9. Pressure Ratio Variation for 3-8x8 Pad

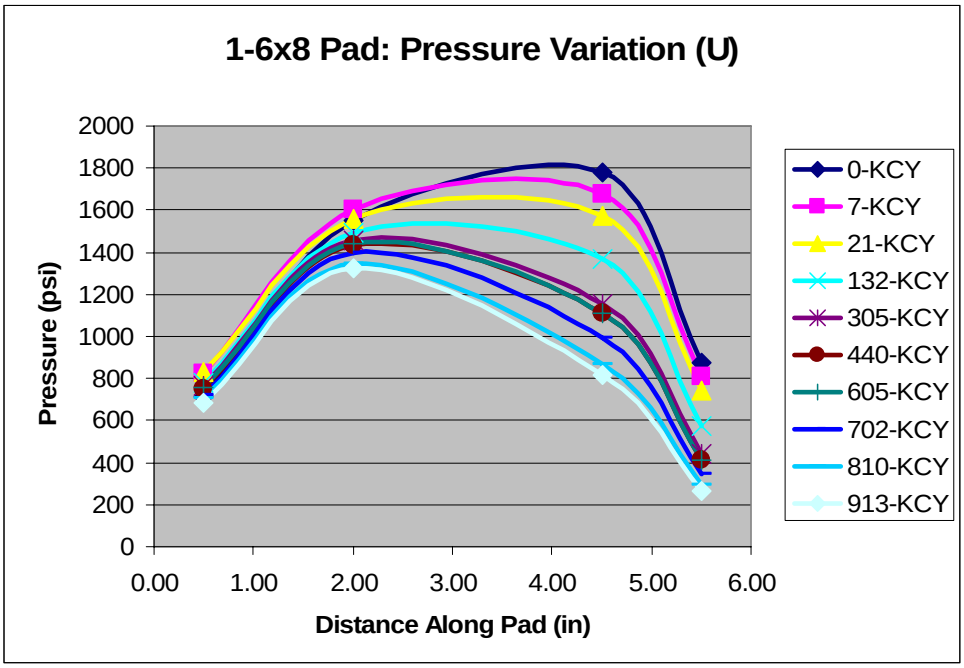

a) Pressure Variation Across the Pad at the Highest Displacement Amplitude

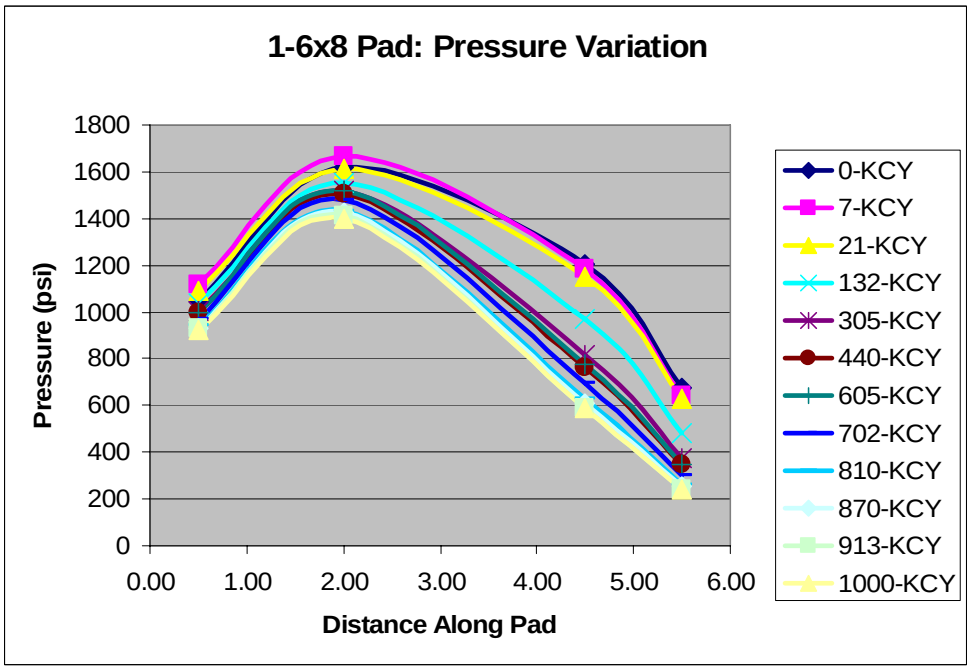

b) Pressure Variation Across the Pad at the Lowest Displacement Amplitude

Figure 6.10. Pressure Variation for 1-6x8 Pad

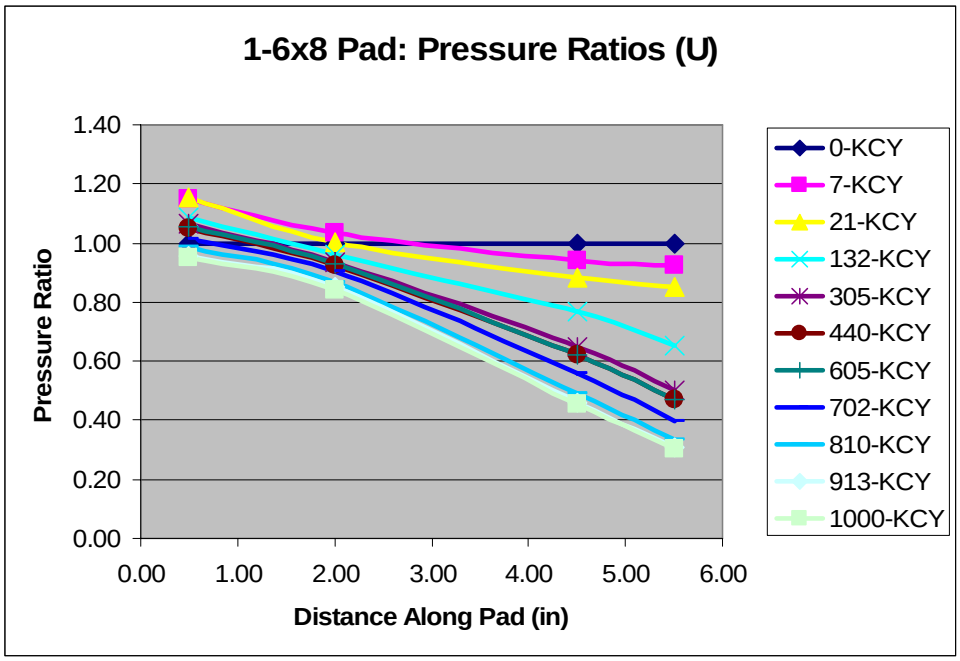

a) Pressure Ratio Variation Across the Pad at the Highest Displacement Amplitude

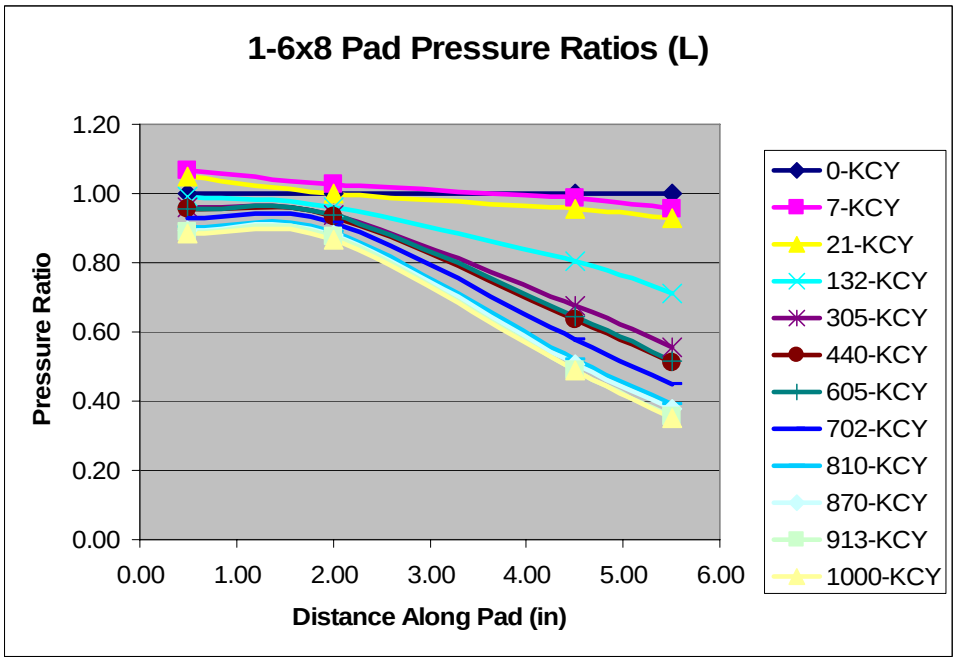

b) Pressure Ratio Variation Across the Pad at the Lowest Displacement Amplitude

Figure 6.11. Pressure Ratio Variation for 1-6x8 Pad

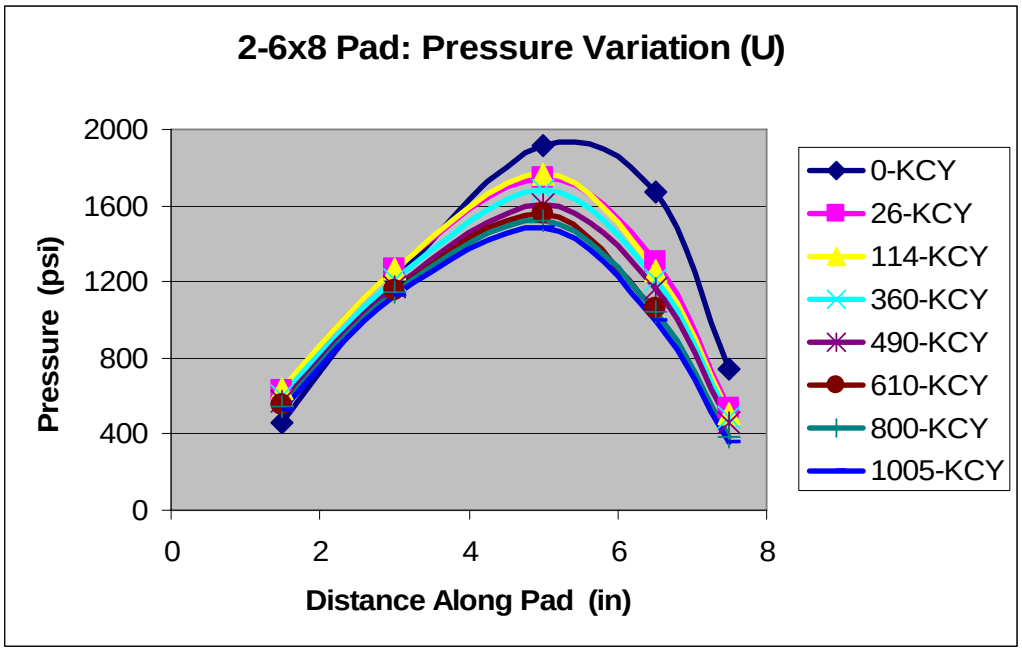

a) Pressure Variation Across the Pad at the Highest Displacement Amplitude

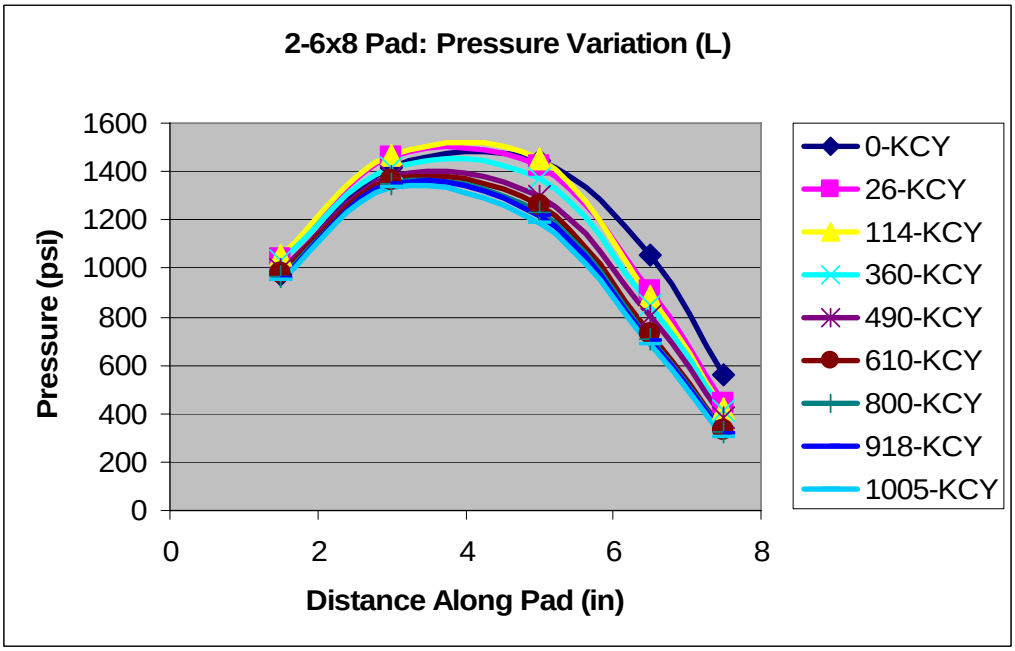

b) Pressure Ratio Variation Across the Pad at the Lowest Displacement Amplitude

Figure 6.12. Pressure Variation for 2-6x8 Pad

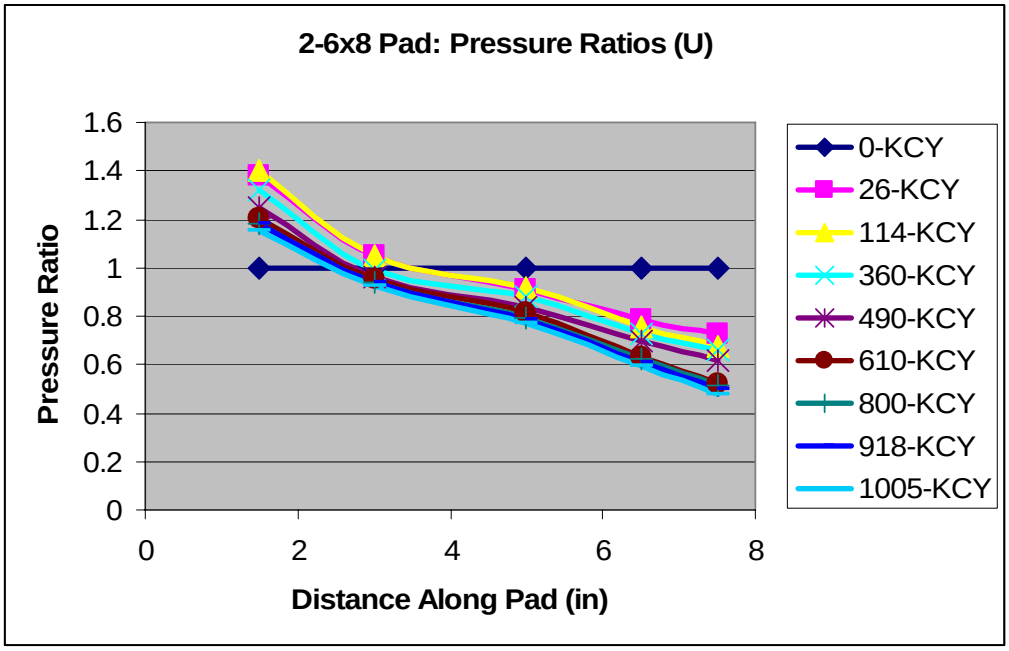

a) Pressure Ratio Variation Across the Pad at the Highest Displacement Amplitude

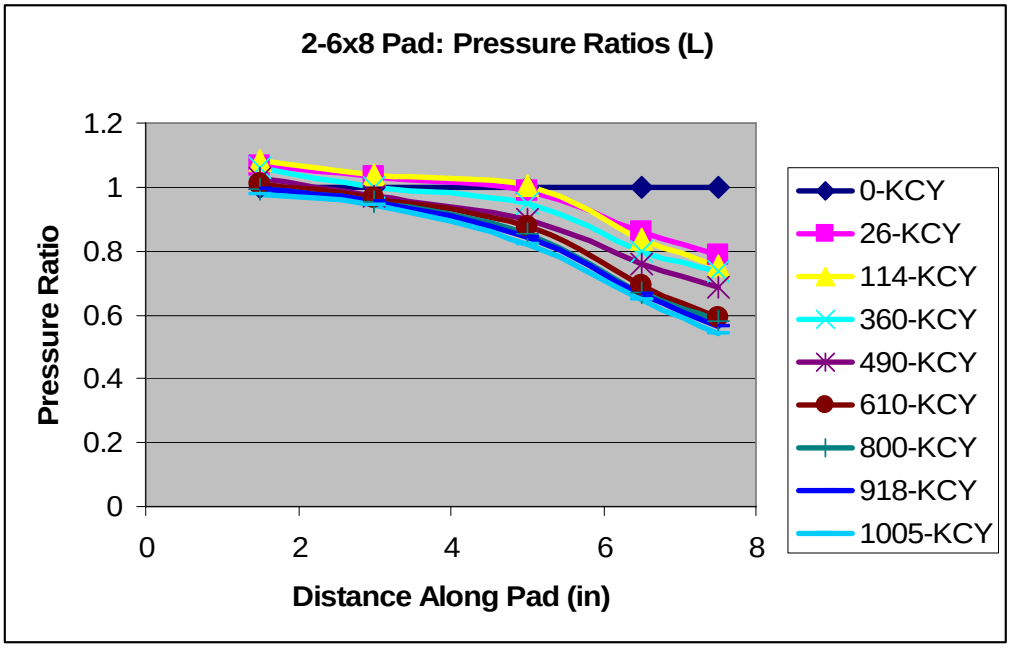

b) Pressure Ratio Variation Across the Pad at the Lowest Displacement Amplitude

Figure 6.13. Pressure Ratio Variation for 2-6x8 Pad

For the results presented in Figures 6.4 through 6.13, “highest displacement amplitude” means when the rotation is the smallest, that is, when the rotating actuator is at its highest point. The “lowest displacement amplitude” means the largest rotational angle, that is the rotating actuator is at it lowest point during the cyclic loading.

The sensor readings were taken after different number of load cycles for the different samples. This was due to the fact that there were a lot of data generated during the testing, thus it was not feasible to record all the data. Instead the recording trigger was activated manually. With records at different number of load cycles it does not make sense to average the results. However, as it can be seen from all the plots, the tendency is very similar across samples of the same size.

As it can be observed in the pressure ratio plots, such as Figure 6.9, at a lower number of load cycles the pressure ratio is close to unity across the length of the pad. At higher number of load cycles such as 918-KCY and 1000-KCY in Figure 6.7 the stress ratio approaches zero at the sloping end of the pad. This phenomenon is very similar (with some degree of quantitative difference) across all the samples tested.

From these observations it can be concluded that in a combined axial compression and rotation, the failure of the pad is limited to the end of the pad with the highest compression strains. This conclusion is supported by the fact that there is very little shift of the plotted curves as the number of load cycles increases beyond the load cycles causing end wedge failure.

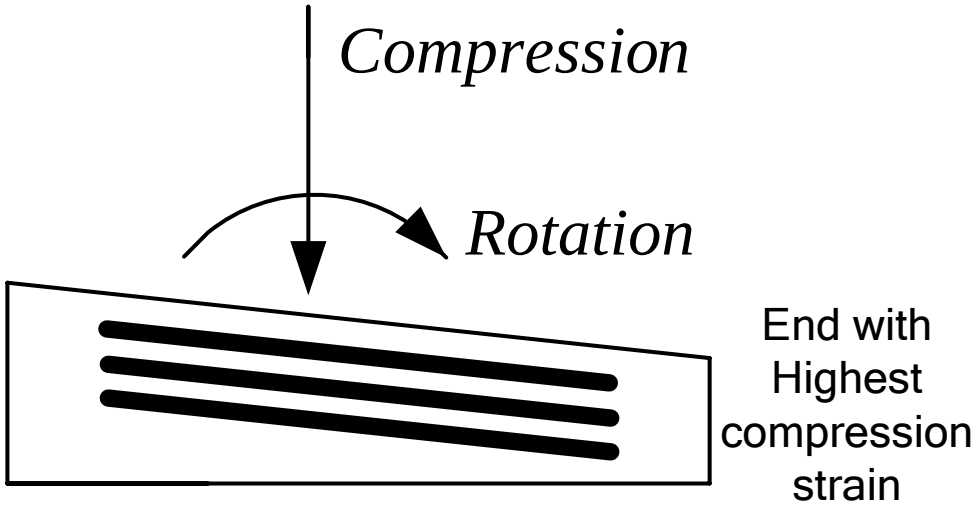

Figure 6.13a : Definition of Sloping End

Finite Element Analysis Results

It is important to recall that the finite element analysis was limited to one cycle of loading and not fatigue. Presented below are some selected plots of the finite element analysis results

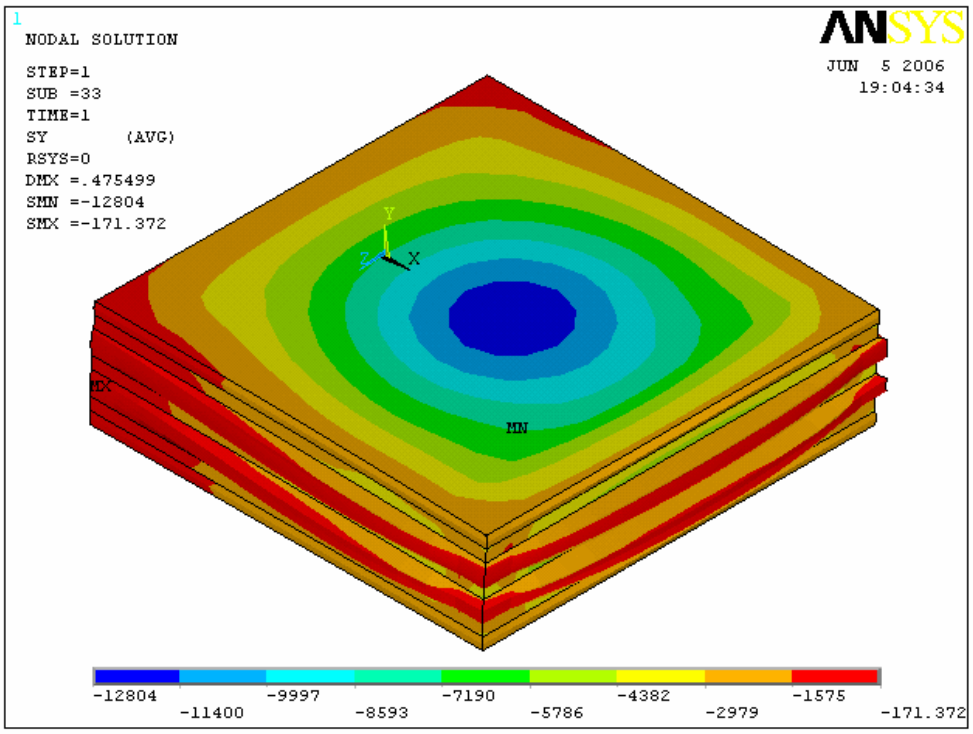

Figure 6.14: Typical Normal Stress Sy Distribution in the Multilayers of the Bearing Pad for 0.5 degree rotation angle

From the results above one can observe the fact that there is a core at the middle where the stresses are the highest. Moreover, the elastomer layers are bulging in the lower end of the rotation just as was evidenced in the test samples.

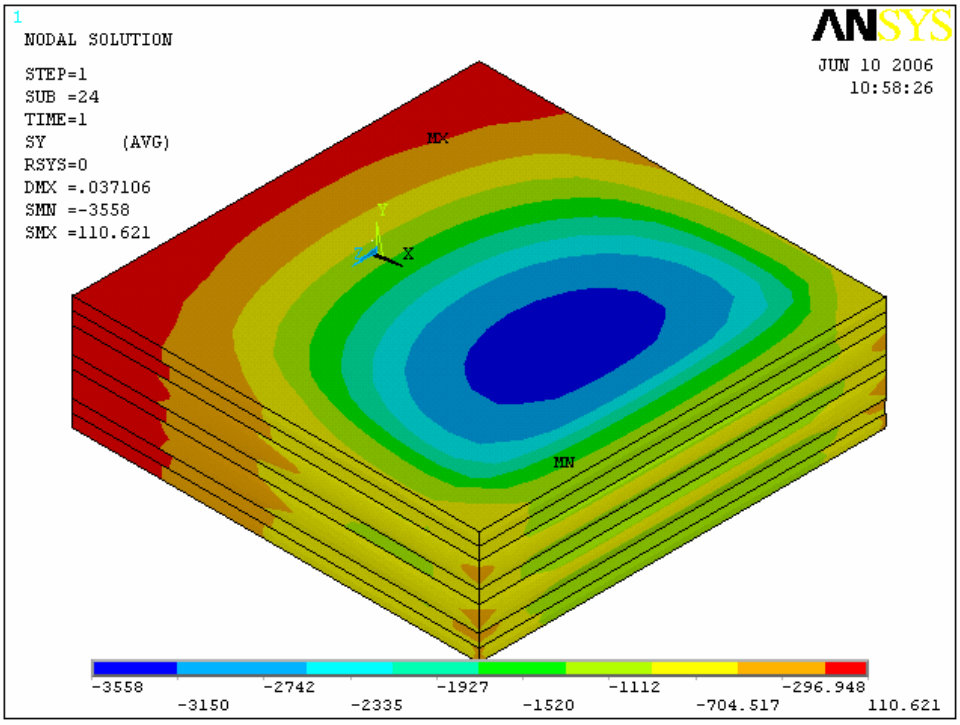

Figure 6.15: Typical Normal Stress Sy Distribution in the Multilayers of the Bearing Pad for high rotation angle

From the results above one can observe the fact that the high compressive stress core moves toward the end with the high compression strains. This behavior is in agreement with the experimental results, i.e., failure that was limited to the end with the highest compression strains.

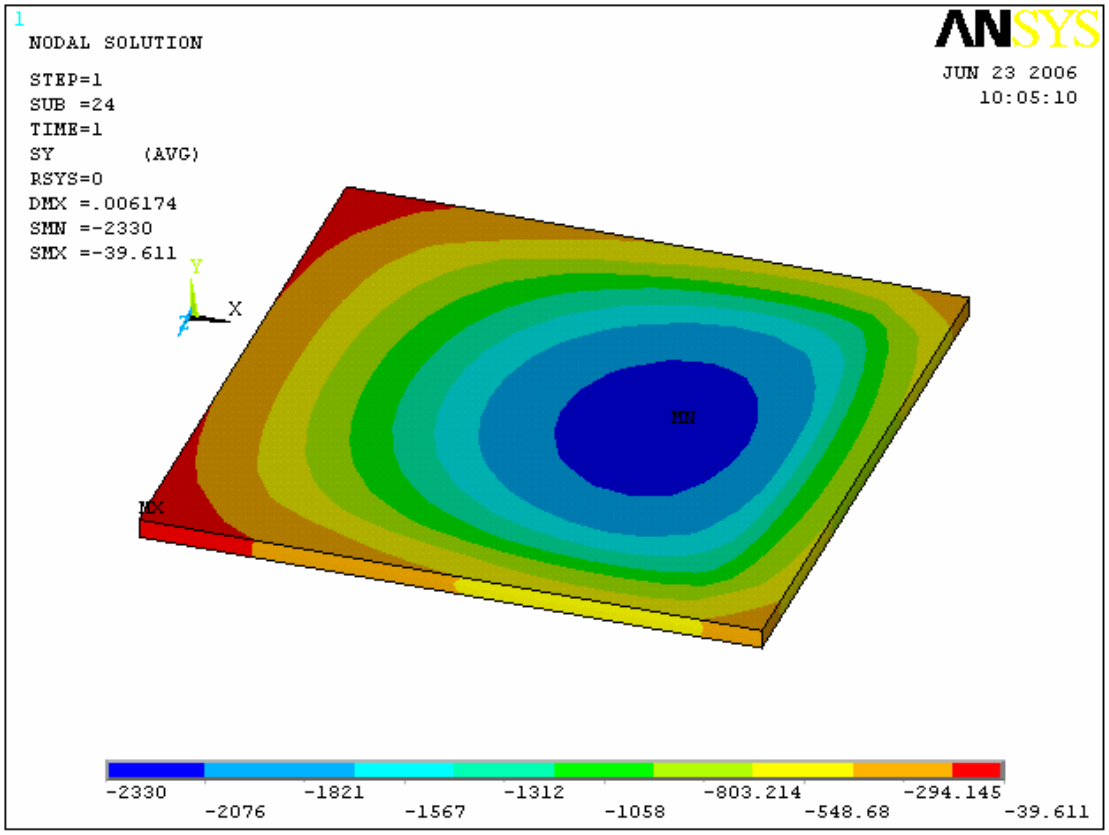

Figure 6.16: Normal Stress Sy Distribution in the Bottom Elastomer Layer for 1-degree Rotation

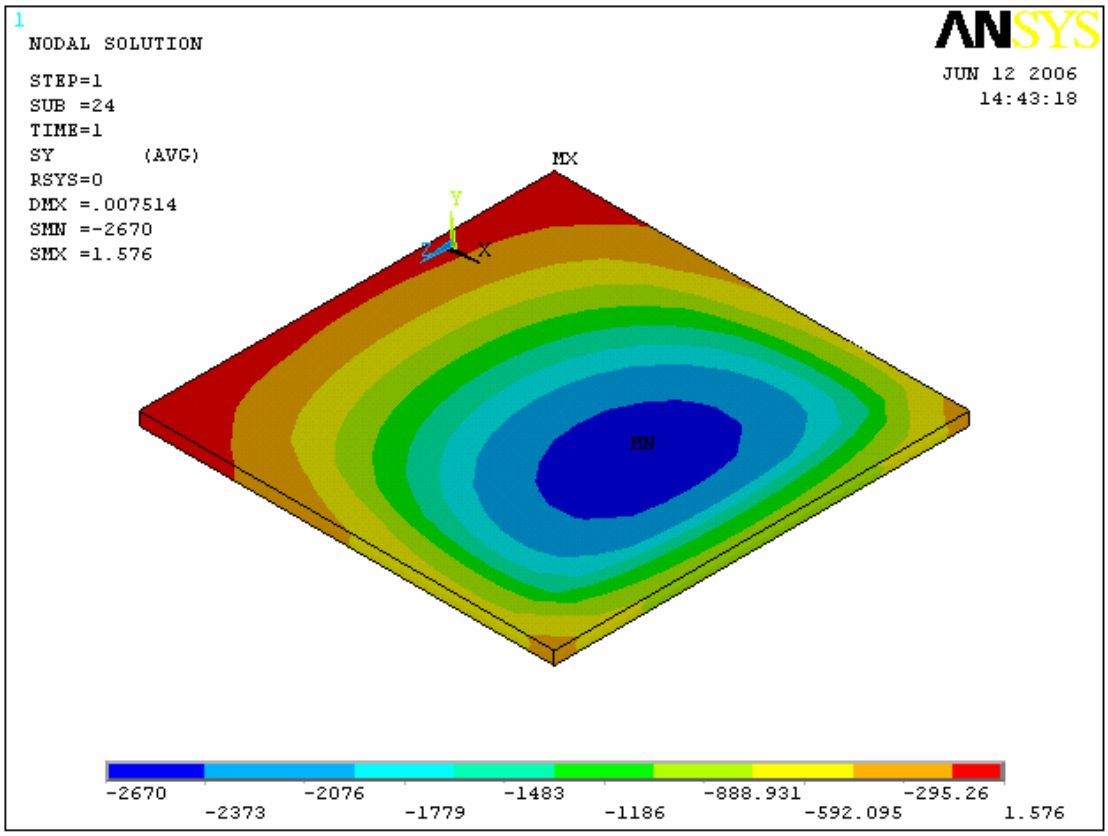

Figure. 6.17: Normal Stress Sy Distribution in the Bottom Elastomer Layer for 1.5-degree Rotation

Presented in Figure 6.18 is a plot of the pressure variation across a 8x8 Pad as measured by the bottom sensors at the initial load cycles and the FEA computed stresses at the same locations. As it can be observed in this plot there is a good agreement between the experimental and the analytical results.

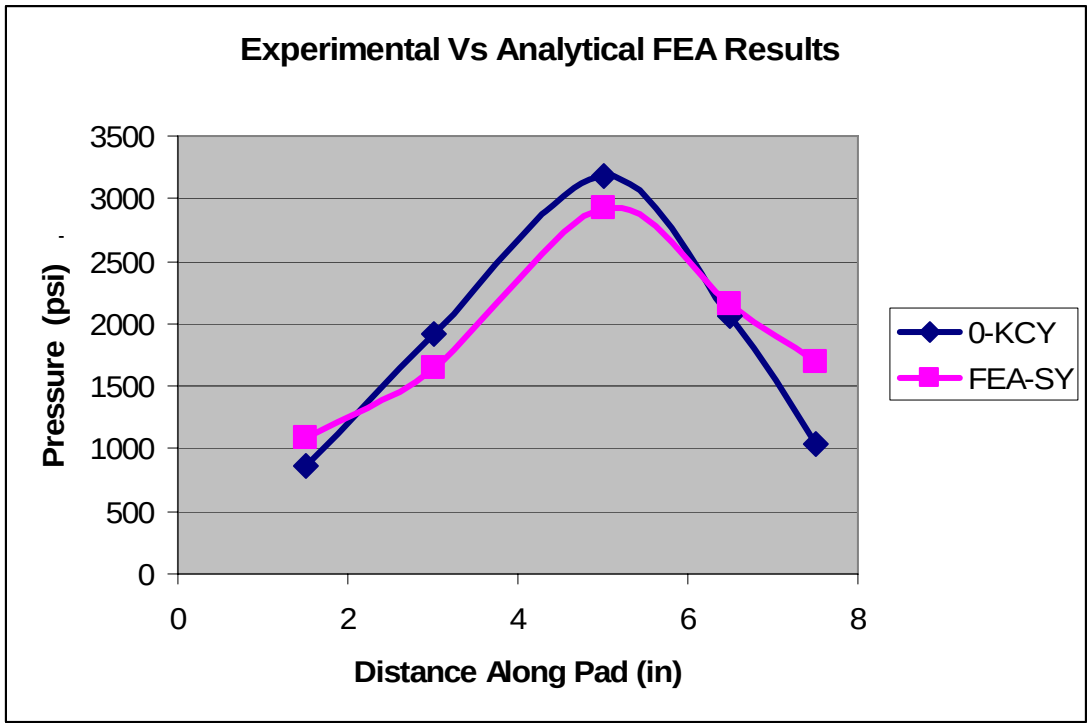

Figure 6.18: Pressure Variation in a 8x8 Pad Experimental Vs FEA Results

CHAPTER 7: NEW ROTATIONAL BEARIN PAD DESIGN FORMULAE

Presented below is the rationale for the proposed bearing pad design formulation

(Next 17 pages of a MATHCAD Document)

DERIVED CUSTOM UNITS

Elastomer Material Properties

Gent presented a table of material properties, which includes the shear modulus G, Young's modulus E0 and the material compressibility coefficient. The material compressibility coefficient is an empirically determined material property, which is included to correct for experimental deviation from theoretical equations

Number of data points $j := 0 .. 9$

Shear Modulus (MPa) $GG_j :=$	Young's Modulus (MPa) $E0_j :=$	Material Compressibility coefficient $\phi G_j :=$
0.296·MPa	0.896·MPa	0.93
0.365·MPa	1.158·MPa	0.89
0.441·MPa	1.469·MPa	0.85
0.524·MPa	1.765·MPa	0.80
0.621·MPa	2.137·MPa	0.73
0.793·MPa	3.172·MPa	0.64
1.034·MPa	4.344·MPa	0.57
1.344·MPa	5.723·MPa	0.54
1.689·MPa	7.170·MPa	0.53
2.186·MPa	9.239·MPa	0.52

Best Fit line parameters between G and E

$\alpha := \text{slope}(GG, E0)$ $\quad c := \text{intercept}(GG, E0)$

$\alpha = 4.515$ $\quad c = -0.488\,\text{MPa}$ $\quad c = -0.071\,\text{ksi}$

$E0_p(G) := \alpha \cdot G + c$

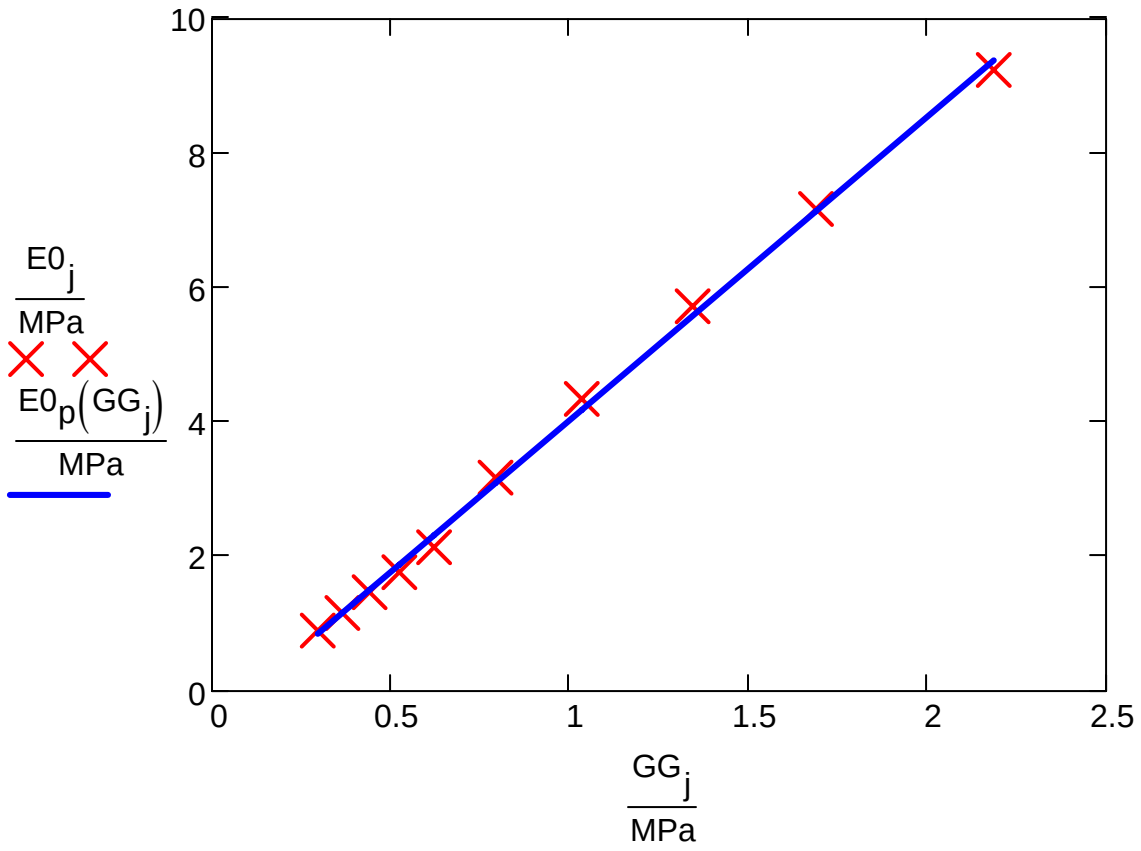

Fig. 7.1 Gent Data and Corresponding Predictor Equation of E_0 Given Shear Modulus G

Thus in computations the following expressions will be used

$E_0 = 4.515 \cdot G - 0.488 \cdot MPa$ where G is in MPa (for SI units)

$E_0 = 4.515 \cdot G - 0.071 \cdot ksi$ where G is in ksi (for US customary units)

Best Fit line parameters between G and ϕ

Hyperbolic function will be a better fit

$hG_j := \frac{1}{GG_j}$

$\alpha_\phi := slope(hG, \phi G)$ $\alpha_\phi = 0.16\,MPa$ $\alpha_\phi = 0.023\,ksi$

$c_\phi := intercept(hG, \phi G)$ $c_\phi = 0.445$ $\phi G_p(G) := \frac{\alpha_\phi}{G} + c_\phi$

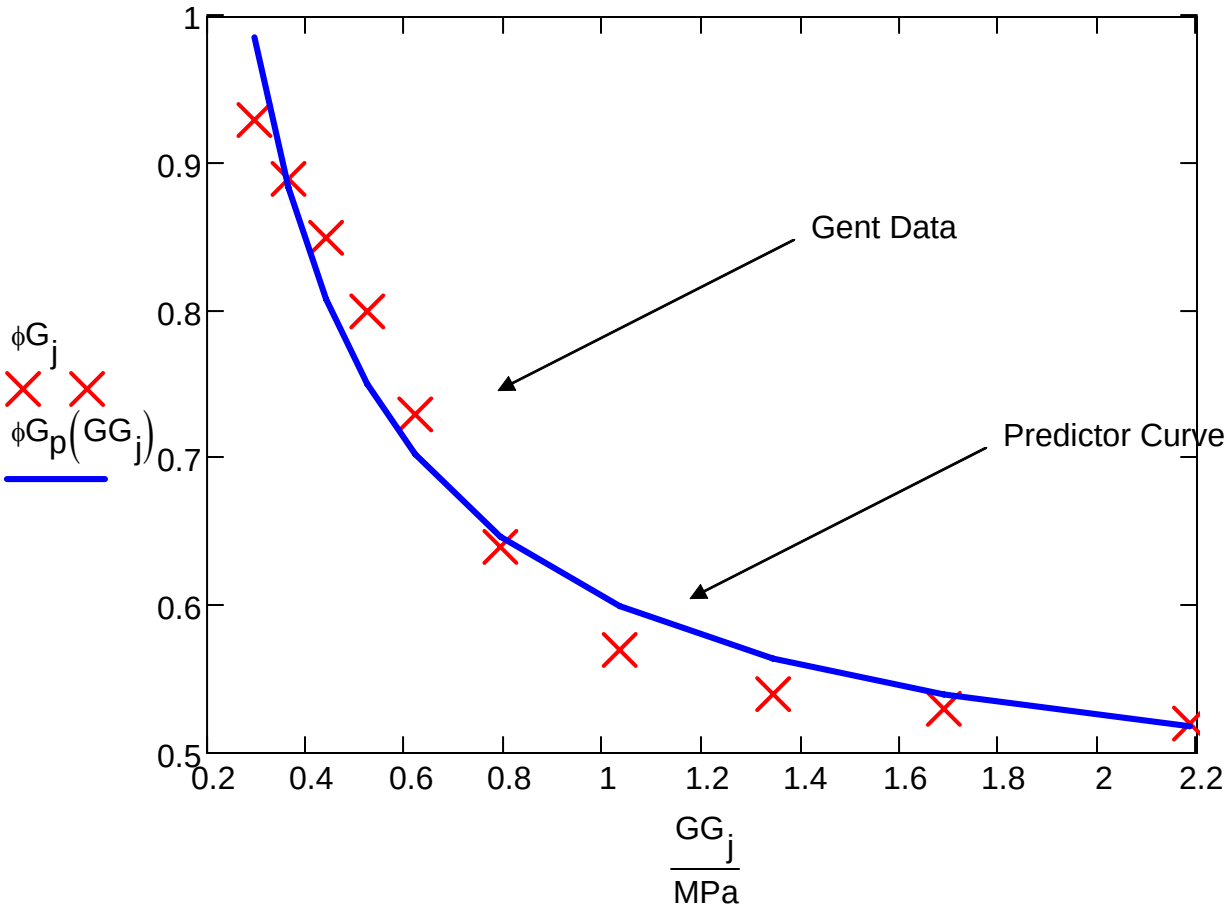

Fig. 7.2 Gent Data and Corresponding Predictor Equation of ϕ Given Shear Modulus G

Thus in computations the following expressions will be used

$$\phi = 0.445 + \frac{0.16 \cdot MPa}{G}$$ where G is in MPa (for SI units)

$$\phi = 0.445 + \frac{0.023 \cdot ksi}{G}$$ where G is in ksi (for US customary units)

For Example an 8 x 8 Bearing Pad

Dimension perpendicular to axis of rotation (length of pad)	$B := 8 \cdot in$
Dimension parallel to axis of rotation (width of pad)	$W := 8 \cdot in$
Thickness of elastomer layer	$h_{ri} := 0.5 \cdot in$
Shear modulus value	$G := 0.12 \cdot ksi$

Bearing shape factor

$$S := \frac{B \cdot W}{2 \cdot h_{ri} \cdot (B + W)} \qquad S = 4$$

$$E_0 := (4.515 \cdot G - 0.488 \cdot MPa) \qquad E_0 = 0.471\,ksi$$

$$\phi := 0.445 + \frac{0.16 \cdot MPa}{G} \qquad \phi = 0.638$$

Effective compression modulus, in accordance with Gent is given as:

$$E_c := E_0 \cdot \left(1 + 2 \cdot \phi \cdot S^2\right) \qquad E_c = 10.09\,ksi$$

According to AASHTO the bearing capacity for a case without rotation is given as

Pure Compression $P_{\alpha 0} = 1.66 \cdot G \cdot S \cdot A$ *[AASHTO Eq. 14.7.5.3.2-1]*

The average axial strain in the case of pure compression can be expressed as

$$\varepsilon_{\alpha 0} = \frac{P_{\alpha 0}}{A \cdot E_c} = \frac{1.66 \cdot G \cdot S}{E_c}$$

For the sample pad (8x8)

$$\varepsilon_{\alpha 0} := \frac{1.66 \cdot G \cdot S}{E_c} \qquad \varepsilon_{\alpha 0} = 0.079$$

As per experimental results and supported by the analytical studies as the rotation increases the extreme end towards which the maximum compressive strain takes place reveals a decrease in vertical pressure.

In the experimental work this zone of reduced pressure was found to have failed in shear. In developing the new formula we are going to neglect this failed zone and treat the pad as a pad of reduced size.

Thus any point with strains exceeding $\varepsilon_{\alpha 0}$ will be considered as a failed part

Capacity with a pad subjected to axial loading and rotation

Strain due to the axial loading

$$\varepsilon_c = \frac{P}{A \cdot E_c}$$

The permissible rotation depends on the vertical strain

Strain reserved for rotation

$$\varepsilon_r = \varepsilon_{\alpha 0} - \varepsilon_c$$

Also $\varepsilon_r = \frac{x_r \cdot \theta}{h_{ri}}$ Thus $\frac{x_r \cdot \theta}{h_{ri}} = \varepsilon_{\alpha 0} - \varepsilon_c$

Which gives $x_r = \left(\varepsilon_{\alpha 0} - \varepsilon_c\right) \cdot \frac{h_{ri}}{\theta} \le \frac{B}{2}$

The new B dimension of the Pad will now be

$$B_{nw} = \frac{B}{2} + x_r$$

For example for the 8x8 pad $A := B \cdot W$ $A = 64\,in^2$

Axial load $P := 0 \cdot kip$ Rotation $\theta := 2 \cdot deg$

$$\varepsilon_c := \frac{P}{A \cdot E_c}$$

$$x_r := \begin{cases} \frac{B}{2} & \text{if } \theta = 0 \\ \left(\varepsilon_{\alpha 0} - \varepsilon_c\right) \cdot \frac{h_{ri}}{\theta} & \text{otherwise} \end{cases} \qquad x_r = 1.131\,in$$

$x_r := \text{if}\left(x_r > \frac{B}{2}, \frac{B}{2}, x_r\right)$ $x_r = 1.131\,in$

$x_r := \text{if}\left(x_r < -\frac{B}{2}, -\frac{B}{2}, x_r\right)$ $x_r = 1.131\,in$

Reduced pad dimension $B_{nw} := \frac{B}{2} + x_r$ $B_{nw} = 5.131\,in$

Shape factor for reduced pad

$$S_{nw} := \frac{B_{nw} \cdot W}{2 \cdot h_{ri} \cdot (B + W)} \qquad S_{nw} = 2.57$$

$A_{nw} := B_{nw} \cdot W$ $A_{nw} = 41.046\,in^2$

$P_{\alpha\theta} := 1.66 \cdot G \cdot S_{nw} \cdot A_{nw}$ $P_{\alpha\theta} = 21\,kip$ $\theta = 2\,deg$

$P_{\alpha 0} := 1.66 \cdot G \cdot S \cdot A$ $P_{\alpha 0} = 51\,kip$

Proposed Florida Design Process for Bearings with Rotation

STEP 1: Compute the Young's modulus of the elastomer from the material shear modulus **G** using the following relationship

$E_0 = 4.515 \cdot G - 0.488 \cdot MPa$ where G is in MPa (for SI units)

$E_0 = 4.515 \cdot G - 0.071 \cdot ksi$ where G is in ksi (for US customary units)

STEP 2: Compute the shape factor using the following relationship

$$S := \frac{B \cdot W}{2 \cdot h_{ri} \cdot (B + W)}$$

STEP 3: Compute the material compressibility coefficient using the following relationship

$$\phi = 0.445 + \frac{0.16 \cdot MPa}{G}$$ where G is in MPa (for SI units)

$$\phi = 0.445 + \frac{0.023 \cdot ksi}{G}$$ where G is in ksi (for US customary units)

STEP 4: Compute the effective compression modulus using the following relationship

$$E_c := E_0 \cdot \left(1 + 2 \cdot \phi \cdot S^2\right)$$

STEP 5: Compute the reduced dimension the pad due to rotation effect using the following relationship

$$B_{nw} = \frac{B \cdot E_c \cdot \theta + 1.66 \cdot G \cdot S \cdot h_{ri}}{2 \cdot E_c \cdot \theta} \leq B$$

That is

$$B_{nw} := \begin{cases} B & \text{if } \theta = 0 \\ \dfrac{B \cdot E_c \cdot \theta + 1.66 \cdot G \cdot S \cdot h_{ri}}{2 \cdot E_c \cdot \theta} & \text{otherwise} \end{cases}$$

and

$$B_{nw} := \text{if}\left(B_{nw} > B, B, B_{nw}\right)$$

STEP 6: Compute the shape factor for the reduced dimension of the pad using the following relationship

$$S_{nw} := \frac{B_{nw} \cdot W}{2 \cdot h_{ri} \cdot \left(B_{nw} + W\right)}$$

STEP 7: Compute the capacity of the bearing pad using the following relationship

$$P_{\theta} := 1.66 \cdot G \cdot S_{nw} \cdot A_{nw}$$

where $A_{nw} = B_{nw} \cdot W$

Specification Changes

Thus, the write up for the new formulation will be as follows:

$$P_{\theta} := 1.66 \cdot G \cdot S_{nw} \cdot A_{nw}$$

where

A_{nw} the area of the reduced pad area equal to $B_{nw} \cdot W$

S_{nw} the shape factor of the reduced pad size.

$$S_{nw} := \frac{B_{nw} \cdot W}{2 \cdot h_{ri} \cdot \left(B_{nw} + W\right)}$$

$$B_{nw} := \begin{cases} B & \text{if } \theta = 0 \\ \dfrac{B \cdot E_c \cdot \theta + 1.66 \cdot G \cdot S \cdot h_{ri}}{2 \cdot E_c \cdot \theta} & \text{otherwise} \end{cases}$$

$$B_{nw} := \text{if}\left(B_{nw} > B, B, B_{nw}\right)$$

$E_c := E_0 \cdot \left(1 + 2 \cdot \phi \cdot S^2\right)$ is the effective compression modulus

$E_0 = 4.515 \cdot G - 0.488 \cdot MPa$ where G is in MPa (for SI units)

$E_0 = 4.515 \cdot G - 0.071 \cdot ksi$ where G is in ksi (for US customary units)

S in the shape factor of the pad.

$$S := \frac{B \cdot W}{2 \cdot h_{ri} \cdot (B + W)}$$

$\phi = 0.445 + \frac{0.16 \cdot MPa}{G}$ where G is in MPa (for SI units)

$\phi = 0.445 + \frac{0.023 \cdot ksi}{G}$ where G is in ksi (for US customary units)

Comparison of proposed formulation to the existing AASHTO formulation

Pad Size 10 by 8

$k := 0 .. 6$

$\theta_k :=$

0·deg
0.25·deg
0.50·deg
0.75·deg
1.0·deg
1.5·deg
2.0·deg

Material

$G := 0.12 \cdot ksi$

$B := 10 \cdot in$

$W := 8 \cdot in$

$S := \frac{B \cdot W}{2 \cdot h_{ri} \cdot (B + W)}$ $S = 4.444$

$A := B \cdot W$ $A = 80\,in^2$

$E_0 := (4.515 \cdot G - 0.488 \cdot MPa)$ $E_0 = 0.471\,ksi$

$\phi := 0.445 + \frac{0.16 \cdot MPa}{G}$ $\phi = 0.64$

Compute effective compressive modulus $E_c := E_0 \cdot \left(1 + 2 \cdot \phi \cdot S^2\right)$ $E_c = 12.35\,ksi$

Compute reduced B dimension

$$B_{nw_k} := \begin{cases} B & \text{if } \theta_k = 0 \\ \dfrac{B \cdot E_c \cdot \theta_k + 1.66 \cdot G \cdot S \cdot h_{ri}}{2 \cdot E_c \cdot \theta_k} & \text{otherwise} \end{cases}$$

$B_{nw_k} := \text{if}\left(B_{nw_k} > B, B, B_{nw_k}\right)$

Compute modified shape factor $S_{nw_k} := \frac{B_{nw_k} \cdot W}{2 \cdot h_{ri} \cdot \left(B_{nw_k} + W\right)}$ $A_{nw_k} := B_{nw_k} \cdot W$

Pad capacity using proposed formulation $P_{\theta_k} := 1.66 \cdot G \cdot S_{nw_k} \cdot A_{nw_k}$

$$n := 2$$

Pad capacity using existing AASHTO formulation

$$P_{AASHTO_k} := A \cdot \left[1.875 \cdot G \cdot S \cdot \left[1 - 0.200 \cdot \left(\frac{\theta k}{n} \right) \cdot \left(\frac{B}{h_{ri}} \right)^2 \right] \right]$$

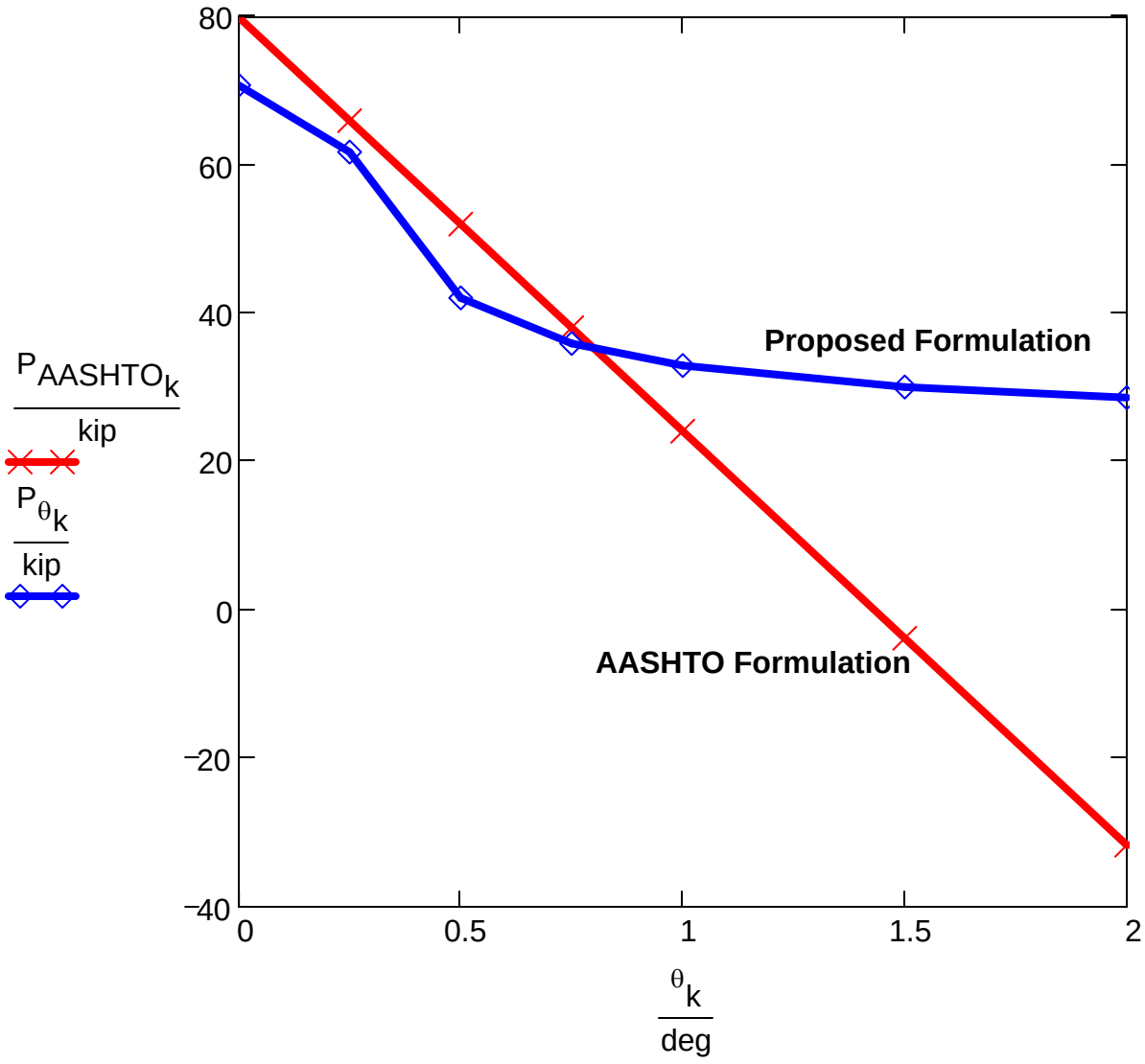

Fig. 7.3 Comparison of Proposed formulation to AASHTO Existing Formulation for a 10 by 8 Bearing Pad

Pad Size 12 by 8

Material $G := 0.12 \cdot ksi$

$B := 12 \cdot in$ $W := 8 \cdot in$

$S := \frac{B \cdot W}{2 \cdot h_{ri} \cdot (B + W)}$ $S = 4.8$

$A := B \cdot W$ $A = 96\,in^2$

$E_0 := (4.515 \cdot G - 0.488 \cdot MPa)$ $E_0 = 0.471\,ksi$

$\phi := 0.445 + \frac{0.16 \cdot MPa}{G}$ $\phi = 0.64$

Compute effective compressive modulus $E_c := E_0 \cdot \left(1 + 2 \cdot \phi \cdot S^2\right)$ $E_c = 14.327\,ksi$

Compute reduced B dimension

$$B_{nw_k} := \begin{cases} B & \text{if } \theta_k = 0 \\ \frac{B \cdot E_c \cdot \theta_k + 1.66 \cdot G \cdot S \cdot h_{ri}}{2 \cdot E_c \cdot \theta_k} & \text{otherwise} \end{cases}$$

$B_{nw_k} := \text{if}\left(B_{nw_k} > B, B, B_{nw_k}\right)$

Compute modified shape factor $S_{nw_k} := \frac{B_{nw_k} \cdot W}{2 \cdot h_{ri} \cdot \left(B_{nw_k} + W\right)}$ $A_{nw_k} := B_{nw_k} \cdot W$

Pad capacity using proposed formulation $P_{\theta_k} := 1.66 \cdot G \cdot S_{nw_k} \cdot A_{nw_k}$

$n := 2$

Pad capacity using existing AASHTO formulation

$$P_{AASHTO_k} := A \cdot \left[1.875 \cdot G \cdot S \cdot \left[1 - 0.200 \cdot \left(\frac{\theta_k}{n} \right) \cdot \left(\frac{B}{h_{ri}} \right)^2 \right] \right]$$

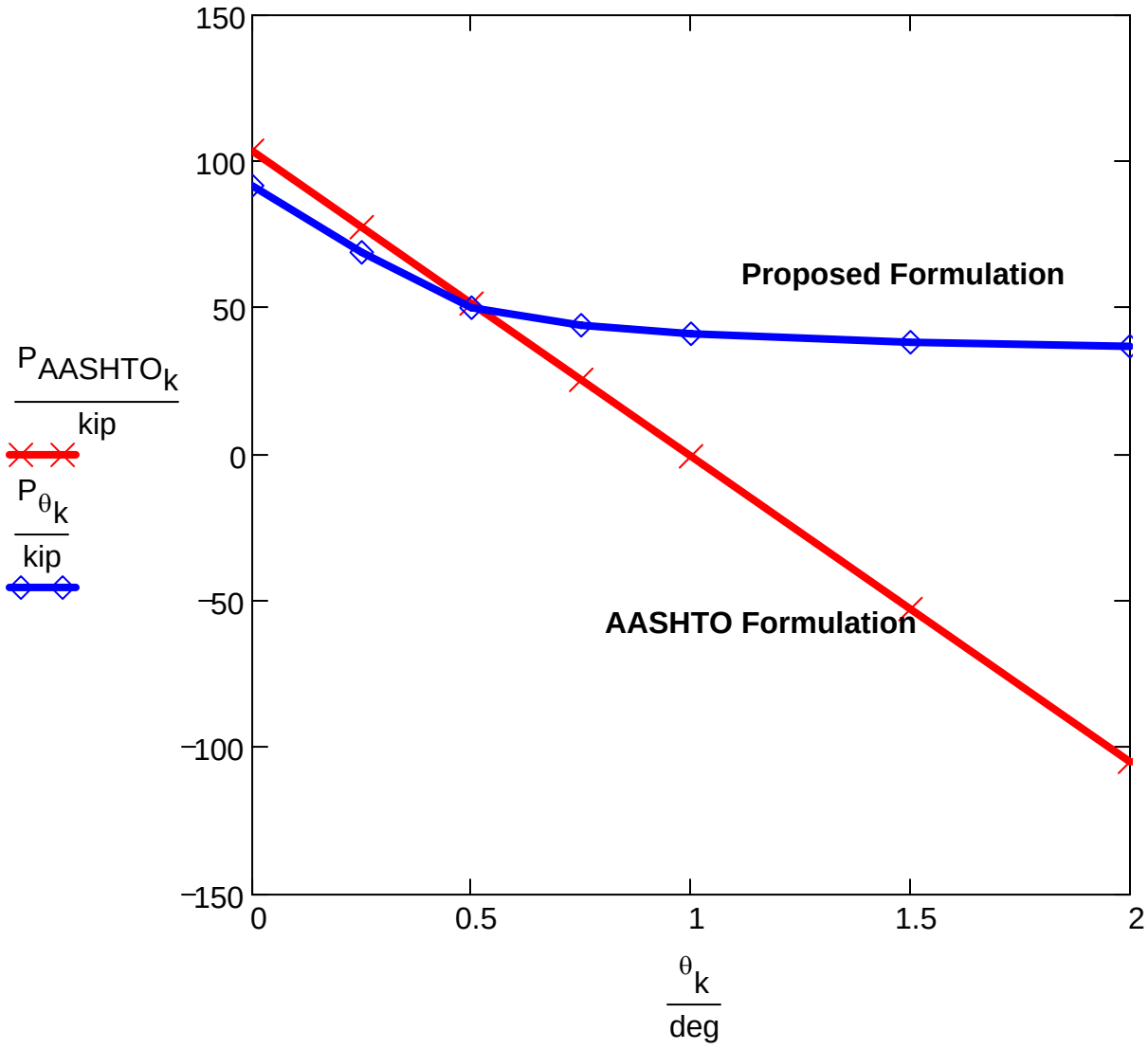

Fig. 7.4 Comparison of Proposed formulation to AASHTO Existing Formulation for a 12 by 8 Bearing Pad

Pad Size 20 by 20

Material

$G := 0.12 \cdot ksi$

$B := 20 \cdot in$

$W := 20 \cdot in$

$S := \frac{B \cdot W}{2 \cdot h_{ri} \cdot (B + W)}$

$S = 10$

$A := B \cdot W$

$A = 400\,in^2$

$E_0 := (4.515 \cdot G - 0.488 \cdot MPa)$

$E_0 = 0.471\,ksi$

$\phi := 0.445 + \frac{0.16 \cdot MPa}{G}$

$\phi = 0.64$

Compute effective compressive modulus

$E_c := E_0 \cdot \left(1 + 2 \cdot \phi \cdot S^2\right)$

$E_c = 60.61\,ksi$

Compute reduced B dimension

$$B_{nw_k} := \begin{cases} B & \text{if } \theta_k = 0 \\ \frac{B \cdot E_c \cdot \theta_k + 1.66 \cdot G \cdot S \cdot h_{ri}}{2 \cdot E_c \cdot \theta_k} & \text{otherwise} \end{cases}$$

$B_{nw_k} := \text{if}\left(B_{nw_k} > B, B, B_{nw_k}\right)$

Compute modified shape factor

$S_{nw_k} := \frac{B_{nw_k} \cdot W}{2 \cdot h_{ri} \cdot \left(B_{nw_k} + W\right)}$

$A_{nw_k} := B_{nw_k} \cdot W$

Pad capacity using proposed formulation

$P_{\theta_k} := 1.66 \cdot G \cdot S_{nw_k} \cdot A_{nw_k}$

$n := 2$

Pad capacity using existing AASHTO formulation

$$P_{AASHTO_k} := A \cdot \left[1.875 \cdot G \cdot S \cdot \left[1 - 0.200 \cdot \left(\frac{\theta k}{n} \right) \cdot \left(\frac{B}{h_{ri}} \right)^2 \right] \right]$$

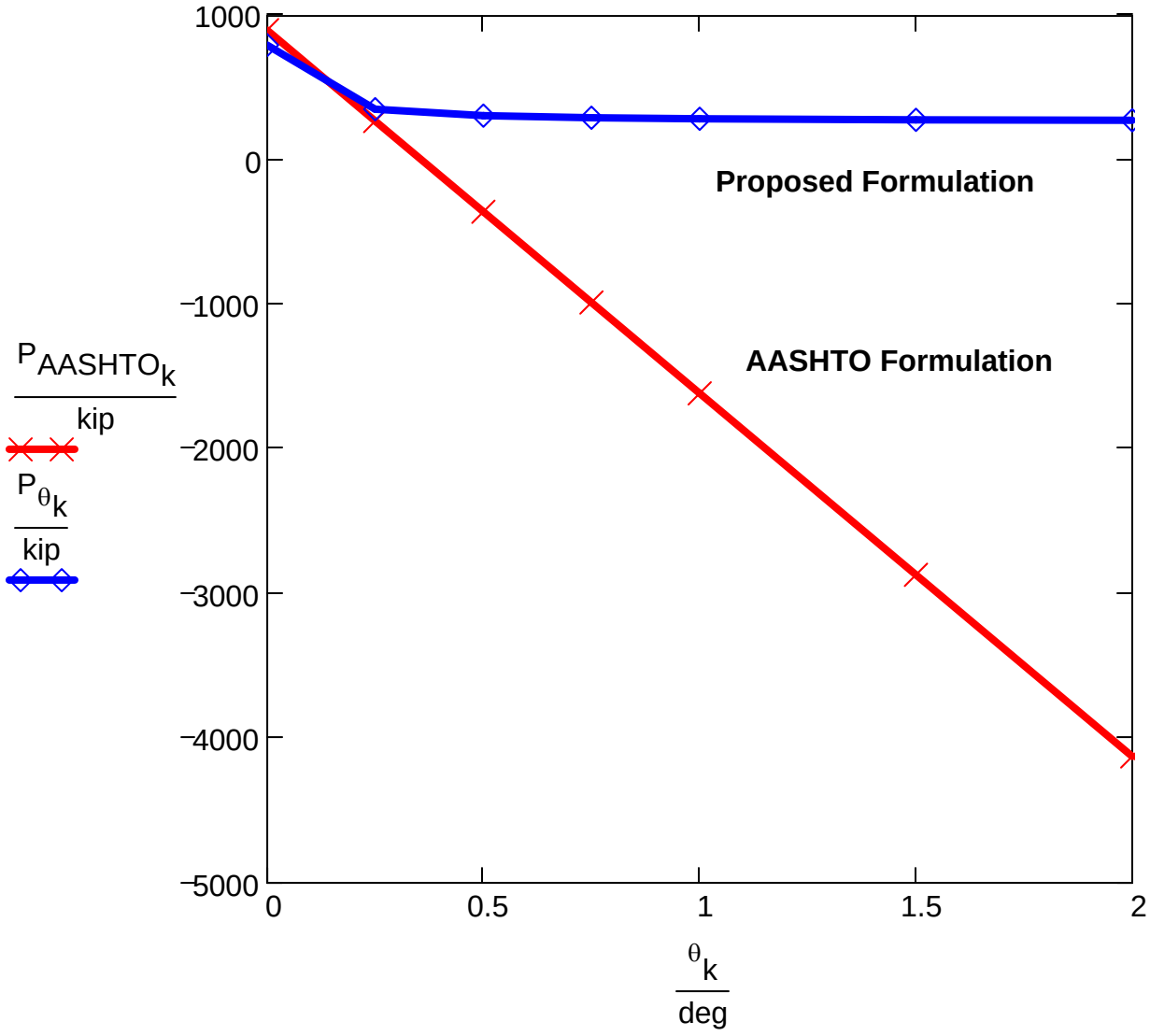

Fig. 7.5 Comparison of Proposed formulation to AASHTO Existing Formulation for a 20 by 20 Bearing Pad

Pad Size 8 by 8

Material

$G := 0.12 \cdot ksi$

$B := 8 \cdot in$

$W := 8 \cdot in$

$S := \frac{B \cdot W}{2 \cdot h_{ri} \cdot (B + W)}$

$S = 4$

$A := B \cdot W$

$A = 64\,in^2$

$E_0 := (4.515 \cdot G - 0.488 \cdot MPa)$

$E_0 = 0.471\,ksi$

$\phi := 0.445 + \frac{0.16 \cdot MPa}{G}$

$\phi = 0.64$

Compute effective compressive modulus

$E_c := E_0 \cdot \left(1 + 2 \cdot \phi \cdot S^2\right)$

$E_c = 10.093\,ksi$

Compute reduced B dimension

$$B_{nw_k} := \begin{cases} B & \text{if } \theta_k = 0 \\ \dfrac{B \cdot E_c \cdot \theta_k + 1.66 \cdot G \cdot S \cdot h_{ri}}{2 \cdot E_c \cdot \theta_k} & \text{otherwise} \end{cases}$$

$B_{nw_k} := \text{if}\left(B_{nw_k} > B, B, B_{nw_k}\right)$

Compute modified shape factor

$S_{nw_k} := \frac{B_{nw_k} \cdot W}{2 \cdot h_{ri} \cdot \left(B_{nw_k} + W\right)}$

$A_{nw_k} := B_{nw_k} \cdot W$

Pad capacity using proposed formulation

$P_{\theta_k} := 1.66 \cdot G \cdot S_{nw_k} \cdot A_{nw_k}$

$n := 2$

Pad capacity using existing AASHTO formulation

$$P_{AASHTO_k} := A \cdot \left[1.875 \cdot G \cdot S \cdot \left[1 - 0.200 \cdot \left(\frac{\theta k}{n} \right) \cdot \left(\frac{B}{h_{ri}} \right)^2 \right] \right]$$

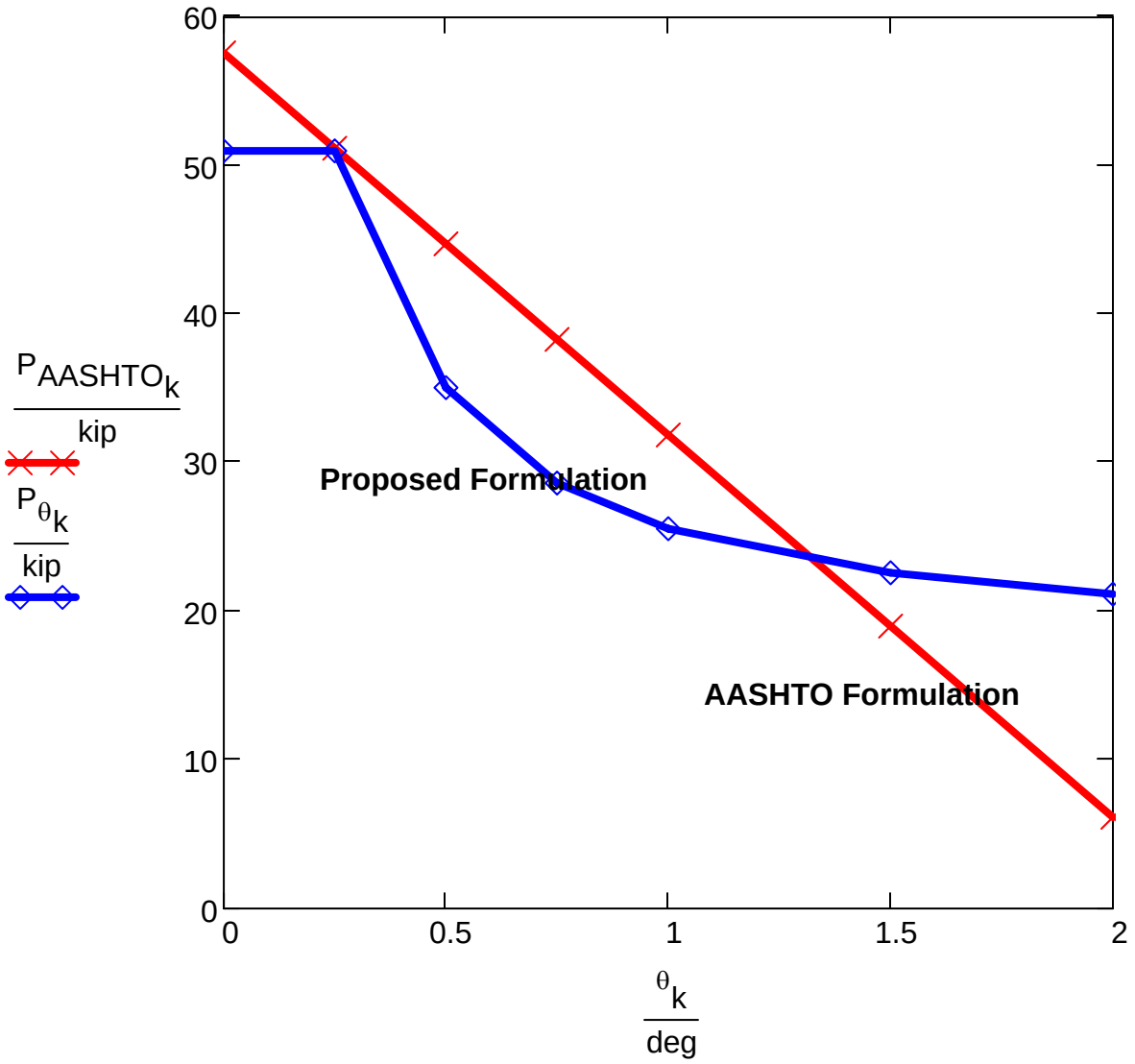

Fig. 7.6 Comparison of Proposed formulation to AASHTO Existing Formulation for a 8 by 8 Bearing Pad

ACKNOWLEDGMENT

Information presented in this paper is as a part of an ongoing project on “Combined Loading of Steel Reinforced Elastomeric Bridge Bearing Pads” been conducted under the sponsorship of the **Florida Department of Transportation**. This support is highly appreciated. In addition the authors would like to thank colleagues at the FL-DOT Structures Laboratory and at the FAMU-FSU College of Engineering for their positive criticism of the ongoing work. Special thanks goes to Mr. Tony Johnston for the fabrication of the testing facility. Mr Steve Eudy for handling all the electronics. Most of all Mr. Marcus Ansley for his patience . The opinions expressed in this paper are solely of the authors and in no way implicate the sponsors of this work.

REFERENCES

Bergstrom.J.S and. Boyce, M.C.2001." Constitutive modeling of the time-dependent and cyclic loading of elastomer and application to soft biological tissues", final version of this draft working paper is published in: Mechanics of Materials, Vol. 33, pp. 523-530.

Clark, Earl .V and Moultrap, K.1966 "load- deformation characteristics of elastomeric bearing pads". Highway Research record # 34, highway Research Board Washington, D.C.

Dawn.E.L, Roeder, C.W, Russel, L, and Kevin, C.2003. "Cotton duck Bearing Pad Engineering Evaluation and Design Recommendations". Departments of civil and Environmental engineering, Seattle Washington.

English, B.A, Klingner, R.E and Yura J.A.1994."Elastomeric bearing Background Information". Research Report 1304-1 Center of Transportation research Bureau of Engineering Research. Texas at Austin.

Euridice A. Oware." Numerical Examination of the Performance of Elastomeric Bearing Pads and Steel Rocker Bearings for Seismic Loads" Dept. of Civil Engineering, Washington University, St. Louis.

Jain, S.K, and Thakkar S.K.2002 "Quasi-static Testing of Laminated Rubber Bearings". Department of Earthquake Engineering at IIT.Roorkee

James M. Kelly "Analysis of Fiber-Reinforced Elastomeric Isolators". Earthquake Engineering Research Center, University of California, Berkeley

Kurt Miller from Axel Product Inc.2000 "Experimental Loading Conditions Used to Implement Hyper elastic and Plastic Material Models"

http://www.axelproduct.com

Muscarella J.V and Yura J.A, 1995 ”Experimental study of elastomeric bridge bearing with design recommendations”. Center of Transportation Research Texas University, Austin.

Muscarella, J.V and Yura, J.V.1996 ”An experimental study of flat and Tapered Elastomeric Bridge Bearing “. ACI Special Publications, Sp 164-6,pp 16

Ozell, A.M and Diniz, J.F, 1960.”Report on tests of the Neoprene pads under repeated shear load, National Research Council Washington, D.C

Pare, R.L and Kenner, E.P.1960 “elastomeric bridge bearing” highway Research board bulletin Highways Research Bulletin # 242 National Research Council Washington, D.C.

Roeder CW, and Stanton FJ. 1982 “ Elastomeric bearing Design, Construction and Materials”. NCHRP Report 248.National Research Council Washington. D.C, Seattle.

Topkaya, C. 2004.“Analysis of specimen size effects in inclined compression test on laminated elastomeric bearings”

Yazdani, N, Eddy, S.M and Cai, C.S.2000.Validation of AASHTO Bearing stiffness for Standard Precast concrete Bridge Girders.”ACI Structural journal, pp 436-443.

Roeder CW, and Stanton FJ.1997. . “Steel bridge bearing selection and design guide” American Iron and Steel Institute.

Muscarella J.V and Yura J.A, 1995 ”Experimental study of elastomeric bridge bearing with design recommendations”. Center of Transportation Research Texas University, Austin.

Clark, Earl .V and Moultrap, K.1966 “load- deformation characteristics of elastomeric bearing pads”. Highway Research record # 34,highway Research Board Washington, D.C.

Pare, R.L and Kenner, E.P.1960 “elastomeric bridge bearing” highway Research board bulletin Highways Research Bulletin # 242 National Research Council Washington, D.C.

Kurt Miller from Axel Product Inc.2000 “Experimental Loading Conditions Used to Implement Hyper elastic and Plastic Material Models”

Lindley Peter B, 1992.”Engineering design with Natural rubber” Malaysia Natural Rubber Producers Research Association Hertford England.

Roeder CW, and Stanton FJ.1982 “ Elastomeric bearing Design, Construction and Materials”. NCHRP Report 248.National Research Council Washington. D.C, Seattle.

Dawn.E.L, Roeder, C.W, Russel, L, and Kevin, C.2003.”Cotton duck Bearing Pad Engineering Evaluation and Design Recommendations”. Departments of civil and Environmental engineering, seatle Washington.

Jain, S.K, and Thakkar S.K.2002 “Quasi-static Testing of Laminated Rubber Bearings”. Department of Earthquake Engineering at IIT.Roorkee

English, B.A, Klingner, R.E and Yura J.A.1994.”Elastomeric bearing Background Information”. Research Report 1304-1 Center of Transportation research Bureau of Engineering Research. Texas at Austin.

Muscarella, J.V and Yura, J.V.1996 ”An experimental study of flat and Tapered Elastomeric Bridge Bearing “. ACI Special Publications, Sp 164-6,pp 16

Topkaya, C.2004.“Analysis of specimen size effects in inclined compression test on laminated elastomeric bearings”

Ozell, A.M and Diniz, J.F, 1960.”Report on tests of the Neoprene pads under repeated shear load, National Research Council Washington, D.C

Bergstrom.J.S and. Boyce, M.C.2001.” Constitutive modeling of the time-dependent and cyclic loading of elastomer and application to soft biological tissues”, final version of this draft working paper is published in: Mechanics of Materials, Vol. 33, pp. 523-530.

Yazdani, N, Eddy, S.M and Cai, C.S.2000.Validation of AASHTO Bearing stiffness for Standard Precast concrete Bridge Girders.”ACI Structural journal, pp 436-443.

Euridice A. Oware.” Numerical Examination of the Performance of Elastomeric Bearing Pads and Steel Rocker Bearings for Seismic Loads” Dept. of Civil Engineering, Washington University, St. Louis.

James M. Kelly “Analysis of Fiber-Reinforced Elastomeric Isolators”. Earthquake Engineering Research Center, University of California, Berkeley.